MODELING, CONTROL AND ANALYSIS OF DOUBLY FED INDUCTION GENERATOR BASED ON WIND TURBINE SYSTEM

2022
MASTER THESIS
ELECTRICAL-ELECTRONICS ENGINEERING

Samatar ABDI YONIS

Thesis Advisor
Prof. Dr. Ziyodulla YUSUPOV

MODELING, CONTROL AND ANALYSIS OF DOUBLY FED INDUCTION GENERATOR BASED ON WIND TURBINE SYSTEM

Samatar ABDI YONIS

T.C.
Karabuk University
Institute of Graduate Programs
Department of Electrical-Electronics Engineering
Prepared as
Master Thesis

Thesis Advisor
Prof. Dr. Ziyodulla YUSUPOV

KARABUK
June 2022

I certify that in my opinion the thesis submitted by Samatar ABDI YONIS titled "MODELING, CONTROL AND ANALYSIS OF DOUBLY FED INDUCTION GENERATOR BASED ON WIND TURBINE SYSTEM" is fully adequate in scope and in quality as a thesis for the degree of Master of Science.

Prof. Dr. Ziyodulla YUSUPOV .....
Thesis Advisor, Department of Electrical-Electronics Engineering

This thesis is accepted by the examining committee with a unanimous vote in the Department of Electrical-Electronics Engineering as a Master of Science thesis. June 16, 2022

Examining Committee Members (Institutions)	Signature
Chairman : Assoc. Prof. Dr. Adem DALCALI (BANU)	.....
Member : Prof. Dr. Ziyodulla YUSUPOV (KBU)	.....
Member : Assist. Prof. Dr. Hüseyin ALTINKAYA (KBU)	.....

The degree of Master of Science by the thesis submitted is approved by the Administrative Board of the Institute of Graduate Programs, Karabuk University.

Prof. Dr. Hasan SOLMAZ .....
Director of the Institute of Graduate Programs

"I declare that all the information within this thesis has been gathered and presented in accordance with academic regulations and ethical principles and I have according to the requirements of these regulations and principles cited all those which do not originate in this work as well."

Samatar ABDI YONIS

ABSTRACT

M. Sc. Thesis

MODELING, CONTROL AND ANALYSIS OF DOUBLY FED INDUCTION GENERATOR BASED ON WIND TURBINE SYSTEM

Samatar ABDI YONIS

Karabuk University
Institute of Graduate Programs
The Department of Electrical-Electronics Engineering

Thesis Advisor:
Prof. Dr. Ziyodulla YUSUPOV
June 2022, 96 pages

In the beginning of the 21st century, there was a growing interest in renewable energy sources particularly the wind energy for power generation. The researchers aimed to enhance the development of the design parameters for wind energy generations. However, doubly fed induction generator (DFIG) has been frequently used in wind turbines because of variable speed operations. DFIG has some merits such as, cost effectiveness, higher efficiency and reliability and the fact that it operates in both standalone and when it's connected to the grid. Complete modeling, control and analysis of DFIG based on wind turbine system has been developed in this thesis.

This thesis includes detailed developments of the wind turbine model such as, wind speed, aerodynamic system, drive train and generator model. Moreover, the dynamic model of DFIG in a rotating dq reference frame has been derived. Vector control approach of electrical machines is employed in the whole system. The complete system which consists of models and sub models are integrated and simulated using MATLAB/Simulink environment. Furthermore, to get the maximum output power from the wind turbine model, it's necessary to design control strategy. This includes rotor side converter (RSC) control, proportional-integral (PI) control, indirect speed control and grid side converter (GSC) control. PI controller has been designed in order the current components follow their references and the current loops has been tuned until the desired value is obtained. The RSC controls torque, flux and active and reactive power. The indirect speed control which is used to drive the torque to follow the maximum power curve is designed at the RSC control. The function of GSC control is to maintain the DC bus voltage constant irrespective of the region of operation and it operates at a unit power factor.

Moreover, the steady-state analysis for the most representative magnitudes of DFIG based wind turbine has been investigated in MATLAB. Correspondingly, the steady-state reactive power capability of DFIG is examined. Two case study is considered during steady-state analysis. In case 1, reactive stator power is set at zero which results the value of the maximum stator current to be lowered. In case 2, direct rotor current is set at zero which provides lower stator current, but the reactive power became high.

Another objective of the study is to compare the performances of most representative magnitudes of DFIG based wind turbine using PI controller and the proposed method in terms of settling time. The simulated result demonstrates that the performances of the proposed method improves and it has less perturbations compared to the PI controller. Moreover, the proposed method gives strong robustness for controlling the system with variable parameters.

The dynamic analysis of current loops behavior in a wind turbine based DFIG has been studied. It is summarized that, to follow properly the dynamic performances of DFIG, it is not required to reach the saturations for the voltage references. Besides, the

behavior of the system under different grid fault conditions such as, symmetrical (balanced) and asymmetrical (unbalanced) voltage dips using crowbar protection are analyzed. The simulation result confirms the effectiveness of the proposed system.

Key Words : Wind turbine, doubly fed induction generator, indirect speed control, dynamic analysis, symmetrical, asymmetrical, crowbar protection.

Science Code : 90526

ÖZET

Yüksek Lisans Tezi

ÇİFT BESLEMELİ ASENKRON GENERTÖRLER TABANLI RÜZGAR TÜRBİNİN MODELLENMESİ, KONTROLÜ VE ANALİZİ

Samatar ABDI YONIS

Karabük Üniversitesi
Lisansüstü Eğitim Enstitüsü
Elektrik-Elektronik Mühendisliği Anabilim Dalı

Tez Danışmanı:
Prof. Dr. Ziyodulla YUSUPOV
Haziran 2022, 96 sayfa

Yirmi birinci yüzyılın başında, yenilenebilir enerji kaynaklarına, özellikle de elektrik üretimi için rüzgar enerjisine artan bir ilgi vardı. Araştırmacılar, rüzgar enerjisi nesilleri için tasarım parametrelerinin gelişimini geliştirmeyi amaçlıyor. Ancak çift beslemeli asenkron generatörler (ÇBAG), değişken hızlı işlemler nedeniyle rüzgar türbinlerinde sıklıkla kullanılmaktadır. ÇBAG'nin maliyet etkinliği, daha yüksek verimlilik ve güvenilirlik ve hem bağımsız hem de şebekeye bağlıyken çalışması gibi bazı avantajları vardır. Bu tezde, ÇBAG'nin rüzgar türbini sistemine dayalı komple modellenmesi, kontrolü ve analizi geliştirilmiştir.

Bu tez, rüzgar hızı, aerodinamik sistem, aktarma organları ve jeneratör modeli gibi rüzgar türbini modelinin detaylı geliştirmelerini içermektedir. Ayrıca, dönen bir dq referans çerçevesinde ÇBAG'nin dinamik modeli türetilmiştir. Tüm sistemde elektrik makinelerinin vektör kontrol yaklaşımı kullanılmıştır. Modeller ve alt modellerden

oluşan sistemin tamamı MATLAB/Simulink ortamı kullanılarak entegre edilmiş ve simüle edilmiştir. Ayrıca rüzgar türbini modelinden maksimum çıkış gücü elde etmek için kontrol stratejisinin tasarlanması gerekmektedir. Buna rotor tarafı dönüştürücü (RTD) kontrolü, oransal-integral (OI) kontrolü, dolaylı hız kontrolü ve şebeke tarafı dönüştürücü (ŞTD) kontrolü dahildir. OI denetleyici, akım bileşenlerinin referanslarını takip etmesi için tasarlanmış ve istenen değer elde edilene kadar akım döngüleri ayarlanmıştır. RTD, torku, akıyı ve aktif ve reaktif gücü kontrol eder. Maksimum güç eğrisini takip etmek için torku sürmek için kullanılan dolaylı hız kontrolü, RTD kontrolünde tasarlanmıştır. ŞTD kontrolünün işlevi, çalışma bölgesinden bağımsız olarak DA bara voltajını sabit tutmaktır ve bir birim güç faktöründe çalışır.

Ayrıca, MATLAB'de ÇBAG tabanlı rüzgar türbininin en temsili büyüklükleri için kararlı durum analizi incelenmiştir. Buna uygun olarak, ÇBAG'nin kararlı durum reaktif güç kapasitesi incelenir. Kararlı durum analizi sırasında iki vaka çalışması ele alınır. Durum 1'de, reaktif stator gücü sıfıra ayarlanır ve bu, maksimum stator akımının değerinin düşürülmesiyle sonuçlanır. 2. durumda, doğrudan rotor akımı, daha düşük stator akımı sağlayan sıfıra ayarlanır, ancak reaktif güç yükselir.

Çalışmanın bir diğer amacı, ÇBAG tabanlı rüzgar türbininin en temsili büyüklüklerinin performanslarını OI kontrolör ve önerilen yöntemin oturma süresi açısından karşılaştırmaktır. Simüle edilen sonuç, önerilen yöntemin performanslarının arttığını ve OI denetleyiciye kıyasla daha az bozulmaya sahip olduğunu göstermektedir. Ayrıca önerilen yöntem, sistemi değişken parametrelerle kontrol etmek için güçlü bir sağlamlık sağlar.

Bir rüzgar türbini tabanlı ÇBAG'de akım döngülerinin davranışının dinamik analizi incelenmiştir. ÇBAG'nin dinamik performanslarını doğru bir şekilde takip etmek için voltaj referansları için doygunluklara ulaşılmasına gerek olmadığı özetlenmiştir. Ayrıca, levye koruması kullanılarak simetrik (dengeli) ve asimetrik (dengesiz) gerilim düşüşleri gibi farklı şebeke arıza koşulları altında sistemin davranışı analiz edilir. Simülasyon sonucu, önerilen sistemin etkinliğini doğrulamaktadır.

Anahtar Kelimeler : Rüzgar türbini, çift beslemeli endüksiyon jeneratör, dolaylı hız kontrolü, dinamik analiz, simetrik, asimetrik, levye koruması.

Bilim Kodu : 90526

ACKNOWLEDGMENT

First and foremost, I would like to express my special thanks to the greatest of all time, ALLAH, the most Gracious, the most Merciful, who has given me the health, strength and patience to complete my Master study.

I would like to give thanks to my supervisor, Prof. Dr. Ziyodulla YUSUPOV, from the bottom of my heart for his support and guidance, outstanding advice and patience during my Master journey.

I would also like to thank my committee members, Assoc. Prof. Dr. Adem DALCALI and Assist. Prof. Dr. Hüseyin ALTINKAYA for their time dedicated to examine and review my work.

Finally, my special gratitude goes to my parents and my brothers, Mr. Saad and Mr. Mahamed and of course my sister, Mrs. Hibo, for their continuous support.

CONTENTS

Page

Page

Page

LIST OF FIGURES

Page

Page

Page

LIST OF TABLES

Page

SYMBOLS AND ABBREVIATIONS INDEX

SYMBOLS

F : frequency

Ps : stator active power

Qs : reactive stator power

V : stator voltage

I : stator current

smax : maximum slip

Rs : stator resistance

Ls : stator inductance

n : rotational speed

Ts : sample time

Vbus : dc-bus voltage

Rr : rotor resistance

Lr : rotor inductance

N : gearbox ratio

U : stator rotor turns ratio

Lm : mutual inductance

Fs : stator flux

D : damping ratio

Vw : wind speed

J : moment of inertia

fsw : switching frequency

idr : direct rotor current

idg : direct grid current

iqr : quadrature rotor current

iqg : quadrature grid current

ABBREVIATIONS

WECS : Wind Energy Conversion System
IEA : International Energy Agency
SFOVC : Stator Flux Oriented Vector Control
GVOVC : Grid Voltage Oriented Vector Control
MPPT : Maximum Power Point Tracking
RSC : Rotor Side Converter
EEWS : Effective Estimations of Wind Speed
GSC : Grid Side Converter
PI : Proportional-Integral
SMC : Sliding Mode Control
DTC : Direct Torque Control
DC : Direct Current
DPC : Direct Power Control
LVRT : Low Voltage Ride Through
DVR : Dynamic Voltage Restorer
SMES : Superconducting Magnetic Energy Storage
FRT : Fault Ride Through
KVL : Kirchhoff's Voltage Law
IGBT : Insulated Gate Bipolar Transistor
FOC : Field Oriented Control
KCL : Kirchhoff's Current Law
PLL : Phase Locked Loop
PWM : Pulse Width Modulation
DFIG : Doubly Fed Induction Generator

PART 1

INTRODUCTION

Normally in order to use the wind energy, a revolving machine called wind turbine is required to exist [1]. For instance, the process where the kinetic energy from the revolving wind turbine is converted in to mechanical energy and this energy is then converted in to electrical energy by generator is known as wind energy conversion system (WECS) [2, 3]. It is commonly used in standalone systems, distributed generation and microgrids, smart grids and grid-connected systems. However, in all these scenarios, proper energy management procedures must be implemented to optimize the power generation of the wind turbines and distribute the generated power to the system with highly efficient and acceptable power quality. In order to do that, the structure of the power converter and effective control strategy must be chosen.

For the last few years, DFIG has been the most preferable options in wind turbines. Due to its numerous advantages compared to other types of generators that are now obtainable in the market. However, DFIG based wind turbines are sensitive to the grid disturbances which is a major problem in the present power situations. This research aims to model and study the operation of a wind turbine based DFIG system. Moreover, it investigates the dynamic behavior of current loops when the system is connected to the grid. It further analyses the behavior of a grid-connected DFIG based wind turbine system during symmetrical and asymmetrical voltage dips. This chapter will provide an introduction to the WECS based on DFIG by first discussing the motivation behind the thesis with some related background, followed by purpose and contribution, methodology of the thesis, literature review and finally, the thesis structure.

1.1. MOTIVATION AND BACKGROUND

Wind energy has been utilized for at least three thousand years. It was employed to produce mechanical energy to pump the water or grind grain until early 20th century [4-8]. In the beginning of the modern industrialization, variable wind energy source was replaced by electrical grids or fossil fuel engines, which supplied a more sustained source of power [6]. After the first oil price changes in the early 1970s, interest in wind power resurfaced. However, the main focus this time was on wind power, as a source of electrical energy rather than mechanical energy. As a result, alternative energy systems such as the electrical grid was used as a backup to offer a stable and consistent power supply [6]. Accordingly, wind energy is one of the most reliable and growing renewable energy sources in the recent years. The most important contributing reasons for the growth of the wind energy system includes: greater public awareness toward the renewable energy, government assistance, and fast improvement in the power electronics sector. According to international energy agency (IEA), in 2020 alone, a total of 1592 TWh of electricity were generated from the wind turbine [9]. Which, for instance, is 12% increase over 2019. Thus, in order to achieve the needed 8000 TWh which is forecasted in 2030, according to IEA report [9], the generation should rise by an average of 18% each year between 2021 and 2030. As previously mentioned, DFIG are commonly used in wind turbines because they employ variable speed turbines. Moreover, DFIG are highly efficient and reliable system and they have the ability to control active and reactive power independently by utilizing partial converters. Normally, DFIG based wind turbines are located far away from the power grid which may result difficulties of controlling the voltages. Correspondingly, they have drawbacks such as being sensitive to the grid disturbance and limited reactive power capability when the system is connected to a weak grid. Therefore, this type of technology requires more research and development in order to be implemented into the grid. Thus, in order to implement the DFIG system into the present energy system, it is essential to analyze the steady-state performance, the dynamic behavior of the system, and the effect on the interconnected power system in terms of voltage control, and active and reactive power capability.

1.2. PURPOSE AND CONTRIBUTION

The main purpose behind this thesis is to implement and model the operation of DFIG based wind turbine system. The major focus of the study presented here is to design and control the wind turbine based DFIG according to the company's manual. It first generates a code created in MATLAB environment to analyze the different steady-state dynamic performance of the system, in order to compare and verify with the designed system. Field oriented or vector control strategy has been employed in order to implement decouple control of active and reactive powers. Moreover, maximum power point tracking (MPPT) strategy by indirect speed control has been carried out to extract the maximum power available from the wind. The main contribution of the thesis is presented as follows:

- Simulation of the DFIG system for the RSC control using stator flux-oriented vector control (SFOVC) strategy.
- Steady-state analysis of the various magnitudes of the DFIG system.
- Comparison between the typical PI controller and the proposed method by investigating the settling time for different wind speed.
- Implementation of DFIG based wind turbine system for the RSC.
- Implementation of the system in GSC using grid voltage-oriented vector control (GVOVC) strategy.
- Dynamic analysis of current loops behavior in a wind turbine based DFIG.

Besides, this thesis investigates the performance analysis of a grid-connected DFIG based wind turbine under symmetrical and asymmetrical voltage dips.

1.3. METHODOLOGY OF THE THESIS

The methodology of this thesis has been performed according to the following steps:

- Complete literature review on relevant publications from journals, conferences and the different books has been investigated.

- Complete modeling of the wind turbine such as: aerodynamic, electrical, and mechanical part has been carried out.
- Dynamic modeling of the DFIG in the dq reference frame is derived to study the operation of the system.
- Developing the steady-state analysis in MATLAB for the various magnitudes of the DFIG.
- Design and control of the DFIG for the RSC.
- Implement and control the most representative magnitudes of a grid-connected DFIG based wind turbine system.

The overall system has been implemented and confirmed in MATLAB/Simulink environment. This software is applied for modeling and controlling the DFIG based wind turbine system because it includes library tools and protection models.

1.4. LITERATURE REVIEW

In DFIG design, two back-to back linked converters supply the desired magnetization current at the rotor side [10]. For instance, the grid power of DFIG based wind turbine is linked to a three-phase converter (GSC), which passes to the DC bus voltage. Moreover, the DC bus voltage can be applied as a source for the other side of the converter, which is directly connected to the rotor windings (RSC).

Ref [11] describes an overview of grid-connected WECS in details. Hence, it is noted that detecting the grid voltage angle correctly is an essential task in most of the control strategies in the GSC. It has been suggested that for grid synchronization, all advanced wind turbines must include a faster and efficient tracking equipment to determine the grid voltage and frequency.

The authors in Ref [12] provides a review on the issue of effective estimations of wind speed (EEWS). Most of the main EEWS strategies and their implementations are extensively addressed. The paper realizes that, accurate estimations of the wind speed to be effective in terms of energy capture.

Improving the effectiveness of vector control strategy has attracted many researchers. In Ref [13-16], the authors presented that the DFIG based wind turbine provides decouple control of active and reactive powers of generator, resulting good dynamic performance, higher efficient energy output, and good power quality.

It is very important to bear in mind that the DFIG is more difficult to control compared to the typical induction generator. Hence, the rotor current is controlled by a power electronics converter in the rotor circuit, this results the control of the DFIG [17]. Vector control is a popular strategy for controlling the DFIG based wind turbine [18, 19]. Different vector control strategy has been presented in the literature. Stator flux-oriented vector control is increasingly employed in the present technology.

Ref [20] introduced a new integrated frequency control technique that dynamically integrates inertial and pitch angle control to improve the performance of DFIG-based wind turbines to the power system frequency control. In Ref [21], a novel controller has been introduced that allows the DFIG based wind turbine to positively contribute to the grid operation.

In Ref [22], comparative analysis between robust sliding mode control (SMC) and typical PI controller in DFIG based WECS has been presented. Their simulated results demonstrates that the proposed SMC provides faster dynamic response with very little steady-state error compared with the PI.

Moreover, Ref [23] compared PI and fuzzy control based DFIG wind turbine, and it is obvious that the fuzzy control is more robust against machine parametric perturbations and delivers faster convergence. From Ref [24] we can understand that using fuzzy-PI controller, settling time and the value of peak overshoot are lowered, and variations are damped down faster compared to the typical PI controller. The transient response given by fuzzy-PI controller has also proved to be superior to the typical PI controller.

Ref [25] proposes a dual-loop control strategy to enhance the dynamic performance of DFIG based wind turbine that may be subjected to the grid disturbance. This strategy

can quickly deteriorate the fluctuations of the stator flux and this can successfully mitigate the impact of stator transient flux on the performances of the DFIG.

Ref [26] studies comparative investigations of control strategies in DFIG based wind turbine. It states that the direct torque control (DTC) is quicker than vector control in terms of transient response, that can be very beneficial and provide a lot of capacity when specific control manipulations are required.

Ref [27] introduced a coordinated control strategy for DFIG with DC connection. The experimental results shows that the control strategy is available for the proposed power grid configuration. It concludes that the DC/DC converter to be the most important component in WECS into the integration of DFIG system. From Ref [28] it can be realized that the study places a PI controller before the conventional DTC or direct power control (DPC) blocks to improve the dynamic performances. Consequently, the study shows that DTC has higher operating performance than DPC, since DTC directly controls the torque.

However, to our knowledge, none of the aforementioned literature investigates the implementation and analysis of the magnitudes of grid-connected DFIG system by using indirect speed control strategy. Moreover, this study describes the comparison of PI controller and the proposed method in terms of settling time.

The authors in Ref [29] presents a review on control approach for DFIG based wind turbine under asymmetrical faults in the GSC. It addresses the difficulties encountered during the dip. Ref [30] presented a crowbar less low voltage ride through (LVRT) strategy to enhance the fault ride through (FRT) capabilities of DFIG based wind turbine under transient state operation. Ref [31] introduced an effective FRT system based DFIG wind turbine. consequently, the design combines the transient stability characteristics of SMC with the active and reactive power capabilities of dynamic voltage restorer (DVR), and the instantaneous power availability of superconducting magnetic energy storage (SMES).

Ref [32] describes the applications of a DVR in DFIG based wind turbine to enable uninterruptible FRT of voltage dips that meet the grid code specifications. The DVR can recompense for the faulty line voltage, allowing the system to keep functioning normally as required by the grid codes.

Ref [33] developed a new organized performance modification strategy to enhance the operations of DFIG during symmetrical and asymmetrical voltage dips. The new strategy efficiently protects the converter by lowering the overcurrent in the RSC and maintaining the dc bus voltage within an appropriate limit.

The authors in Ref [34] investigates the improvement of crowbar hardware design for FRT capabilities in DFIG based wind turbines. The simulated results shows that the oscillation that occurred after the transient event, were immediately damped with the linkage of the DFIG to the crowbar hardware element, which was improved by the stator and rotor dynamic model.

1.5. THESIS STRUCTURE

The structure of this thesis is classified into seven chapters. As previously stated, chapter 1 provides an introduction to the WECS based on DFIG by first discussing the motivation behind the thesis with some related backgrounds, followed by purpose and contribution, methodology of the thesis, literature review and finally, the structure of the thesis.

Chapter 2 studies the different categories of wind turbine system. It further presents the detailed model of the wind turbine system by first modeling the wind speed, followed by the aerodynamic model, drive train model, and generator model.

Chapter 3 describes the dynamic modeling of the DFIG in the dq reference frame. Moreover, it presents DFIG model in the ABC representation and the transformation techniques.

Chapter 4 presents the control design of DFIG based wind turbine for the RSC and when the system is connected to the grid. PI control and indirect speed control strategy has been studied. Moreover, it investigates the steady-state analysis of DFIG and the derivations of the transfer function for the RSC and GSC.

Chapter 5 investigates the analysis of grid-connected DFIG based wind turbine during symmetrical and asymmetrical voltage dips.

Chapter 6 demonstrates the design and implementation of the DFIG based wind turbine using PI controller and indirect speed control strategy. Detailed simulation results are presented and discussed.

Chapter 7 gives the conclusion and recommendations for future work on the operation and control of DFIG based wind turbine system.

PART 2

WIND ENERGY SYSTEM

Wind energy is among the most well-known renewable energy sources, and its use is increasing steadily around the world. In 2019, alone, more than 60 GW of wind energy capacity was installed globally, which is a 19% rise over installation in 2018, showing that wind energy is gradually dominating the energy industry. DFIG has been an extensively known machine compared to other forms of the wind energy system. It contains a wind turbine attached to the shaft of an induction generator. A DFIG is built such that: the stator part connects to the power grid directly, whereas the rotor part links to the grid via a pulse width modulation (PWM) converter that controls the slip energy. This section includes the different types of wind turbines both according to the position of the axis of rotation and by the operation of their system. Moreover, it presents the mathematical modeling of the wind turbine system.

2.1. WIND ENERGY CONVERSION SYSTEM

WECS is the entire system that uses mechanical power to convert wind energy into useable electrical power. It is mainly divided into three parts: aerodynamic, mechanical, and electrical [35]. Figure 2.1 depicts the primary parameters of a typical wind power conversion system.

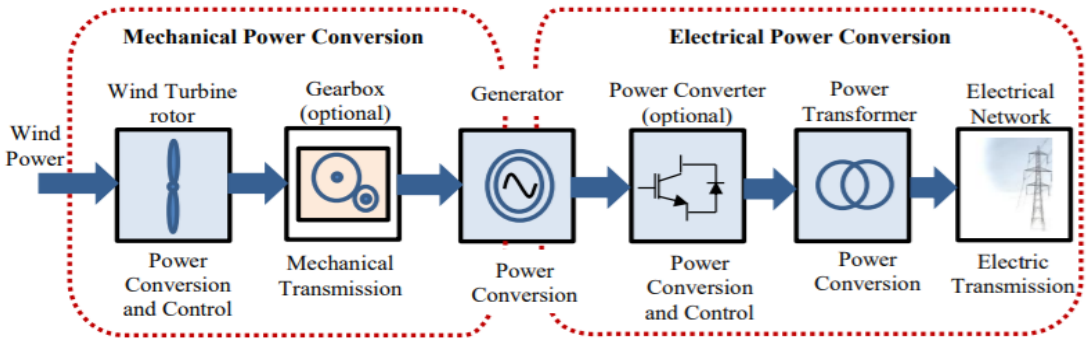

Figure 2.1. Shows components of grid-connected WECS [35].

Wind turbines can be categorized into two types of rotational axis; horizontal axis wind turbines (HAWTs) and vertical axis wind turbines (VAWTs) [36]. HAWTs currently account for most installed solutions around the world. As a result, HAWTs account for about 75% of wind turbines, which is owing to their great efficiency when compared to installation and maintenance expenses [37]. The name HAWT is given based upon the fact that its blades spin on an axis parallel to the earth's surface. HAWTs can be classified into two parts: downwind HAWTs and upwind HAWTs, as shown in Figure 2.2.

It can be seen that the rotational blade of downwind is on the backside of the turbine. Unlike downwind, the rotor blade of the upwind turbine is directly toward the wind. Furthermore, they don’t self-align toward the wind, necessitating the use of a tail vane or a yaw system to keep the rotor facing the wind. For this purpose, most of the wind turbines that are used nowadays are upwind HAWTs. Thereby, upwind HAWTs are mostly presented in this work.

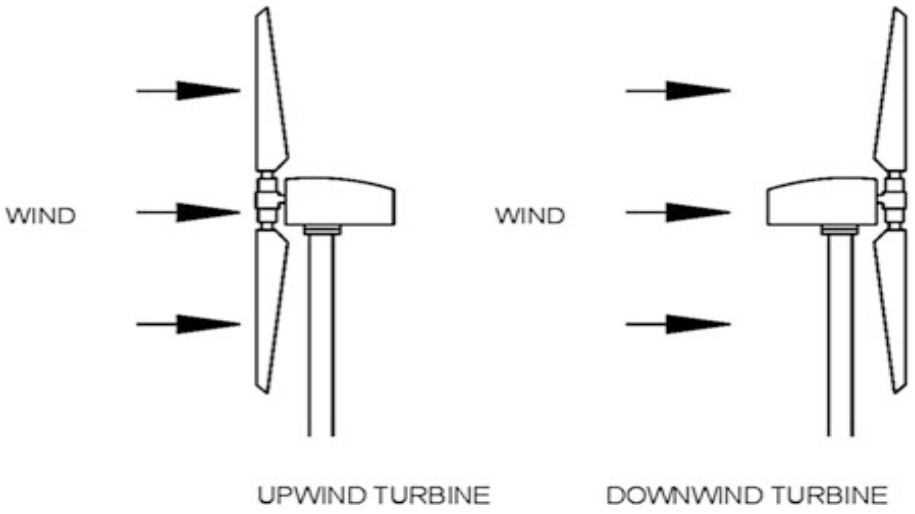

Figure 2.2. Upwind and downwind type wind turbines [38].

2.2. WIND TURBINE SYSTEM

Wind turbine systems may be divided into two categories based on how their system works: Fixed and variable speed wind turbines.

2.2.1. Fixed Speed Wind Turbines

The rotor speed of a fixed-speed wind turbine (FSWT) can be specified and governed by the frequencies of the grid, the gear ratio, and generator design, regardless of wind speed [39]. A typical configuration of FSWT can be seen in Figure [2.3]. FSWTs include a squirrel cage induction generator (SCIG) that links to a Soft-Starter that connects to a capacitor which is linked to the grid through a transformer to adjust the reactive power [39]. The main disadvantage is that these wind turbine generators are unable to track whenever the value of the speed of the wind is changed. Furthermore, the efficiency of power harvesting may not be good like in variable speed turbines. For this reason, in this thesis, we consider variable speed turbines.

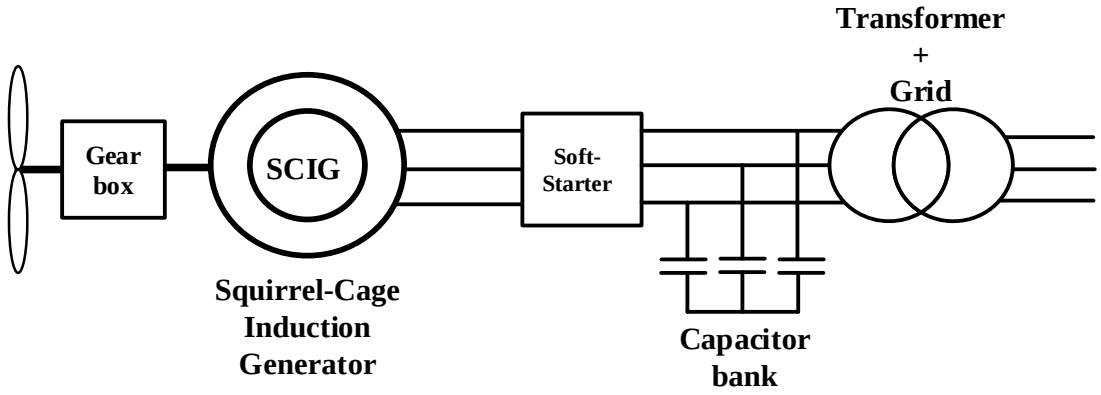

Figure 2.3. Configuration of fixed speed wind turbine.

2.2.2. Variable Speed Wind Turbines

Variable speed generators, differs from the fixed speed turbines in that, they can adjust the rotational speed, as the speed of wind changes to maximize energy capturing from the wind. The rotational speed of the turbine can be continuously modified in response to wind speed. Furthermore, lambda (λ) can be kept at an optimal range to ensure maximum power conversion efficiency at different wind speed [40]. The configuration of variable speed turbines can be seen in Figure 2.4. A PWM converter links the generator to the power grid then the converter allows the wind turbines to operate at various speeds. Variable speed generator has several benefits, including enhanced

wind power output, greater power quality, and less mechanical impacts. Contrarily, higher manufacturing costs and power losses are associated with the usage of power converters [40].

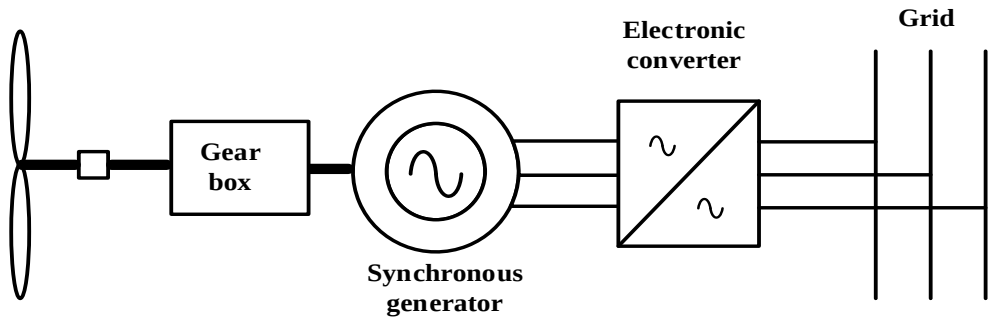

Figure 2.4. Scheme of variable speed synchronous generator.

2.3. WIND TURBINE MODEL

It is very important to note that the data provided by the company in their manual is relatively limited. The purpose of this section is to present some basic data and concepts for a wind turbine model. A practical wind turbine has a nominal output power of 1.5 to 3 MW. For this purpose, in this thesis, a 2.4 MW of wind turbine has been chosen for the system simulation. A schematic diagram of the Mitsubishi MWT 92 wind turbine is presented in Figure 2.5. From the information gathered from the company's manuals and other technical references, several factors that characterize wind turbine's dynamic performance and its basic electrical and mechanical behavior can be presented. To model, we need to consider the parameters of some features including, the ratio of the blade, the nominal power for a certain wind speed, the gearbox ratio, rotational speed, and the maximum speed of the blade's tip which are all presented in Appendix A.

Wind turbines produce electrical power by converting the mechanical energy provided by kinetic energy in the wind [41]. They can be described as a dimensionless power coefficient curve function of lambda and inclination angle. In this section, we assume that the wind turbine model comprises several parts: a wind speed, an aerodynamic model, a drive train model, and a generator. The corresponding wind speed supplied

to the aerodynamic system is estimated using a wind speed model [42]. The amount of rotational speed divided by the real wind speed (v_w) is called lambda. Wind speed, blade's pitch angle and speed of the rotor are all together fed into the aerodynamic system as shown in Figure 2.6. The output torque is fed to the drive train model along with the speed of the generator. Drive train model, thereby generates electromagnetic torque on high-speed shaft (hss), which is then transmitted to the generator system.

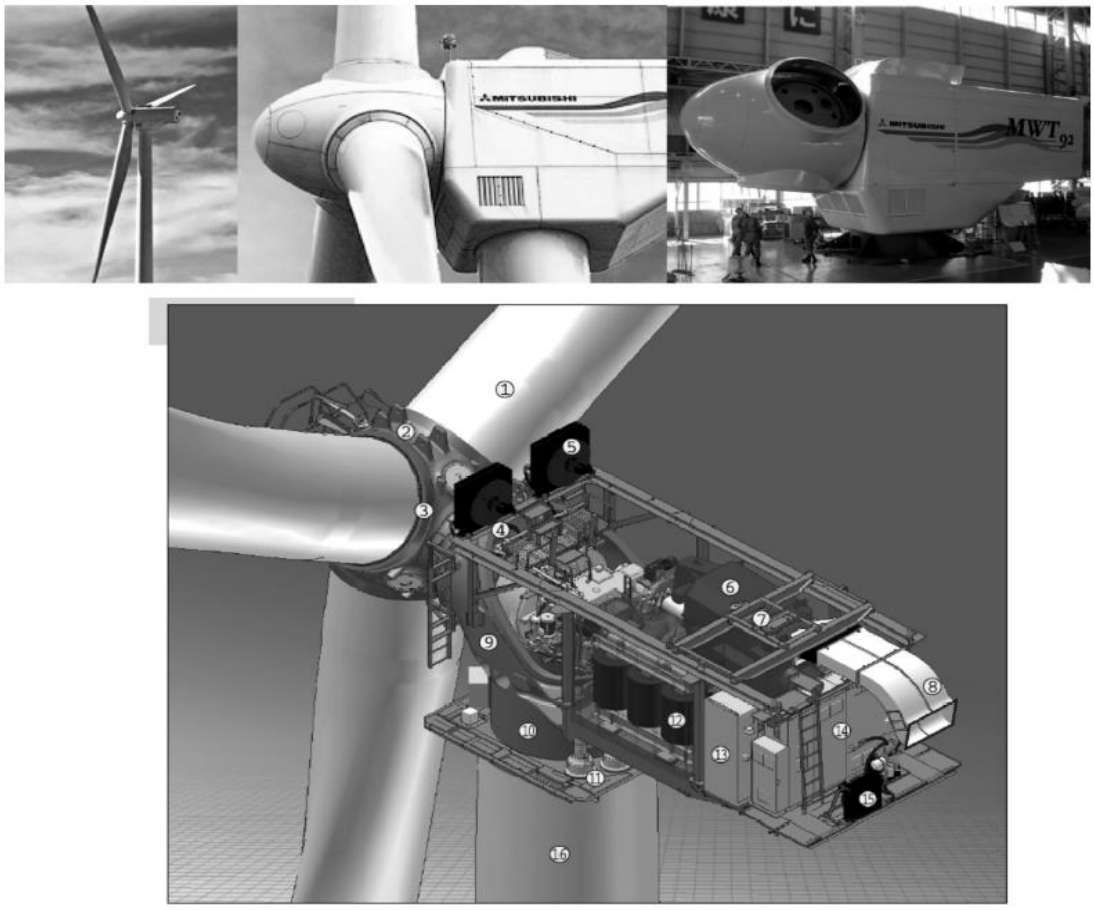

Figure 2.5. Schematic diagram of Mitsubishi MWT 92 wind turbine [42].

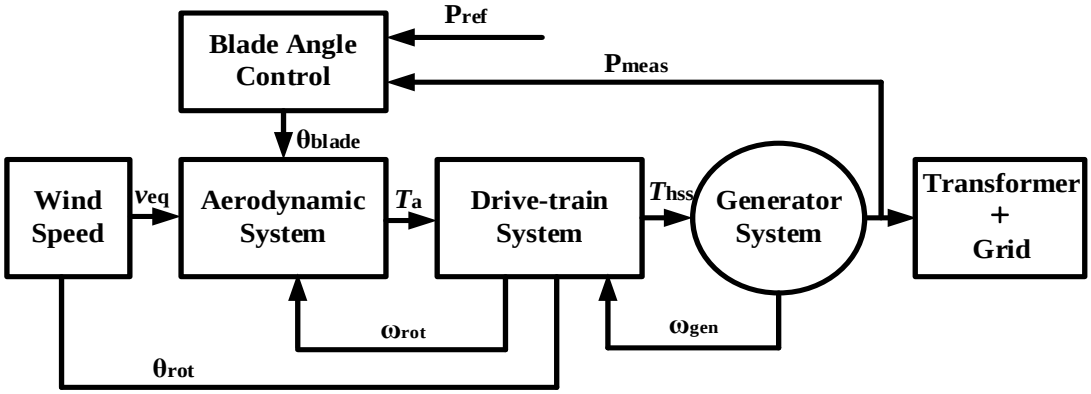

Figure 2.6. Shows a typical block design of the wind turbine model.

2.3.1. Wind Speed Model

Wind speed varies depending on the environment and it can also fluctuate randomly over time. This explains the fact that it has a significant impact on the electromagnetic torque and hence it seems to have a major impact on the power generated by the three blades [43]. For this purpose, in order to simulate the dynamic behavior of the wind turbine model, we need to take into consideration the wind speed. In this work, wind speed can be modeled by adding the following four constituents:

$$v_w(t) = v_{wa}(t) + v_{wt}(t) + v_{wr}(t) + v_{wg}(t) \tag{2.1}$$

Where $v_{wa}(t)$, $v_{wr}(t)$, $v_{wg}(t)$ and $v_{wt}(t)$ are the constant, turbulence, ramp, and gust constituents, respectively. The gust constituent can be modeled to represent unusual transient increases in wind speed and can be expressed as follows:

$$v_{wg}(t) = \begin{cases} 0, & for\ t < T_{sg} \\ A_g\left(1 - cos\left[2\pi\left(\frac{t-T_{sg}}{T_{eg}-T_{sg}}\right)\right]\right), & for\ T_{sg} \le t \le T_{eg} \\ 0, & for\ T_{eg} < t \end{cases} \tag{2.2}$$

Where T_{sg} and T_{eg} are start and end time of gust constituents and A_g is gust amplitude. Finally, the turbulence constituent can be represented by a signal with the following power density [43].

$$P_{Dt}(f) = \frac{l v_w\left[\ln\left(\frac{h}{z_o}\right)\right]^{-2}}{\left[1+1.5\frac{fl}{v_w}\right]^{5/3}} \tag{2.3}$$

Where l is turbulence scale, h is the height and $l = 20h$, that has maximum height of 300 meter; z_0 is the raggedness length value that varies due to topography type as it can be seen in Table 2.1 [43].

Table 2.1. Indicates different value of z_o for various topology type [43].

Types of topologies	**Scale of z_o in meter**
High seas	0.001-0.01
Snow surface	0.01-0.05
Mown grass	0.01-0.03
Rocky ground	0.02-0.1
Mountainous	2-6

Since we know all the other values, the next stage is to generate a signal with power spectrum. Considering that the P_{Dt} is close to the responses of first-order filter, then the suggested transfer function is as follows:

$$H(s) = \frac{K}{s+p} \tag{2.4}$$

Where p and K are formulated as follows:

$$p = \frac{2\pi\left(\left(K_1^2\right)^{3/5}-1\right)}{K_2\sqrt{K_1^2-1}} \tag{2.5}$$

$$K = K_1 p \tag{2.6}$$

And K_1 and K_2 are expressed as:

$$K_1 = lv_w\left[\ln\left(\frac{h}{z_o}\right)\right]^{-2} \tag{2.7}$$

$$K_2 = 1.5\frac{l}{v_w} \tag{2.8}$$

The calculated signal of the power spectrum is defined as:

$$P_{filter} = \frac{\frac{k^2}{p^2}}{1+\frac{4\pi^2}{p^2 f^2}} \tag{2.9}$$

2.3.2. Aerodynamic Model

Aerodynamic model calculates electromagnetic torque as a function of rotational speed on the blades. A simple aerodynamic system is presented in Figure 2.7. The torque coefficient can be obtained by using look up table from Simulink/MATLAB. In order to calculate the average electromagnetic torque in the low-speed shaft, wind speed can be defined as the average incidence of wind speed on the brushed area by the blade. The torque generated by the three-blade wind turbine can be formulated as [42].

$$T_t = 0.5\rho\pi R^3 V_w^2 C_t \tag{2.10}$$

Where, ρ, R, V_w, and C_t are air density, ratio (meter), wind speed and torque coefficient of wind turbine, respectively.

The most basic approach to characterize the power and torque coefficient is by a mathematical calculation as a function of lambda and pitch angle, as we presented in section (2.3). The power coefficient can be represented by the following expression:

$$C_p = 0.773\left(\frac{151}{\lambda_i} - 0.58\beta - 0.002\beta^{2.14} - 13.2\right)\left(e^{-18.4/\lambda_i}\right) \tag{2.11}$$

With

$$\lambda_i = \frac{1}{\lambda + 0.02\beta} - \frac{0.003}{\beta^3 + 1} \tag{2.12}$$

The tip step ratio λ is obtained as:

$$\lambda = \frac{R\Omega_t}{V_w} \tag{2.13}$$

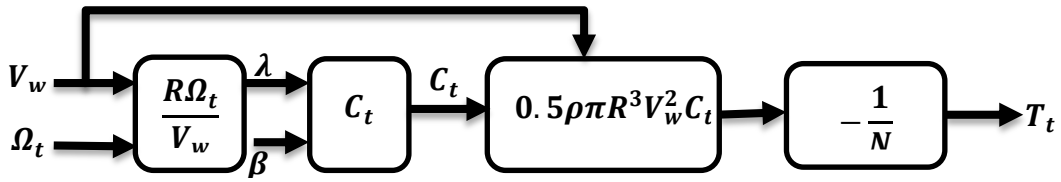

Figure 2.7. Aerodynamic system.

2.3.3. Drive Train Model

The drive train system of wind turbine can be used to characterize either by 1-mass, 2-mass, 3-mass or even 6-mass model [44]. The drive train system consists of a turbine, generator, low-speed shaft, gearbox, and a high-speed shaft [45, 46]. In order to model drive train system, we need to include both dynamic and typical parameters. At first, we need to consider power train's resonance frequency. The power transmission train is formed by the blades connected to the hub, attached to the slow shaft, which is coupled to the gearbox, which multiplies the rotational speed of the fast shaft attached to the generator [42]. In this thesis, we consider the 2-mass model as illustrated in Figure 2.8. The second resonant frequency is very higher but it's lower in magnitude. All the magnitudes are supposed to be in the fast shaft. Inertia (J_t) affects the turbine side masses, whereas (J_m) affects the electrical generator. The stiffness coefficient (k) and damping coefficient (c) represent the dynamic linkage between the two inertias. The dynamics of the system is characterized using Newton's laws as follows:

$$\begin{Bmatrix} \dot{\omega}_m \\ \dot{\omega}_t \\ \omega_m \\ \omega_t \end{Bmatrix} = \begin{pmatrix} \frac{-v^2 c}{J_m} & \frac{vc}{J_m} & -\frac{v^2 k}{J_m} & \frac{vk}{J_m} \\ \frac{vc}{J_t} & -\frac{c}{J_t} & \frac{vk}{J_t} & -\frac{k}{J_t} \\ 1 & 0 & 0 & 0 \\ 0 & 1 & 0 & 0 \end{pmatrix} \begin{Bmatrix} \omega_m \\ \omega_t \\ \theta_m \\ \theta_t \end{Bmatrix} + \begin{pmatrix} \frac{1}{J_m} & 0 \\ 0 & \frac{1}{J_t} \\ 0 & 0 \\ 0 & 0 \end{pmatrix} \begin{Bmatrix} \tau_m \\ \tau_t \end{Bmatrix} \tag{2.14}$$

Where θ_t, θ_m, ω_t and ω_m are turbine angle, generator angle, turbine angular speed and generator angular speed, respectively. τ_t is torque supplied to rotor shaft and τ_m is the generator torque.

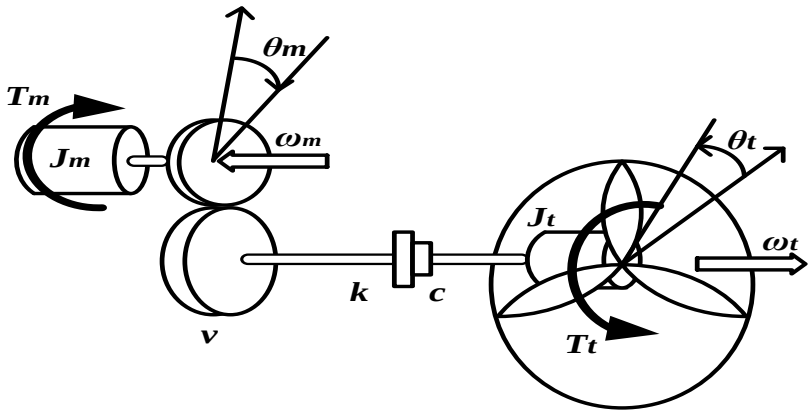

Figure 2.8. Drive train model.

2.3.4. Generator Model

A wound rotor asynchronous machine is the generator of doubly fed wind turbine system. The impact of magnetic saturations and the capacitance of all windings are ignored, and the neutrality of the stator and rotor windings is assumed to be moving and the currents flowing toward the machine are supposed to be positive and assuming that the stator and rotor windings to be placed symmetric and sinusoidal. It is possible to implement the relationship between voltage and current on the generator, as well as their first derivatives using synchronous dq representation and can be formulated as follows [43].

$$\begin{Bmatrix} v_{sq} \\ v_{sd} \\ v_{rq} \\ v_{rd} \end{Bmatrix} = \begin{bmatrix} L_s & 0 & M & 0 \\ 0 & L_s & 0 & M \\ M & 0 & L_r & 0 \\ 0 & M & 0 & L_r \end{bmatrix} \frac{d}{dt} \begin{Bmatrix} i_{sq} \\ i_{sd} \\ i_{rq} \\ i_{rd} \end{Bmatrix} + \begin{bmatrix} r_s & L_s\omega_s & 0 & M\omega_s \\ -L_s\omega_s & r_s & -M\omega_s & 0 \\ 0 & sM\omega_s & r_r & sL_r\omega_s \\ -sM\omega_s & 0 & -sL_r\omega_s & r_r \end{bmatrix} \begin{Bmatrix} i_{sq} \\ i_{sd} \\ i_{rq} \\ i_{rd} \end{Bmatrix} \quad (2.15)$$

Where L_s and L_r are the coefficients of stator and rotor inductance, M is magnetizing inductance and s is the slip.

Moreover, the torque and stator reactive power (Q_s), which is used to control the (rotor side) can be represented as follows:

$$T_m = \frac{3}{2} PM\left(i_{sq} i_{rd} - i_{sd} i_{rq}\right) \quad (2.16)$$

And

$$Q_s = \frac{3}{2}\left(v_{sq} i_{sd} - v_{sd} i_{sq}\right) \tag{2.17}$$

Where, P is the number of pole pair.

PART 3

DYNAMIC MODELING OF DOUBLY FED INDUCTION GENERATOR

Recently, the doubly fed induction machine is commonly utilized in wind generation system. These thesis presents the dynamic model and the performance analysis of steady-state in DFIG. The dynamic model of DFIG allows one to know the continual performance (not only under steady-state) of machine parameters, but also during various voltage providing situations. This section first develops the dynamic model of DFIG in abc stationary natural frame. The dynamics of the system is then converted to a rotating dq reference frame using Clarke and Park transformation method for cancellation of coupling between the two stator and rotor windings. The dynamic model of DFIG in a rotating dq axis is very important for designing the properties of synchronous and hyper-synchronous operating system as well as implementing vector control strategy for controlling active and reactive output power. In this section, a brief model of DFIG, a dc-link model, power electronic converter model and power and torque calculation has been presented.

3.1. DFIG MODEL IN ABC REPRESENTATION

The generalized form of the DFIG model can be represented as three phase stator and rotor windings, as shown in Figure 3.2. These three phase windings are the idealized form of the real system. Figure 3.1 shows the relation between stationary abc natural frame and rotating space vector. Whereby the space vector spins with a random speed ω with respect to abc natural frame. The space vector and abc references are separated 120^0 each other [42]. By using Kirchhoff's voltage law (KVL) it's possible to characterize the instantaneous voltage, current and flux in the stator side of the machine as follows:

$$\begin{cases} v_{as}(t) = R_s i_{as} + \frac{d\psi_{as}(t)}{dt} \\ v_{bs}(t) = R_s i_{bs} + \frac{d\psi_{bs}(t)}{dt} \\ v_{cs}(t) = R_s i_{cs} + \frac{d\psi_{cs}(t)}{dt} \end{cases} \quad (3.1)$$

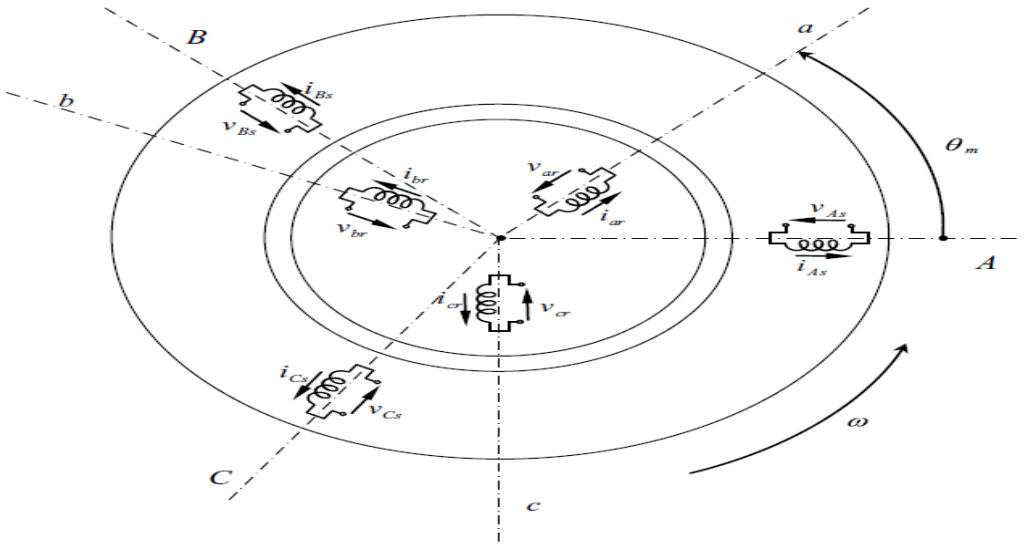

Figure 3.1. Shows stationary abc reference frame [42].

These idealistic *abc* representations are the actual machine, which facilitates the development of an equivalent electrical circuits as illustrated in Figure 3.2.

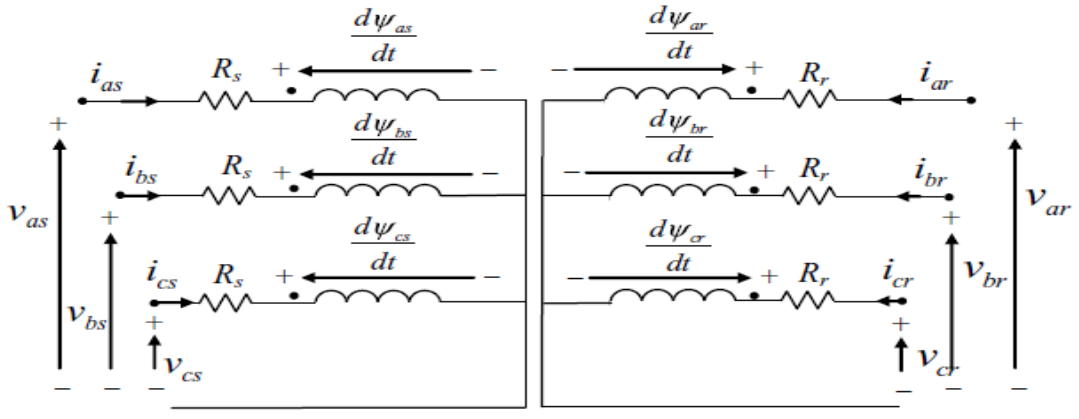

Figure 3.2. DFIG equivalent circuits [42].

Where $i_{as}(t)$, $i_{bs}(t)$, and $i_{cs}(t)$ are the currents of the stator in the a, b, c phases respectively; $v_{as}(t)$, $v_{bs}(t)$, and $v_{cs}(t)$ are the voltages supplied in the stator; $\psi_{as}(t)$, $\psi_{bs}(t)$, and $\psi_{as}(t)$ are stator fluxes and R_s is the resistance of the stator.

For instance, the magnitudes in the rotor side can also be expressed as follows:

$$\begin{cases} v_{ar}(t) = R_r i_{ar} + \frac{d\psi_{ar}(t)}{dt} \\ v_{br}(t) = R_r i_{br} + \frac{d\psi_{br}(t)}{dt} \\ v_{cr}(t) = R_r i_{cr} + \frac{d\psi_{cr}(t)}{dt} \end{cases} \tag{3.2}$$

Where $i_{ar}(t)$, $i_{br}(t)$, and $i_{cr}(t)$ are the currents of the rotor in the a, b, c phases respectively; $v_{ar}(t)$, $v_{br}(t)$, and $v_{cr}(t)$ are the voltages supplied in the stator refer to rotor; $\psi_{ar}(t)$, $\psi_{br}(t)$, and $\psi_{ar}(t)$ are fluxes of the rotor and R_r is the resistance of the rotor. Moreover, the magnitudes of the rotor have constant rotational frequencies ω_r during steady-state condition. The relationship between stator and rotor angular frequency is described as follows:

$$\omega_s = \omega_r + \omega_m \tag{3.3}$$

with

$$\omega_m = P\Omega_m \tag{3.4}$$

Where ω_m is the electric rotational frequency, Ω_m is the mechanical rotor speed and P is the number of poles of the machine.

3.2. THE TRANSFORMATION TECHNIQUE

In order to use the vector control approach, we need to model the dynamic equation of doubly fed induction machine (DFIM), which then provides the instantaneous voltages and currents in order to compute and control the parameters. Even though the rotor currents cannot be determined with cage motors, thus the current is substituted by an

appropriate amount expressed in a rotating dq representation by using a well-known technique called the Clarke and Park transformation.

3.2.1. The Clarke Transformation

The Clarke transform is a mathematical technique that converts a 3-phase abc natural frame into an orthogonally structure $(\alpha\beta)$ [47]. Let's consider a symmetric 3-phase induction generator having stationary abc axis with 120^0 apart as illustrated in Figure 3.3. Then it's possible to convert the abc constituents into $\alpha\beta$ through the Clarke method and it can be expressed as the following matrix equation:

$$\begin{bmatrix} x_\alpha \\ x_\beta \\ x_0 \end{bmatrix} = T_C \begin{bmatrix} x_a \\ x_b \\ x_c \end{bmatrix} \tag{3.5}$$

Where, T_C is the Clarke transform matrix that can be represented as,

$$T_C = \frac{2}{3}\begin{bmatrix} 1 & -\frac{1}{2} & -\frac{1}{2} \\ 0 & \frac{\sqrt{3}}{2} & -\frac{\sqrt{3}}{2} \\ \frac{1}{2} & \frac{1}{2} & \frac{1}{2} \end{bmatrix} \tag{3.6}$$

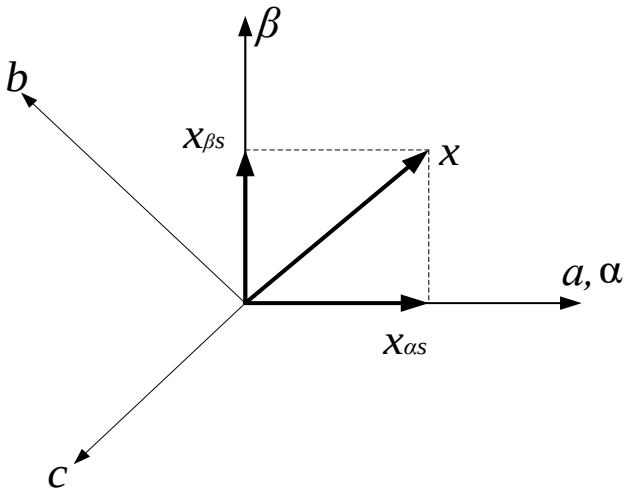

Figure 3.3. The Clarke transform representation.

For a symmetric 3-phase, x_0 is equal to zero and the transform representation for stator and rotor current shown in Figure 3.4 is defined as:

$$\begin{bmatrix} i_{\alpha s} \\ i_{\beta s} \\ i_{0s} \end{bmatrix} = T_C \begin{bmatrix} i_{as} \\ i_{bs} \\ i_{cs} \end{bmatrix} \tag{3.7}$$

And the rotor side can be defined as:

$$\begin{bmatrix} i_{\alpha r} \\ i_{\beta r} \\ i_{0r} \end{bmatrix} = T_C \begin{bmatrix} i_{ar} \\ i_{br} \\ i_{cr} \end{bmatrix} \tag{3.8}$$

Where, i_{0s} and i_{0r} are the stator and rotor currents at zero constituents respectively.

For instance, it's also possible to transform the rotor representation refer to the stator and it can be expressed by the following matrix equation:

$$\begin{bmatrix} i_{\alpha r}^{s} \\ i_{\beta r}^{s} \end{bmatrix} = T_{\theta r} \begin{bmatrix} i_{\alpha r} \\ i_{\beta r} \end{bmatrix} \tag{3.9}$$

with

$$T_{\theta r} = \begin{bmatrix} \cos\theta_r & -\sin\theta_r \\ \sin\theta_r & \cos\theta_r \end{bmatrix} \tag{3.10}$$

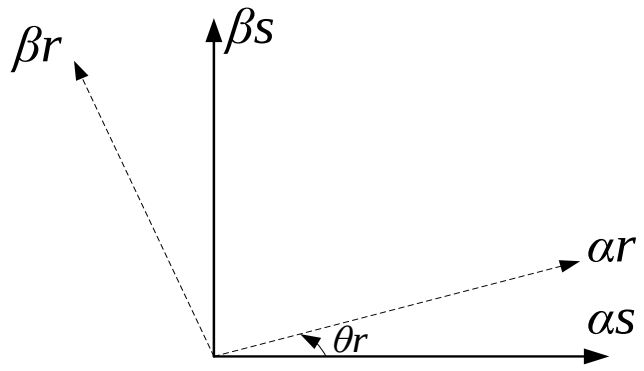

Figure 3.4. Transform representation between stator and rotor parameters.

3.2.2. The Park Transformation

The Park transform technique was first introduced by an American engineer known as R.H. Park in the late 1920s to simplify a new strategy for the analysis of a 3-phase electrical machine. This method was introduced to transform a 2-phase $\alpha\beta$ reference frame into a rotating dq reference frame (see Figure 3.5) through a rotating transform matrix $T_P(\theta)$ that can be expressed as:

$$\begin{bmatrix} i_{ds} \\ i_{qs} \end{bmatrix} = T_P(\theta) \begin{bmatrix} i_{\alpha s} \\ i_{\beta s} \end{bmatrix} \tag{3.11}$$

Where, $T_P(\theta)$ is the transform matrix and is given as:

$$T_P(\theta) = \begin{bmatrix} \cos\theta & -\sin\theta \\ \sin\theta & \cos\theta \end{bmatrix} \tag{3.12}$$

Where, θ is the angle between d and q axis.

Figure 3.6 represents the general transformation design which is transforming from 3-phase abc to 2-phase $\alpha\beta$ stationary reference frame and to rotating dq representation.

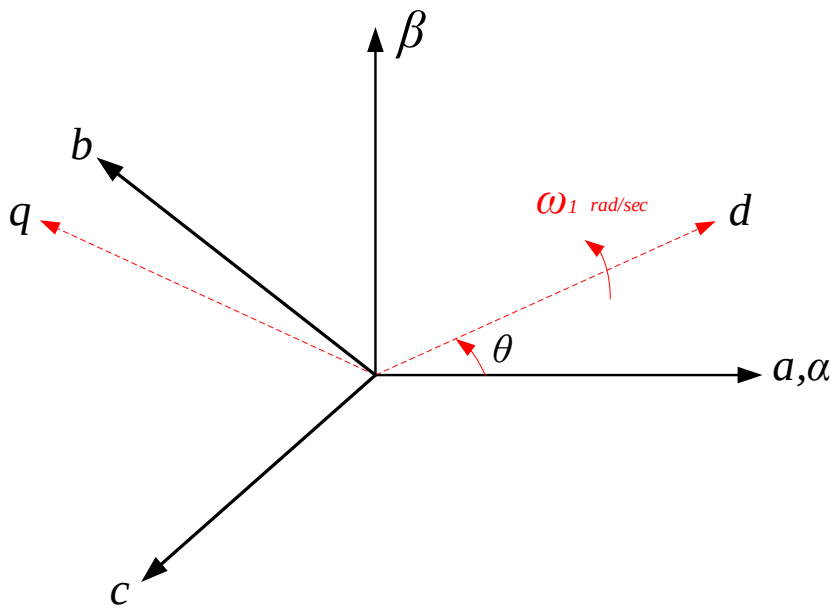

Figure 3.5. The representation of Park transforms.

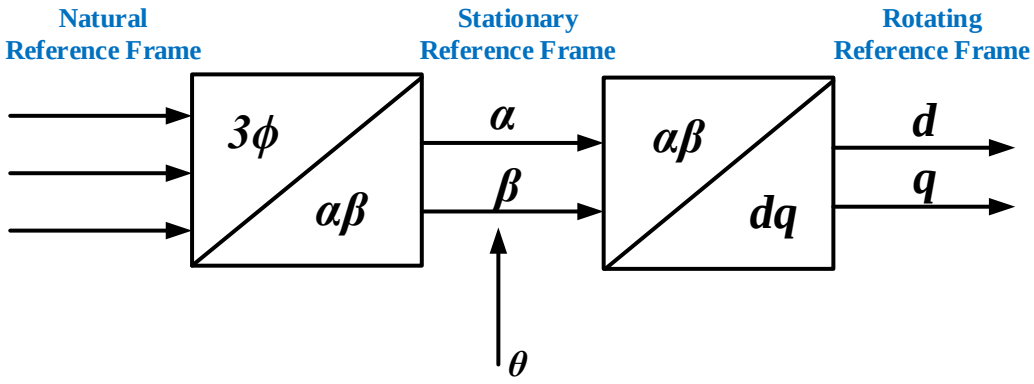

Figure 3.6. General diagram of the transformation techniques.

3.3. THE DYNAMIC MODEL OF DFIG IN DQ REPRESENTATION

For a proper understanding of the behaviors of a DFIG, it is important to use a basic and special model. In order to do that it's necessary to model a rotating 2-phase dq that is provided by Park transform technique [48]. The equivalent electrical circuit can be seen in Figure 3.7. The dynamic equation of DFIG is described as a fourth order state space based synchronous dq representation, the stator and rotor voltage equations can be expressed as follows [49]:

$$\begin{cases} v_{ds} = R_s i_{ds} + \frac{d\psi_{ds}}{dt} - \omega_s \psi_{qs} \\ v_{qs} = R_s i_{qs} + \frac{d\psi_{qs}}{dt} + \omega_s \psi_{ds} \\ v_{dr} = R_r i_{dr} + \frac{d\psi_{dr}}{dt} - \omega_r \psi_{qr} \\ v_{qr} = R_r i_{qr} + \frac{d\psi_{qr}}{dt} + \omega_r \psi_{dr} \end{cases} \quad (3.13)$$

the stator and rotor fluxes can be determined as:

$$\begin{cases} \psi_{ds} = L_s i_{ds} + L_m i_{dr} \\ \psi_{qs} = L_s i_{qs} + L_m i_{qr} \\ \psi_{dr} = L_r i_{dr} + L_m i_{ds} \\ \psi_{qr} = L_r i_{qr} + L_m i_{qs} \end{cases} \quad (3.14)$$

We can solve Equation (3.14) in terms of current as follows:

$$\begin{cases} I_{ds} = \frac{1}{\sigma L_s}\psi_{ds} - \frac{L_m}{\sigma L_s L_r}\psi_{dr} \\ I_{qs} = \frac{1}{\sigma L_s}\psi_{qs} - \frac{L_m}{\sigma L_s L_r}\psi_{qr} \\ I_{dr} = \frac{1}{\sigma L_r}\psi_{dr} - \frac{L_m}{\sigma L_s L_r}\psi_{ds} \\ I_{qr} = \frac{1}{\sigma L_r}\psi_{qr} - \frac{L_m}{\sigma L_s L_r}\psi_{qs} \end{cases} \quad (3.15)$$

Where v_{ds}, v_{qs}, ψ_{ds}, ψ_{qs}, i_{ds}, i_{qs} and ω_s are the stator side voltages, fluxes, currents and angular speed of the dq representation respectively; v_{dr}, v_{qr}, ψ_{dr}, ψ_{qr}, i_{dr}, i_{qr} and ω_r are the rotor side voltages, fluxes, currents and angular speed of the dq representation respectively; R_s and L_s are the stator side resistance and inductance; R_r and L_r are the rotor side resistance and inductance; and L_m is the magnetizing inductance and σ is the leakage coefficients formulated as; $\sigma = \frac{L_s L_r - L_m^2}{L_s L_r}$

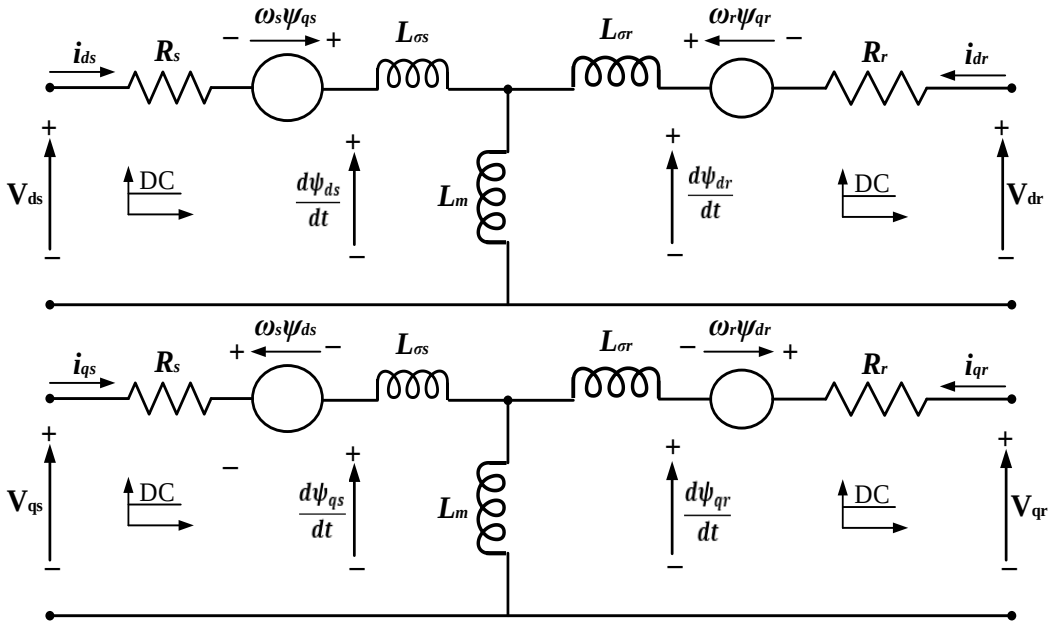

Figure 3.7. Electrical circuit for DFIG model in dq representation.

Once we get the parameters such as voltages, currents, fluxes and inductance of the stator and rotor side of the dq representation and magnetizing inductance, in order to finalize the system, it's important to adjust the active and reactive power in stator and rotor side of the machine (let's assume we neglect power loss) and it's formulated as follows:

$$\begin{cases} P_s = \frac{3}{2}(v_{ds}i_{ds} + v_{qs}i_{qs}) \\ P_r = \frac{3}{2}(v_{dr}i_{dr} + v_{qr}i_{qr}) \\ Q_s = \frac{3}{2}(v_{qs}i_{ds} - v_{ds}i_{qs}) \\ Q_r = \frac{3}{2}(v_{qr}i_{dr} - v_{dr}i_{qr}) \end{cases} \tag{3.16}$$

Electromagnetic torque can be formulated as follows:

$$T_{em} = \frac{3}{2}P\frac{L_m}{L_s}(\psi_{qs}i_{dr} - \psi_{ds}i_{qr}) \tag{3.17}$$

It's important to represent the dynamics of DFIG in state space equation to perform the simulation. The state space is commonly used during transient conditions. The basic equation used for time dependent state space is expressed as:

$$\begin{cases} \dot{X}(t) = AX(t) + BU(t) \\ Y(t) = CX(t) + DU(t) \end{cases} \tag{3.18}$$

Where A, B, C and D are state, input, output and forward matrixes respectively; X and Y are the state and output vector.

For instance, substitute Equation (3.15) into Equation (3.13) it gives (considering the flux as a state variable) as follows:

$$\begin{cases} \frac{d\psi_{ds}}{dt} = -\frac{R_s}{\sigma L_s}\psi_{ds} + \omega_s\psi_{qs} + \frac{R_sL_m}{\sigma L_sL_r}\psi_{dr} + v_{ds} \\ \frac{d\psi_{qs}}{dt} = -\omega_s\psi_{ds} - \frac{R_s}{\sigma L_s}\psi_{qs} + \frac{R_sL_m}{\sigma L_sL_r}\psi_{qr} + v_{qs} \\ \frac{d\psi_{dr}}{dt} = \frac{R_rL_m}{\sigma L_sL_r}\psi_{ds} - \frac{R_r}{\sigma L_r}\psi_{dr} + \omega_r\psi_{qr} + v_{dr} \\ \frac{d\psi_{qr}}{dt} = \frac{R_rL_m}{\sigma L_sL_r}\psi_{qs} - \omega_r\psi_{dr} - \frac{R_r}{\sigma L_r}\psi_{qr} + v_{qr} \end{cases} \tag{3.19}$$

From Equation (3.18) the state space equation can be written as:

$$\begin{bmatrix}\dot{\psi}_{ds}\\ \dot{\psi}_{qs}\\ \dot{\psi}_{dr}\\ \dot{\psi}_{qr}\end{bmatrix}=\begin{bmatrix}-\frac{R_s}{\sigma L_s} & \omega_s & \frac{R_s L_m}{\sigma L_s L_r} & 0\\ -\omega_s & -\frac{R_s}{\sigma L_s} & 0 & \frac{R_s L_m}{\sigma L_s L_r}\\ \frac{R_r L_m}{\sigma L_s L_r} & 0 & -\frac{R_r}{\sigma L_r} & \omega_r\\ 0 & \frac{R_r L_m}{\sigma L_s L_r} & -\omega_r & -\frac{R_r}{\sigma L_r}\end{bmatrix}\begin{bmatrix}\psi_{ds}\\ \psi_{qs}\\ \psi_{dr}\\ \psi_{qr}\end{bmatrix}+\begin{bmatrix}1 & 0 & 0 & 0\\ 0 & 1 & 0 & 0\\ 0 & 0 & 1 & 0\\ 0 & 0 & 0 & 1\end{bmatrix}\begin{bmatrix}v_{ds}\\ v_{qs}\\ v_{dr}\\ v_{qr}\end{bmatrix} \quad (3.20)$$

3.4. CONVERTER AND DC LINK MODEL

The power circuit of DFIG in wind turbine (shown in Figure 3.8) consists of a DFIG, a dc bus (commonly employs dc capacitor), a two back-to-back power electronic converter, each converter is connected to the rotor and grid circuit, in which both the rotor and grid side converter are connected to a controller namely RSC control and GSC control respectively. The converters are mainly voltage source converters (VSC) that allows power to flow in two directions [50].

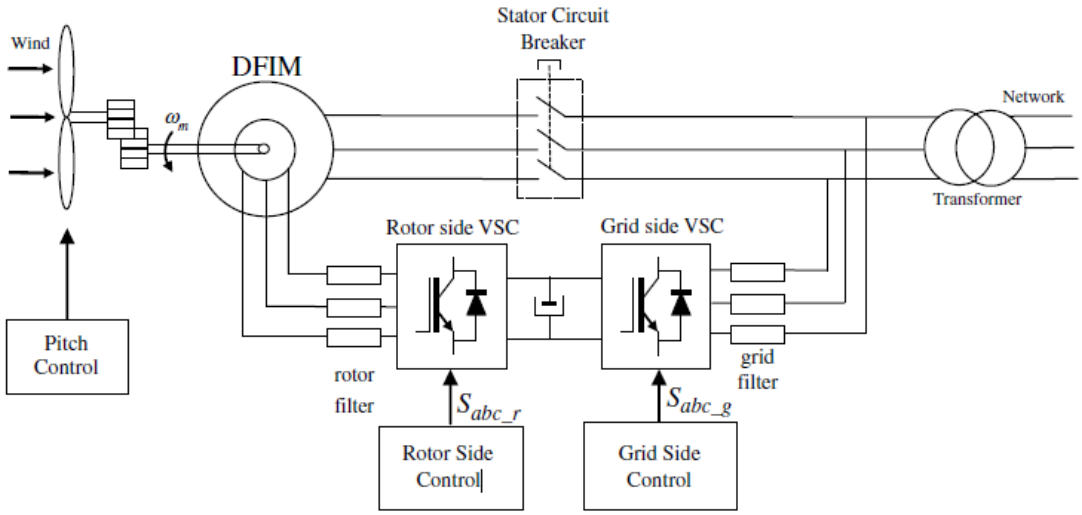

Figure 3.8. Power circuit of DFIG in wind turbine [42].

The inverter gate uses an IGBTs equipped with flyback diodes. An *LC* filters is supplied on each side of converters output in order to minimize the harmonics and insulate the components [43]. In this work, *RL* grid side filter is used. Modeling the converters is not an easy operation, and various level of details can be obtained by taking some considerations. In this thesis, it's considered a high value of switching frequency (fsw) of 4000 Hz in order to completely filter the voltage signals produced

by the converters and switching power losses are considered to be neglected. By taking into this consideration, the dynamics equation of the machine between the voltage of the grid side and the rotor side of the converter (assume current to be positive while it flows to the machine) can be formulated as:

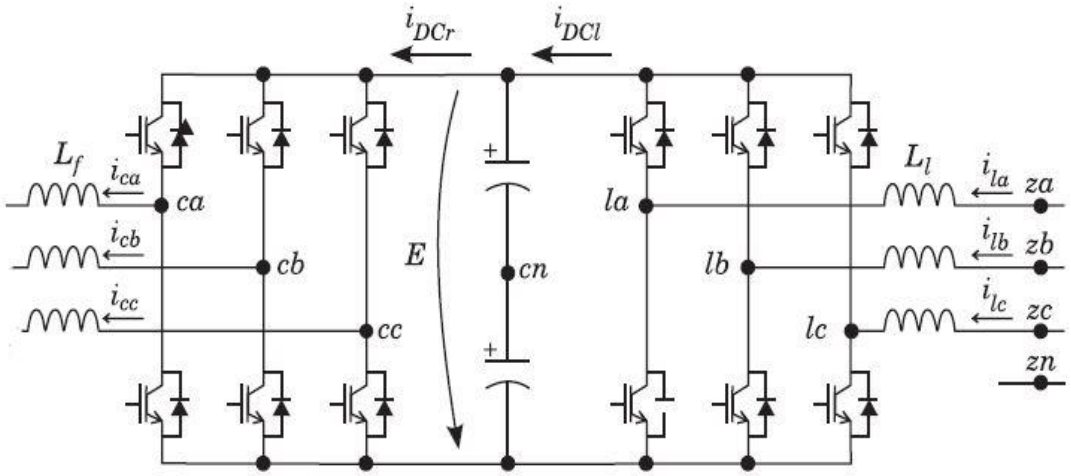

Figure 3.9. DFIG power converter circuit [43].

$$v_z^{abc} - v_l^{abc} - (v_{cn} - v_{zn})\begin{Bmatrix}1\\1\\1\end{Bmatrix} = r_l i_l^{abc} + L_l \frac{d}{dt} i_l^{abc} \tag{3.21}$$

and

$$(v_{cn} - v_{zn}) = \frac{1}{3}(v_{za} + v_{zb} + v_{zc} - v_{la} - v_{zb} - v_{zc}) \tag{3.22}$$

Where v_l^{abc} and v_z^{abc} are the rotor and grid side abc vector voltages of the converters; r_l and L_l are the resistance and inductance filters.

The DC component of the power electronics converter is commonly known as the DC link [51]. The dc link stores the energy in the capacitor and the purpose of the capacitor is to keep the voltage terminals constant. The dc link is connected between the rotor side and grid side converters [52]. The energy storage through the capacitor can be formulated as:

$$W_c = \frac{1}{2} C_{dc} v_{dc}^2 \tag{3.23}$$

Considering the converter losses to be small and negligible, the active power in the dc link can be given as [53]:

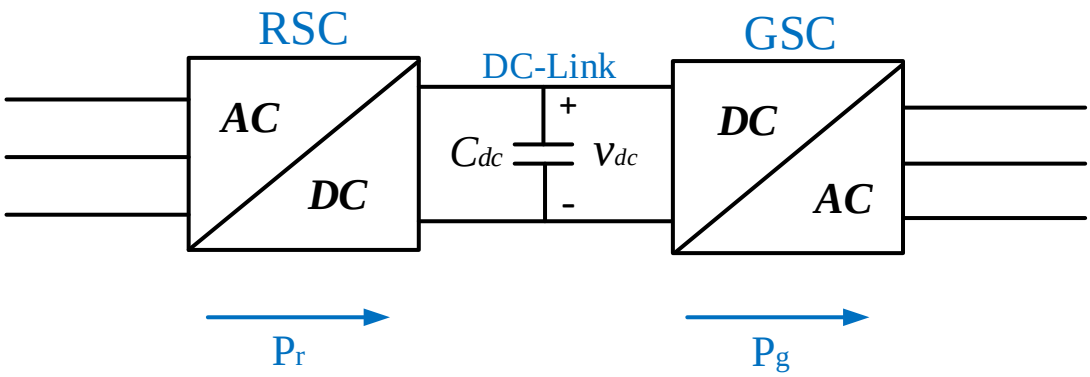

Figure 3.10. DC link model.

$$P_{dc} = \frac{dW_c}{dt} = C_{dc} \frac{dv_{dc}}{dt} = P_r - P_g \tag{3.24}$$

Where C_{dc} and v_{dc} are the capacitor and the voltage in the dc link, P_r and P_g are the rotor side and grid side active power. The currents in the dc link can be obtained by using Kirchhoff's current law (KCL).

$$i_c = i_{DCl} - i_{DCr} \tag{3.25}$$

For instance, the dc bus voltage can be expressed as:

$$v = v_0 + \frac{1}{C} \int_0^t (i_{DCl} - i_{DCr})\, dt \tag{3.26}$$

Where i_{DCr} and i_{DCl} are the DC current in the rotor side and grid side converter respectively.

PART 4

CONTROL DESIGN OF DFIG BASED WIND TURBINE

There are different strategies for controlling the DFIG. In this thesis vector control (VC) which is also called field oriented control (FOC) of electrical machines has been implemented. VC employs in both the rotor side and grid side converter. Using this control strategy it is possible to decouple and construct the control of d component and q component separately. Which minimizes the control design complication and accomplishes various control goals. The main purpose of the RSC is to control the active and reactive power. That allows the turbine to capture the maximum power from the wind, while also providing reactive power supports to the grid. Correspondingly, GSC aims to keep the DC bus voltage constant. In this section, the control of RSC is presented. In RSC control, we have the current loops of the DFIG and the mechanical speed (rotor speed controller). Direct current (i_{dr}) is proportional and controls the reactive power, whereas, the quadrature currents are proportional to the toque or stator active power. This section also presents the GSC control, this control includes the bus voltage references and controls the grid reactive power reference ($Q_{g\_}ref$). It also includes the derivation of the transfer function of a closed-loop second order system for the rotor side and grid side of a DFIG. Moreover, an angle calculator also called phase-locked loop (PLL) is designed in both RSC and GSC control, in order to achieve a three-phase stator voltage grid synchronization, that offers the reliability to estimate and reject smaller harmonics. Furthermore, PI controller and the MPPT approach using indirect speed controller has been applied in order for the mechanical torque (T_t) to follow the maximum power curve in response to the wind speed variations.

4.1. RSC CONTROL

One of the main objectives of RSC control is the mechanical speed to obtain the maximum power available from the wind and vary according to the MPPT of the wind [54]. Figure 4.2 shows the control design of RSC (of current control loops). The control of RSC contains two control loops: internal and external current control loops. The internal current loop controls direct current (i_{dr}) and quadrature current (i_{qr}) and the external current loop controls the speed of the machine (ω_m) and reactive stator power (Q_s). The q rotor current is in proportion to the electromagnetic torque (T_{em}), which makes i_{qr} to control the electromagnetic torque as well as the mechanical speed (ω_m) if requires. Correspondingly, direct rotor current (i_{dr}) is responsible of stator reactive power (Q_s).

As it can be seen from Figure 4.2 that the difference of the stator reactive power and its reference as well as the difference of the machine speed and its references are both fed to the regulators and gives an output of direct (i_{dr} & i_{dr}^*) and quadrature (i_{qr} & i_{qr}^*) rotor currents, respectively. The values of i_{qr}^* and i_{qr} is subtracted and fed to the regulator and, similarly, the values of i_{dr}^* and i_{dr} is subtracted and fed to the regulator. The vector control of a DFIG can be carried out in a synchronous rotating dq reference frame [56], where for instance, the d-axis is lined up with the stator flux (ψ_s) as shown in Figure 4.1.

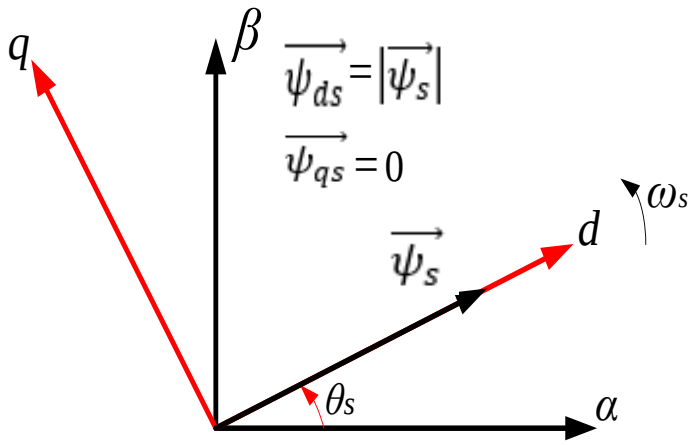

Figure 4.1. Phasor diagram of a synchronous rotating dq reference frame.

For instance, from section (3.3), DFIG model in synchronous dq representation, if we substitute Equation (3.14) into the rotor voltages of Equation (3.13), we get the rotor voltages (consider $\psi_{qs} = 0$):

$$\begin{cases} v_{dr} = R_r i_{dr} + \sigma L_r \frac{di_{dr}}{dt} - \omega_r \sigma L_r i_{qr} + \frac{L_m}{L_s} \frac{d}{dt} \left|\overrightarrow{\psi_s}\right| \\ v_{qr} = R_r i_{qr} + \sigma L_r \frac{di_{qr}}{dt} + \omega_r \sigma L_r i_{dr} + \omega_r \frac{L_m}{L_s} \left|\overrightarrow{\psi_s}\right| \end{cases} \quad (4.1)$$

In DFIG the stator side is directly linked to the grid at a constant AC voltage, so the ψ_s is constant; therefore, the derivatives of $\frac{d}{dt}\left|\overrightarrow{\psi_s}\right| = 0$. Equation (4.1) demonstrates that the direct and quadrature current controls can be achieved by using a PI controller for each component, as shown in Figure 4.2. At the output of the current control, cross terms of functions can be added in order to support the PI controllers.

After implementing the current control loops and flux angle calculations, the overall control design can be presented. As it can be seen in Figure 4.1, the d-axis reference is lined up with a stator flux ($\overrightarrow{\psi_s}$), the torque equation in dq representation is expressed as follows:

$$T_{em} = \frac{3}{2} p \frac{L_m}{L_s} (\psi_{qs} i_{dr} - \psi_{ds} i_{qr}) \Rightarrow T_{em} = -\frac{3}{2} p \frac{L_m}{L_s} \left|\overrightarrow{\psi_s}\right| i_{qr} \Rightarrow T_{em} = K_T i_{qr} \quad (4.2)$$

Equation (4.2) shows that the quadrature rotor current i_{qr} is directly proportional to the electromagnetic torque (T_{em}), that is, i_{qr} controls T_{em}. Similarly, it is possible to derive stator reactive power (Q_s) equation in the dq frame, which indicates that the direct rotor current (i_{dr}) is responsible for Q_s.

$$Q_s = \frac{3}{2} (v_{qs} i_{ds} - v_{ds} i_{qs}) = -\frac{3}{2} \omega_s \frac{L_m}{L_s} \left|\overrightarrow{\psi_s}\right| \left(i_{dr} - \frac{\left|\overrightarrow{\psi_s}\right|}{L_m} \right) \Rightarrow Q_s = K_Q \left(i_{dr} - \frac{\left|\overrightarrow{\psi_s}\right|}{L_m} \right) \quad (4.3)$$

Hence, because of the orientation we chose, we can see that both current (i_{qr}, i_{qr}^*) and (i_{dr}, i_{dr}^*) allow us to control the torque and active/reactive power independently. Based on the above expressions, Figure 4.2 shows the control design of RSC.

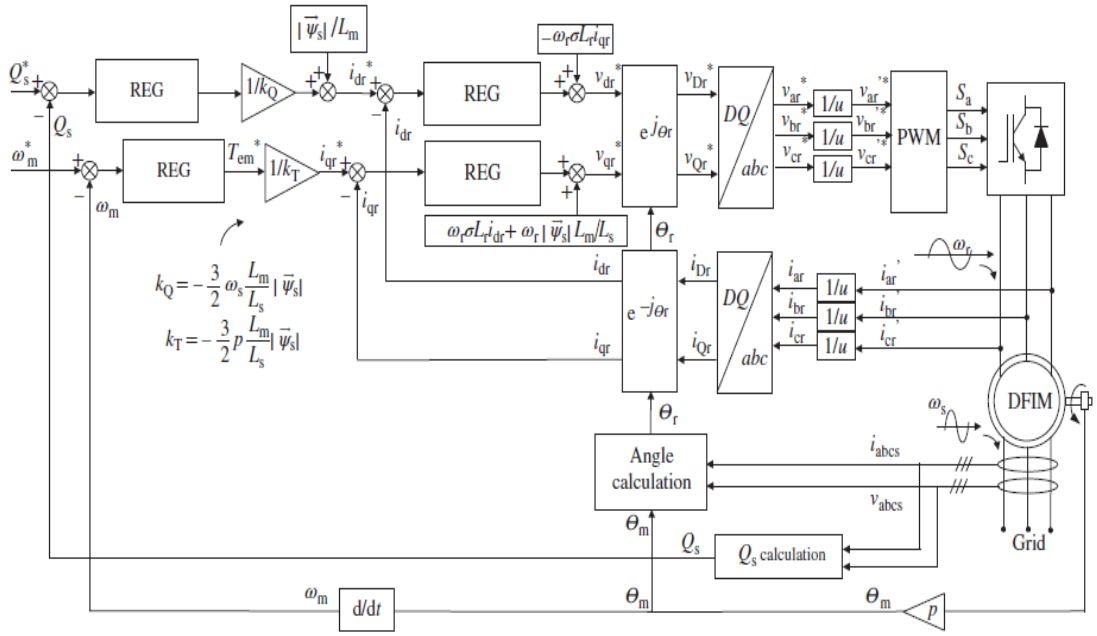

Figure 4.2. Control design of the RSC [55].

4.1.1. Transfer Function for the RSC

Figure 4.3 shows the equivalent block diagram of a second order closed loop system for i_{dr}, i_{qr} and their references, where both current loops are equals, having two poles and a zero with a PI controller.

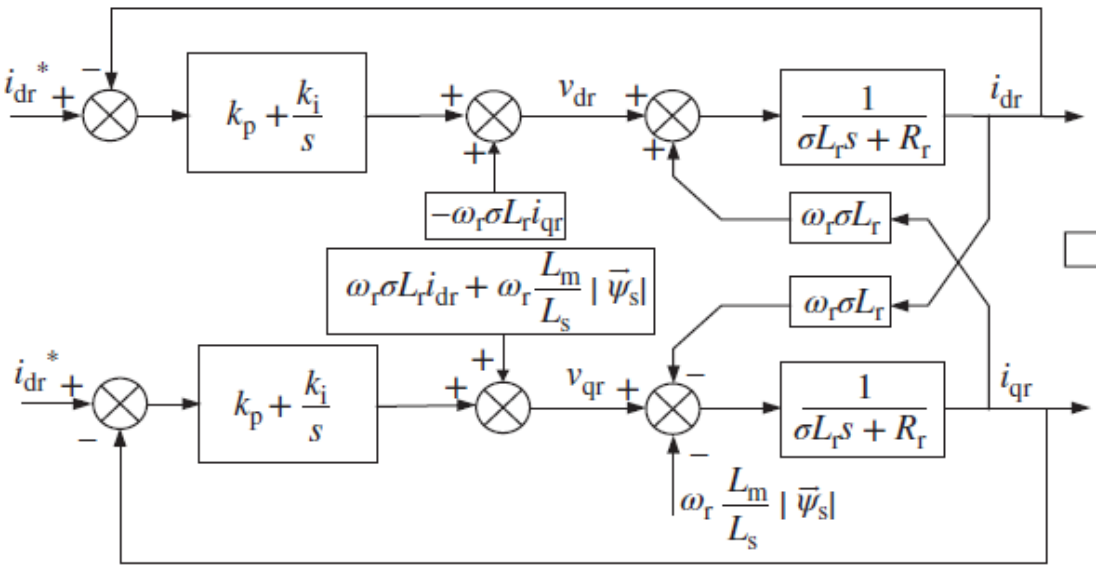

Figure 4.3. Equivalent second order system of a closed loop current control with regulator [55].

The transfer function for both current control loops can be expressed as follows:

$$TF = \frac{i_{dr}(s)}{i^*_{dr}(s)} = \frac{i_{qr}(s)}{i^*_{qr}(s)} = \frac{sk_p+k_i}{\sigma L_r s^2+(k_p+R_r)s+k_i} = \frac{sk_p+k_i}{L_f s^2+(k_p+R_f)s+k_i} \quad (4.4)$$

This can be equivalent to:

$$TF = \frac{i_{dr}(s)}{i^*_{dr}(s)} = \frac{i_{qr}(s)}{i^*_{qr}(s)} = \frac{i(s)}{i^*(s)} = \frac{(sk_p+k_i)/L}{s^2+\frac{(k_p+R)}{L}s+\frac{k_i}{L}} \Rightarrow \frac{(sk_p+k_i)/L}{s^2+2\xi\omega_n s+\omega_n^2} = \frac{(sk_p+k_i)/L}{(s+\omega_n)^2} \quad (4.5)$$

Where:

$$k_p = 2\omega_n L - R \; and \;\; k_i = \omega_n^2 L \quad (4.6)$$

So here in Equation (4.5), we can put as a general inductance and general resistance, and it can be applied to many machines. Furthermore, the proportional and integral gains can be obtained by Equation (4.6) and we can choose ω_n, which are the poles of the Closed loop transfer functions according to the dynamic performance we want to achieve. Figure 4.4 represents the bode plot diagram of dq closed loop transfer function for the RSC.

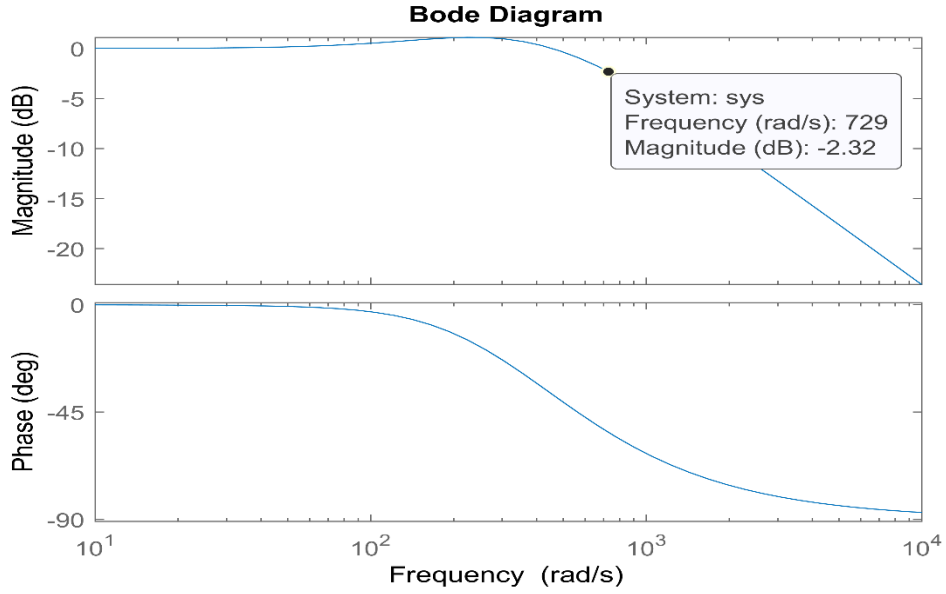

Figure 4.4. Bode plot diagram of the closed loop for RSC.

4.2. GSC CONTROL

It is very important to control some components in the GSC. Because it is impossible to make it operate effectively without controlling certain magnitudes in the grid side system. one of the purposes of the GSC control is to maintain the DC bus voltage constant, irrespective of the region of operation. It also operates at a unit power factor. In this section, vector control strategy in the GSC is presented. Figure 4.5 describes the power flow design from the GSC to the grid.

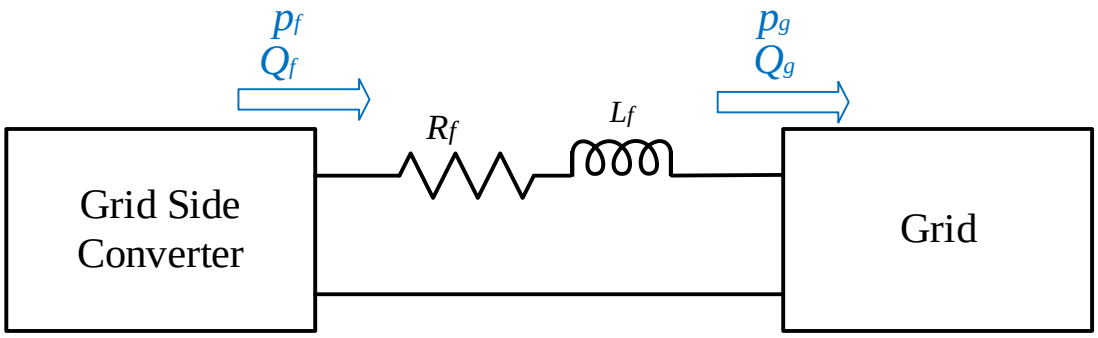

Figure 4.5. Power flow design.

The GSC is responsible for controlling parts of the power flow of the DFIG. The power produced by the three-blade wind turbine is partially supplied through the rotor of the DFIG. For instance, the power flow that passes through the rotor also passes through the dc-link and then sent to the grid by the GSC. Figure 4.6 represents grid voltage alignment with the d-axis. The GSC is connected to the grid through an RL filter. Modifying the grid voltages to be lined up with the d component (v_{qg}), the filter voltages of the dq references can be described as:

$$\begin{cases} v_{df} = R_f i_{dg} + L_f \frac{di_{dg}}{dt} + v_{dg} - \omega_s L_f i_{qg} \\ v_{qf} = R_f i_{qg} + L_f \frac{di_{qg}}{dt} + \omega_s L_f i_{dg} \end{cases} \tag{4.7}$$

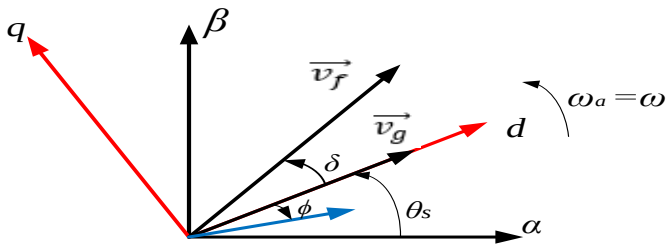

Figure 4.6. Grid voltage alignment with the d-axis.

Voltage oriented vector filters for the LCL filter can be given as:

$$\begin{cases} v_{df} = R_f i_{df} + L_f \frac{di_{df}}{dt} + R_g i_{dg} + L_g \frac{di_{dg}}{dt} + v_{dg} - \omega L_f i_{qf} - \omega L_g i_{qg} \\ v_{qf} = R_f i_{qf} + L_f \frac{di_{qf}}{dt} + R_g i_{dg} + L_g \frac{di_{qg}}{dt} + \omega L_f i_{df} + \omega L_g i_{dg} \end{cases} \quad (4.8)$$

So, the filters active and reactive power can be given as follows:

$$\begin{cases} P_g = \frac{3}{2}(v_{dg} i_{dg} + v_{qg} i_{qg}) \\ Q_g = \frac{3}{2}(v_{qg} i_{dg} - v_{dg} i_{qg}) \end{cases} \quad (4.9)$$

Moreover, the topology used for controlling the GSC is a two-level voltage source converter (2L-VSC). The pulses for the controlled switches (S_{a_g}, S_{b_g}, S_{c_g}) of the 2L-VSC are, for instance, the output voltages of the converter, are generated in order to control the DC bus voltage (V_{bus}) and the grid reactive power (Q_g). In this section grid voltage-oriented vector control (GVOVC) approach has been presented.

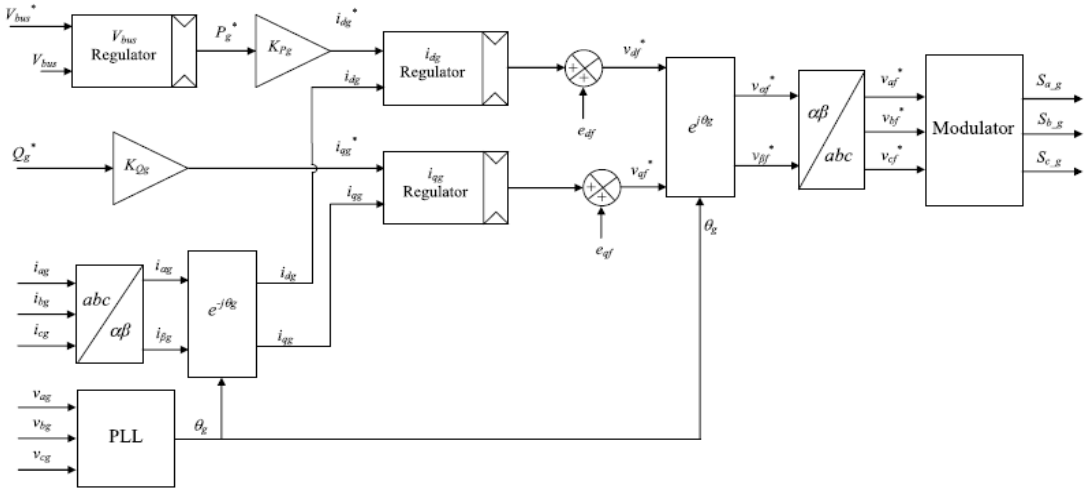

Figure 4.7. Control block design of the GSC [42].

For instance, the control block design of the GSC can be seen in Figure 4.7. From the references (V_{bus}, Q_g^*), it creates pulses for the controlled switches S_{a_g}, S_{b_g}, S_{c_g}. Therefore, the modulator produces the pulses from the abc voltage references for the GSC: v_{af}^*, v_{bf}^*, v_{cf}^*. Thus, these abc voltage references are first produced in dq axis (v_{df}^*, v_{qf}^*), then converted to $\alpha\beta$ axis ($v_{\alpha f}^*$, $v_{\beta f}^*$), and eventually generates abc voltage

references. Then the dq voltage references (v_{df}^*, v_{qf}^*) are separately produced by the dq current (i_{dg}^*, i_{qg}^*) references. This indicates that by changing v_{df}; i_{dg} is mainly changed. Moreover, there is also cancellation of coupling terms at the output of the current PI regulators, for a good dynamic performance and it can be given as:

$$\begin{cases} e_{df} = -\omega_s L_f i_{qg} \\ e_{qf} = \omega_s L_f i_{dg} \end{cases} \tag{4.10}$$

As shown in Figure 4.7, the direct grid current references (i_{dg}^*) is proportional and controls the grid active power (P_g^*) and the quadrature grid current (i_{qg}^*) implies and controls grid reactive power (Q_g^*). Note that, under ideal conditions, the term v_{dg} is equal to the amplitude of the grid voltage and is constant. Thus, the constant terms required can be deduced from Equation (4.8) and is given by:

$$\begin{cases} k_{Pg} = \frac{1}{\frac{3}{2}v_{dg}} \\ k_{Pg} = \frac{1}{-\frac{3}{2}v_{dg}} \end{cases} \tag{4.11}$$

4.2.1. Transfer Function for the GSC

Figure 4.8 demonstrates the current loops of the L filter. From the voltage Equation (4.7), the L filters at an open loop can be represented as:

$$\begin{cases} v_{df} = R_f i_{dg} + L_f \frac{di_{dg}}{dt} \\ v_{qf} = R_f i_{qg} + L_f \frac{di_{qg}}{dt} \end{cases} \tag{4.12}$$

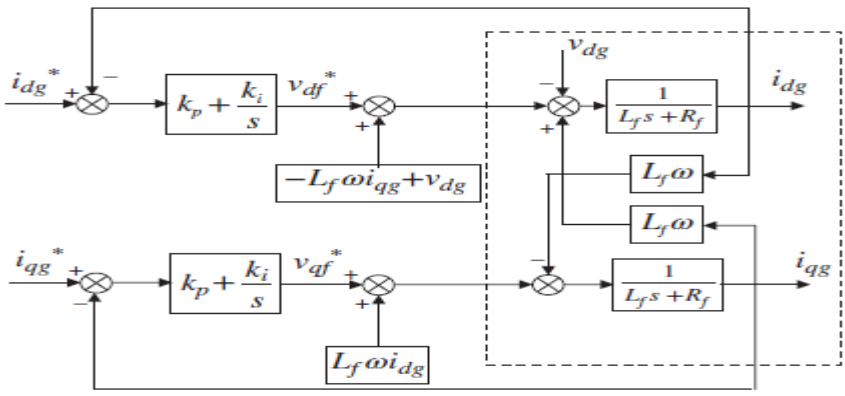

Figure 4.8. Current loops for the L filter [42].

By using Laplace transform the following transfer function is obtained:

$$\frac{i_{dg}(s)}{v_{df}(s)} = \frac{1}{L_f s + R_f} \tag{4.13}$$

and

$$\frac{i_{qg}(s)}{v_{qf}(s)} = \frac{1}{L_f s + R_f} \tag{4.14}$$

As a result, the control block design can be used to express this fact, as shown in Figure 4.8 using this method, we take into consideration an ideal PI regulator. As a result, transfer function of the current closed loop can be given as:

$$\frac{i_{ds}(s)}{i_{ds}^{*}(s)} = \frac{sk_p + k_i}{s^2(L_f) + s(R_f + k_p) + k_i} \tag{4.15}$$

and

$$\frac{i_{qs}(s)}{i_{qs}^{*}(s)} = \frac{sk_p + k_i}{s^2(L_f) + s(R_f + k_p) + k_i} \tag{4.16}$$

Now, if we equate the denominator of Equation (4.15) or (4.16) to the denominator of standard second order transfer function, we get:

$$s^2(L_f) + s(R_f + k_p) + k_i = s^2 + 2\xi\omega_n s + \omega_n^2 \tag{4.17}$$

Thus, the integral (k_i) and proportional (k_p) constant values are:

$$\begin{cases} k_i = L_f \omega_n^2 \\ k_p = L_f 2\xi\omega_n - R_f \end{cases} \tag{4.18}$$

As we explained in previous section, we can choose ω_n and ξ according to the dynamic performance we want to achieve (Mitsubishi MWT 92 manuals).

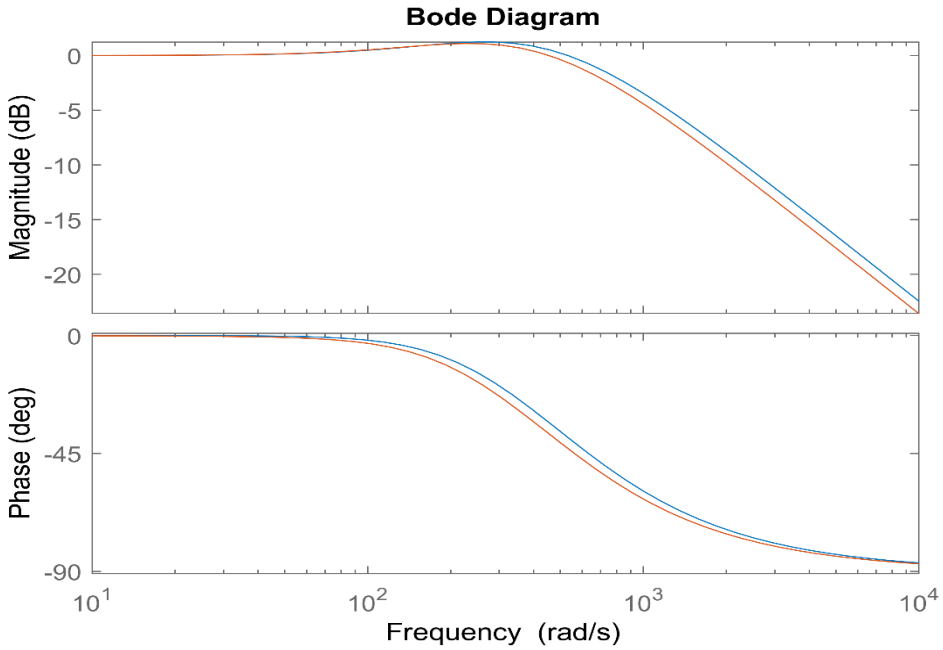

Figure 4.9. Bode plot diagram of both RSC and GSC.

In Figure 4.9, the blue one indicates the GSC current loops and the red one shows RSC current loops, we have current loops of both GSC and RSC with a band width very similar. Figure 4.10 illustrates the step response for the grid side and in 15 milliseconds it reaches the steady state.

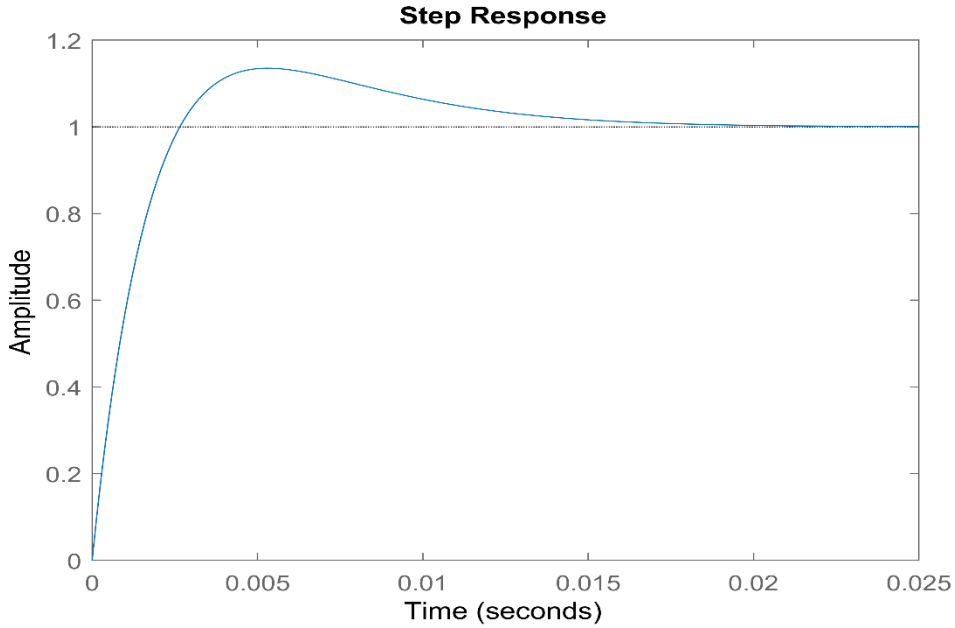

Figure 4.10. Step response of the GSC.

4.3. PHASE LOCKED LOOP

An angle calculator called PLL is designed in both the RSC control and GSC control, for voltage and current coordinate transformations. Beacause of it's closed loop nature, it assures the stability and rejection of perturbations to the angle estimation. Figure 4.11 shows the PLL block design at the grid, that takes an input of grid abc voltages from the measured DFIG and then transforms to dq reference frame. Then the PLL aligns the quadrature grid voltage (v_{qg}) by comparing direct grid voltage (v_{qg}) with zero reference voltage. The error signal passes through the PI regulator that provides the angular frequency (ω_s) of the grid voltages. The conversion method and the PLL MATLAB/Simulink design is shown in Appendix B.

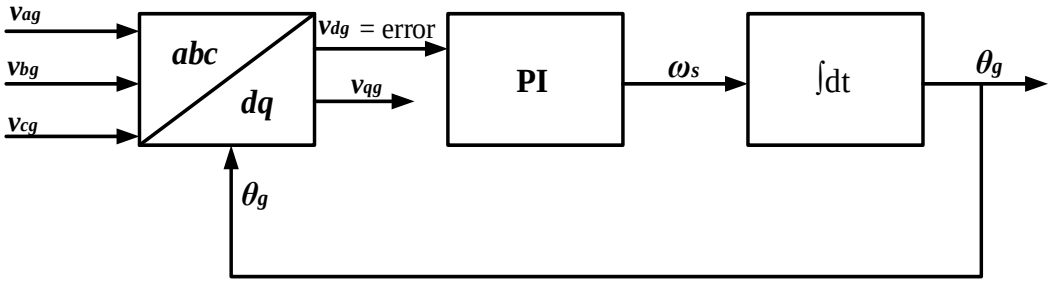

Figure 4.11. Classical PLL block design.

Finally, the control strategy (GVOVC) that has been presented is able to control the DC bus voltage (V_{bus}) and grid reactive power (Q_g) as specified, it also provides good performance in the dynamic response because of the vector control structure. The Simulations results in detail is presented in Part 7.

4.4. CONTROL STRATEGY

This section presents the control strategy we applied in this work. This includes typical PI control and MPPT by indirect speed control strategy.

4.4.1. Proportional and Integral Control

The PI controllers are some kinds of regulators that combines proportional and integral operation in one unit [57]. It is important to create a PI regulator, in order to assure

that the rotor speed, generated torque, the direct (i_{dr}) and quadrature (i_{qr}) rotor currents follow their references. Figure 4.12 illustrates the PI controller of rotor speed and its reference.

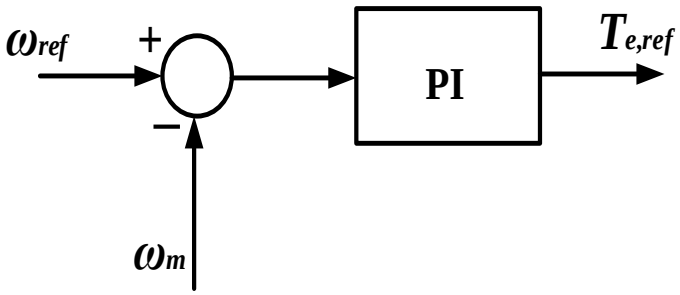

Figure 4.12. PI with rotor speed.

$$G(s) = \frac{p}{Js} \tag{4.19}$$

and

$$R(s) = k_p + k_i/s \tag{4.20}$$

Transfer function for closed loop can be expressed as:

$$H(s) = \frac{R(s)G(s)}{1+R(s)G(s)} \tag{4.21}$$

Which gives:

$$H(s) = \frac{k_p s+k_i}{j/ps^2+k_p s+k_i} \tag{4.22}$$

Second order transfer function is represented as:

$$(s) = \frac{\omega_c^2}{s^2+2\xi\omega_c s+\omega_c^2} \tag{4.23}$$

If we equate the denominator of Equation (4.22) with (4.23) it gives:

$$\begin{cases} k_p = \frac{2J}{p}\xi\omega_n \\ k_i = \frac{\omega_n^2 J}{p} \end{cases} \tag{4.24}$$

Here we can have the PI controller for direct current of the RSC.

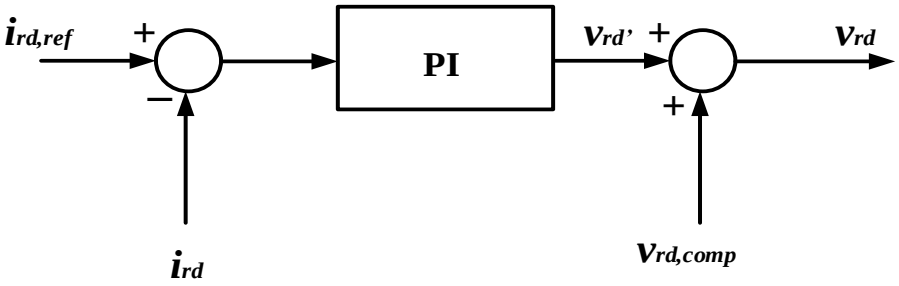

Figure 4.13. PI with direct rotor current and voltage.

Since the GSC controls the dc bus voltage, we can have the PI controller for V_{bus} and i_{dg} component.

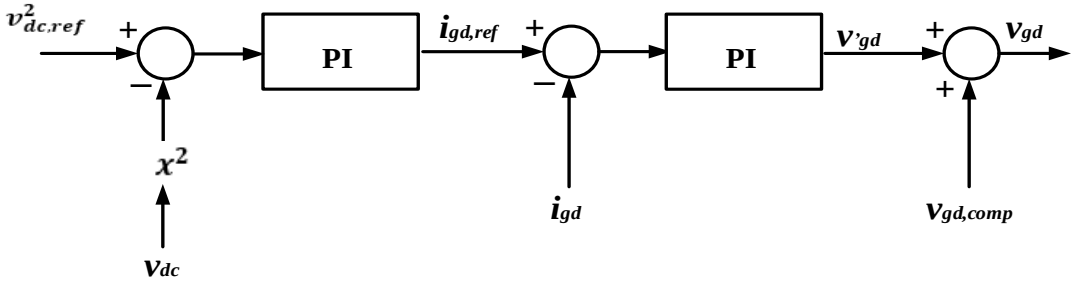

Figure 4.14. PI in the GSC.

Typical wind turbine has a nominal power between 1.5 and 3 MW. One of the most significant models presented in this thesis is Mitsubishi MWT 92. Mitsubishi started with variable speed wind turbine (VSWT) DFIG based technology with models: MWT 92 rated at 2300 kW, MWT 95, 100 and 102 rated at 2400 kW and MWT 92 rated at 2.4 MW.

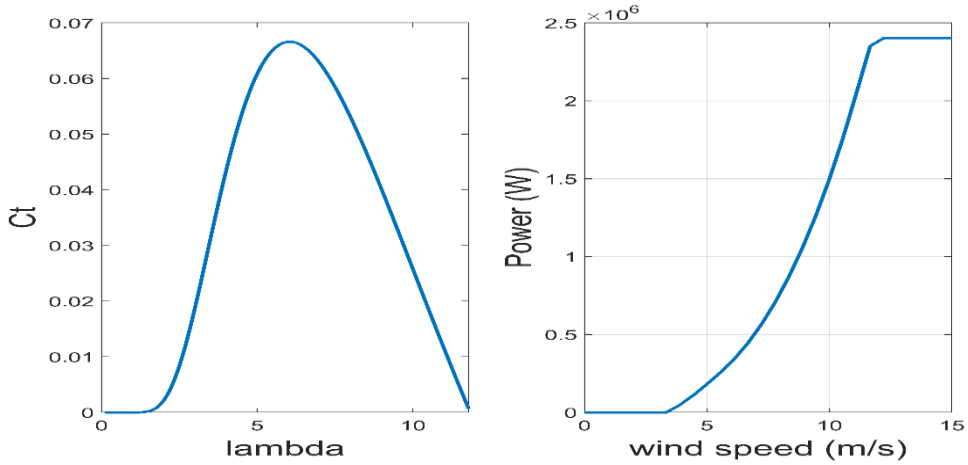

Figure 4.15. Torque coefficient versus lambda and power curve.

The proposed output power curve shown in Figure 4.15 has been confirmed by comparing with the output of the generated power with different wind speed. Table shows the values of different wind speed and the generated output power.

Table 4.1. The values of wind speed and the generated power.

Wind speed	**Power**
7.50 m/s	0.6342 MW
9.50 m/s	1.2840 MW
11.8 m/s	2.3635 MW

For instance, from Equation (4.6), we can obtain the values of proportional (k_p) and integral (k_i) gains for the rotor side and can be given as (note: k_i has the same value in both d and q current components and k_p also has the same values for both d and q components):

$$\begin{cases} k_p = 0.5771 \\ k_i = 491.5995 \end{cases}$$

Moreover, when we consider PI controller as a control strategy, from Equation (4.24) the value of k_p and k_i will be:

$$\begin{cases} k_p = 5080 \\ k_i = 203200 \end{cases}$$

The same is applied to the grid side. The values of the PI controller coefficients for the grid side are:

$$\begin{cases} k_p = 0.3016 \\ k_i = 56.8489 \end{cases}$$

The value of gains, considering PI controller as a control strategy (having an input of bus voltage and its reference) has been chosen until the desired value is obtained:

$$\begin{cases} k_p = -1000 \\ k_i = -300000 \end{cases}$$

4.4.2. Indirect Speed Control

Different strategies have been presented in the literature to control the wind turbine under partial load while tracking the maximum power extraction. At this point, there are two types of speed control: Direct and Indirect speed control. In this thesis, we consider MPPT by indirect speed control. This approach is important because it ensures a variable speed operating system, to optimizes the power output across a given wind speed. The power generated by the three blades becomes maximum if we consider maximizing the power coefficient (C_p).

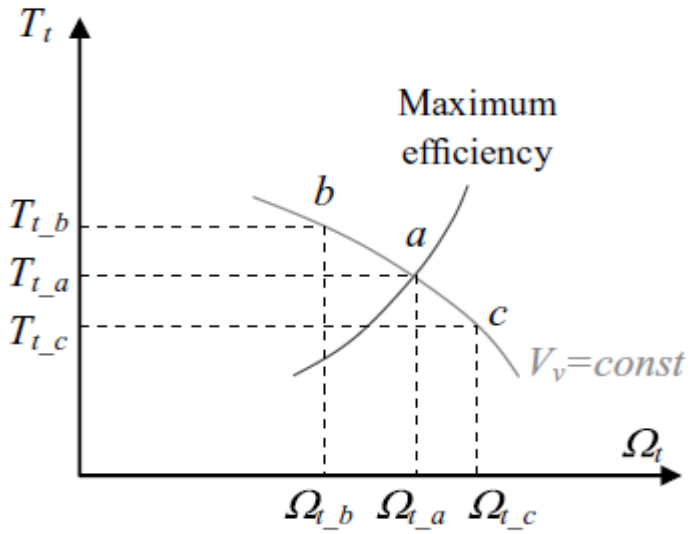

Figure 4.16. MPPT stability curve [42].

As a result, we need to maximize lambda (λ) such that the blades capture maximum amount of wind energy. Assume the variable speed turbine is functioning at 'a' level of the curve that can be seen in Figure 4.16 with speed of the wind and rotor torque constant. When the rotor speed is lowered to Ω_{t-b}, the operational level shifts to level 'b' and torque becomes T_{t-b}. Mechanical torque is held at the previous level relating to T_{t-a}, thus T_{t-b} is greater than electromagnetic torque T_{em} and rotor speed rises till it stabilizes near Ω_{t-a} level once again. Thus, the reference of rotor speed at optimum lambda can be given as:

$$\omega_{ref}(u) = \frac{\lambda_{opt} v}{R} \tag{4.25}$$

Figure 4.17 shows the scheme of MPPT by indirect speed control strategy.

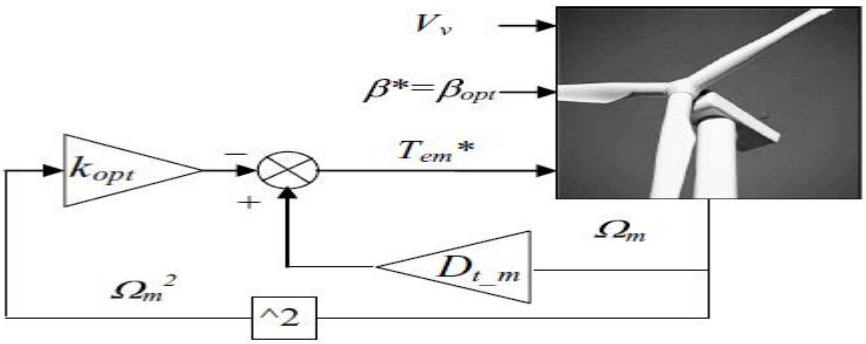

Figure 4.17. Indirect speed control strategy [42].

The electromagnetic torque (T_{em}) generated can be expressed as:

$$T = \frac{1}{2}\rho\pi R^3 \frac{R^2\Omega^2}{(\lambda_{opt})^2}\frac{(C_p)max}{\lambda_{opt}} \tag{4.26}$$

Equation (4.26) can be simplified as

$$T = -k_{opt}\Omega^2 \tag{4.27}$$

Equation (4.27) leads to the control strategy shown in Figure 4.17.

4.5. STEADY-STATE ANALYSIS OF THE DFIG

It is very important to study the operation of the steady-state analysis of DFIG, in order to know the stable operating point of the system. This study can be important for determining the appropriate magnetizing method in terms of efficiency and estimating the necessary rotor currents at a specific operating point for dimensioning the power electronic converter. Thus, to analyze the steady-state, the following equations in Table 4.2 and Table 4.3 are applied.

4.5.1. Case 1: When Reactive Stator Power is Zero

Reactive stator power (Q_s) is set to zero and all the magnitudes of the DFIG at steady-state is analyzed by using steady-state equations shown in Table 4.2.

Table 4.2. Steady-state magnitudes of the DFIG for Qs=0 [55].

Stator fluxes	$\lvert\vec{\psi}_s\rvert = \sqrt{\frac{-B \pm \sqrt{B^2 - 4AC}}{2A}}$	$C = \left[\frac{2}{3}\frac{R_s}{L_m}\right]^2 \left(\frac{T_{em}}{p}\right)^2$	$B = \frac{4}{3}R_s T_{em}\omega_s - \lvert\vec{v}_s\rvert^2$	$A = \omega_s^2$
Rotor fluxes	$\psi_{dr} = L_m i_{ds} + L_r i_{}$	$\psi_{qr} = L_m i_{qs} + L_r i_{qr}$	$\lvert\vec{\psi}_r\rvert^2 = \psi_{dr}^2 + \psi_{qr}^2$	$\theta_{\psi_r} = a\tan\left(\frac{\psi_{qr}}{\psi_{dr}}\right)$
Stator currents	$i_{ds} = 0$	$i_{qs} = \frac{T_{em}}{\frac{3}{2}p\lvert\vec{\psi}_s\rvert}$	$\lvert\vec{i}_s\rvert^2 = i_{ds}^2 + i_{qs}^2$	$\theta_{i_s} = a\tan\left(\frac{i_{qs}}{i_{ds}}\right)$
Rotor currents	$i_{dr} = \frac{\lvert\vec{\psi}_s\rvert - L_s i_{ds}}{L_m}$	$i_{qr} = -\frac{L_s}{L_m} i_{qs}$	$\lvert\vec{i}_r\rvert^2 = i_{dr}^2 + i_{qr}^2$	$\theta_{i_s} = a\tan\left(\frac{i_{qs}}{i_{ds}}\right)$
Stator voltages	$v_{ds} = R_s i_{ds}$	$v_{qs} = R_s i_{qs} + \omega_s\lvert\vec{\psi}_s\rvert$	$\lvert\vec{v}_s\rvert^2 = v_{ds}^2 + v_{qs}^2$	$\theta_{v_s} = a\tan\left(\frac{v_{qs}}{v_{ds}}\right)$
Rotor voltages	$v_{dr} = R_r i_{dr} - \omega_r\sigma L_r i_{qr}$	$v_{qr} = R_r i_{qr} + \omega_r\sigma L_r i_{dr} + \omega_r\frac{L_m}{L_s}\lvert\vec{\psi}_s\rvert$	$\lvert\vec{v}_r\rvert^2 = v_{dr}^2 + v_{qr}^2$	$\theta_{v_r} = a\tan\left(\frac{v_{qr}}{v_{dr}}\right)$
Slip	$\omega_r = \omega_s - \omega_m$		$s = \omega_r/\omega_s$	
Active powers	$P_m = T_{em}\frac{\omega_m}{p}$	$P_s = \frac{3}{2}(v_{ds}i_{ds} + v_{qs}i_{qs})$	$P_r = \frac{3}{2}(v_{dr}i_{dr} + v_{qr}i_{qr})$	
Reactive powers	$Q_s = 0$	$PF_s = \cos a$	$Q_r = \frac{3}{2}(v_{qr}i_{dr} - v_{dr}i_{qr})$	$PF_r = \cos(a\tan(Q_r/P_r))$
Efficiency	$\eta = \frac{P_m}{P_s + P_r}$ if $P_m >$		$\eta = \frac{P_s + P_r}{P_m}$ if $P_m < 0$	

4.5.2. Case 2: When Direct Rotor Current is Zero

Here, the quadrature rotor current is set to zero and all the magnitudes of the DFIG at steady-state is analyzed by using steady-state equations shown in Table 4.3.

Table 4.3. Steady-state magnitudes of the DFIG for idr=0 [55].

Stator fluxes	$\lvert\vec{\psi}_s\rvert = \sqrt{\frac{-B \pm \sqrt{B^2 - 4AC}}{2A}}$	$C = \left[\frac{2}{3}\frac{R_s}{L_m}\right]^2 \left(\frac{T_{em}}{p}\right)^2$	$B = \frac{4}{3}R_s T_{em}\omega_s - \lvert\vec{v}_s\rvert^2$	$A = \left(\frac{R_s}{L_s}\right)^2 + \omega_s^2$
Rotor fluxes	$\psi_{dr} = L_m i_{ds} + L_r i_{dr}$	$\psi_{qr} = L_m i_{qs} + L_r i_{qr}$	$\lvert\vec{\psi}_r\rvert^2 = \psi_{dr}^2 + \psi_{qr}^2$	$\theta_{\psi_r} = a\tan\left(\frac{\psi_{qr}}{\psi_{dr}}\right)$
Stator currents	$i_{ds} = \frac{\lvert\vec{\psi_s}\rvert}{L_s}$	$i_{qs} = -\frac{L_m}{L_s} i_{qr}$	$\lvert\vec{i}_s\rvert^2 = i_{ds}^2 + i_{qs}^2$	$\theta_{i_s} = a\tan\left(\frac{i_{qs}}{i_{ds}}\right)$
Rotor currents	$i_{dr} = 0$	$i_{qr} = \frac{T_{em}}{-\frac{3}{2}p\frac{L_m}{L_s}\lvert\vec{\psi}_s\rvert}$	$\lvert\vec{i}_r\rvert^2 = i_{dr}^2 + i_{qr}^2$	$\theta_{i_s} = a\tan\left(\frac{i_{qs}}{i_{ds}}\right)$
Stator voltages	$v_{ds} = R_s i_{ds}$	$v_{qs} = R_s i_{qs} + \omega_s\lvert\vec{\psi}_s\rvert$	$\lvert\vec{v}_s\rvert^2 = v_{ds}^2 + v_{qs}^2$	$\theta_{v_s} = a\tan\left(\frac{v_{qs}}{v_{ds}}\right)$
Rotor voltages	$v_{dr} = R_r i_{dr} - \omega_r\sigma L_r i_{qr}$	$v_{qr} = R_r i_{qr} + \omega_r\sigma L_r i_{dr} + \omega_r\frac{L_m}{L_s}\lvert\vec{\psi}_s\rvert$	$\lvert\vec{v}_r\rvert^2 = v_{dr}^2 + v_{qr}^2$	$\theta_{v_r} = a\tan\left(\frac{v_{qr}}{v_{dr}}\right)$
Slip	$\omega_r = \omega_s - \omega_m$		$s = \omega_r/\omega_s$	
Active powers	$P_m = T_{em}\frac{\omega_m}{p}$	$P_s = \frac{3}{2}(v_{ds}i_{ds} + v_{qs}i_{qs})$	$P_r = \frac{3}{2}(v_{dr}i_{dr} + v_{qr}i_{qr})$	
Reactive powers	$Q_s = \frac{3}{2}(v_{qs}i_{ds} - v_{ds}i_{qs})$	$PF_s = \cos(a\tan(Q_s/P_s))$	$Q_r = \frac{3}{2}(v_{qr}i_{dr} - v_{dr}i_{qr})$	$PF_r = \cos(a\tan(Q_r/P_r))$
Efficiency	$\eta = \frac{P_m}{P_s + P_r}$ if $P_m > 0$		$\eta = \frac{P_s + P_r}{P_m}$ if $P_m < 0$	

PART 5

ANALYSIS OF DFIG BASED WIND TURBINE DURING VOLTAGE DIPS

Voltage dips are short term drops in rms voltages that can be caused by an overload, short circuit or the beginning of electrical generators. It mostly occurs when the rms voltage reduces between 10 to 90 percent of its normal value during 0.5 cycles to 1 minute. Voltage dips affect all electrical drives attached to a grid varying degree. On the other hand, one of the principal disadvantages of the DFIG is that they are very sensitive to this grid disturbances. In this section, basic space vector magnitudes for certain typical voltage dips are presented. It also presents the analysis of DFIG system during symmetrical and asymmetrical voltage dips. The aim of this vector magnitude is to investigate the positive and negative sequence voltage vectors for various forms of dips.

5.1. SYMMETRICAL VOLTAGE DIPS

In this section, the analysis of symmetrical voltage dips is only presented. For instance, when the voltage dip is observed immediately by the stator of the DFIG, it is very important to analyze the behavior of the stator flux in order to comprehend the difficulties that results from the disturbance of the dip. In order to do that, it must be taken into consideration with park transformation model from chapter 3 (Figure 3.5), the stator side voltage and flux references can be given as:

$$\overrightarrow{v_s}^s = R_s\overrightarrow{\imath_s}^s + \frac{d\overrightarrow{\psi_s}^s}{dt} \tag{5.1}$$

and

$$\overrightarrow{\psi_s}^s = L_s\overrightarrow{\imath_s}^s + L_m\overrightarrow{\imath_r}^s \tag{5.2}$$

Thus, by comparing stator current $\overrightarrow{\imath_s}^s$ of Equation (5.1) and (5.2) we get:

$$\frac{d\overrightarrow{\psi_s}^s}{dt} = \overrightarrow{v_s}^s - \frac{R_s}{L_s}\overrightarrow{\psi_s}^s + R_s\frac{L_m}{L_s}\overrightarrow{\imath_r}^s \tag{5.3}$$

Alternatively, it is important to change the equivalent electrical circuit of the DFIG, that we explained in section (3.3), to a smaller equivalent circuit. Therefore, from Equation (5.1) and (5.2), the following expressions are obtained. Which leads to the circuit diagram shown in Figure 5.1 (a).

$$\overrightarrow{v_r}^r = \frac{L_m}{L_s}\left(\overrightarrow{v_s}^r - j\omega_m\overrightarrow{\psi_s}^r\right) + \left[R_r + \left(\frac{L_m}{L_s}\right)^2 R_s\right]\overrightarrow{\imath_r}^r + \sigma L_r\frac{d}{dt}\overrightarrow{\imath_r}^r \tag{5.4}$$

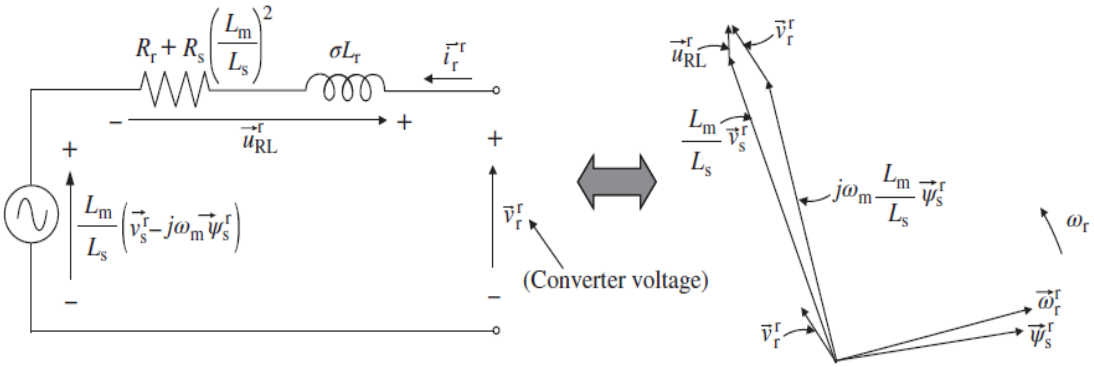

(a) (b)

Figure 5.1. (a) Equivalent circuit for voltage dips analysis of DFIG and (b) Space vector phasor diagram as sub synchronous mode [42].

From Equation (5.4), it can be seen that the rotor voltage is described as a function of rotor current, stator voltage and flux and equivalent resistance and inductance. Figure 5.1 (b) shows the space vector phasor diagram.

5.1.1. Crowbar Protection

In [42] it is very recommendable to work with the equivalent circuit of the DFIG represented in Figure 5.2 (a) and at steady state and normal operation conditions shown in Figure 5.2 (b). What happens is that when there is a smaller voltage dip, the stator voltage ($\overrightarrow{v_s}^r$) that was in normal operation is suddenly reduced to a much smaller value ($\overrightarrow{u_{RL}}^r$). For this purpose, the stator flux cannot evolve rapidly to a very small value. Therefore, in order to keep the voltage ($\overrightarrow{u_{RL}}^r$) small, we need a big rotor voltage ($\overrightarrow{v_r}^r$).

Normally, the back-to-back converters are not dimensions with such big voltages ($\vec{v_r}^r$), for that purpose it loses control. Thus, in order to avoid this problematic issue, it's very important to put a hardware element called crowbar protection.

There are different hardware crowbar configurations but most of them are equivalent. In this thesis, the crowbar protection has been chosen as one diode bridge, one switch and one resistance. Figure 5.2 (a) and (b) illustrates DFIG system supplied with three phase DC crowbar protection and one phase equivalent circuit of DFIG system when the crowbar is activated, respectively.

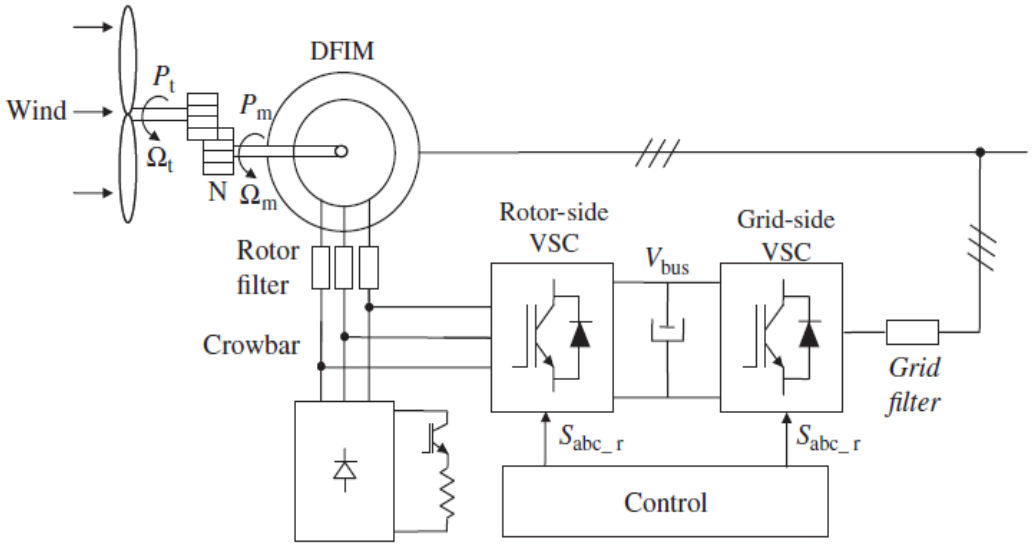

(a)

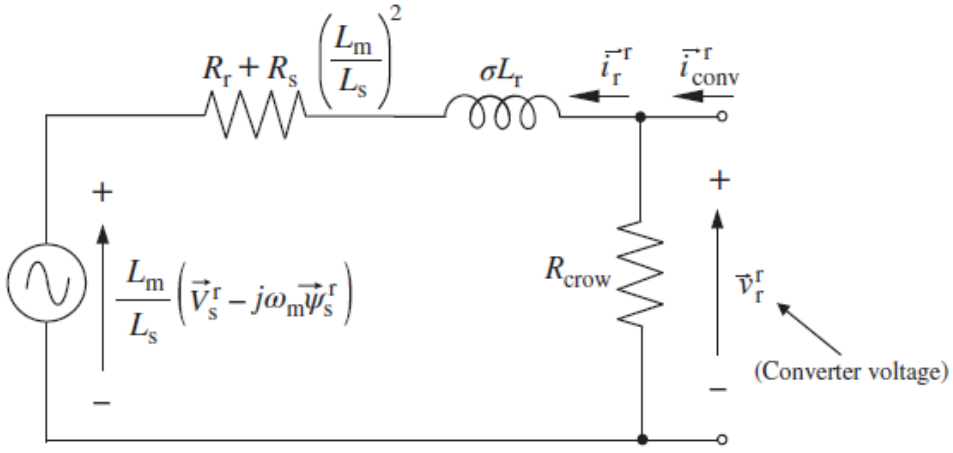

(b)

Figure 5.2. (a) DFIG system supplied with three phase DC crowbar protection and (b) one phase equivalent circuit of DFIG system when the crowbar is activated [42].

As shown in Figure 5.2 (b) the crowbar resistance is placed in each terminal of the rotor. Thus, it is possible to make the stator flux ($\overrightarrow{\psi_s}^r$) evolution more faster during the dip and reach the new steady state much faster with the reduced voltages ($\overrightarrow{v_s}^r$) at the grid and therefore at the stator.

5.2. ASYMMETRICAL VOLTAGE DIPS

This section presents analysis of asymmetrical voltage dips. Practically, asymmetrical (unbalanced) faults are mostly experienced than symmetrical faults. DFIG can be required to work under unbalanced grid voltages in a certain circumstances and applications, such as in weak grids where the nonlinear loads cause unbalance of grid voltages. For instance, the unbalanced voltage has direct impact on the operation of the DFIG. Which affects the performance of DFIG, if no additional action is performed [42]. The unbalanced occurrence can be investigated using a technique called sequence decomposition. Accordingly, this unbalanced voltage indicates the existence of both a positive and negative sequence. Therefore, in order to overcome these kinds of problematic issues, it's better to use a control strategy called dual vector control strategy of a DFIG.

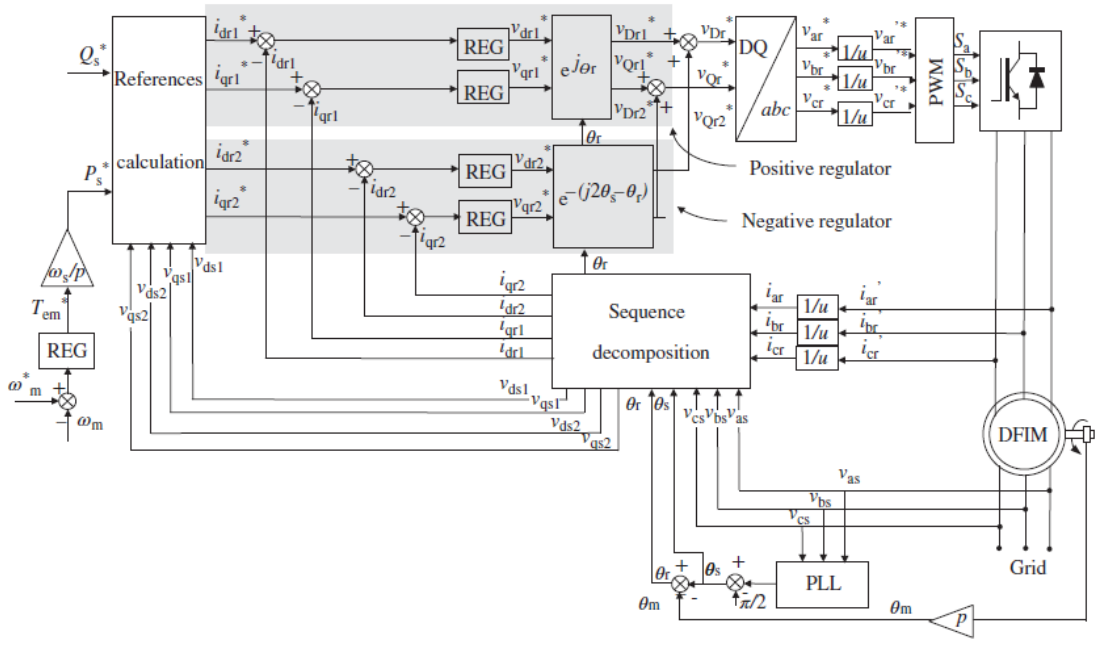

Figure 5.3. Dual vector control strategy of a DFIG [55].

Since Figure 5.3 deals with positive and negative sequence of voltages and currents with the DFIG, it should include negative sequence current loops in order to be able to properly control the generator. Furthermore, the filter (in Figure 5.4) is set in order to eliminate the coupling oscillations between the sequences. Thus, the filter could be tuned up to 100 Hz (which is double of the frequency of the stator) and in order to get an acceptable performance of the loops, this double frequency should be removed.

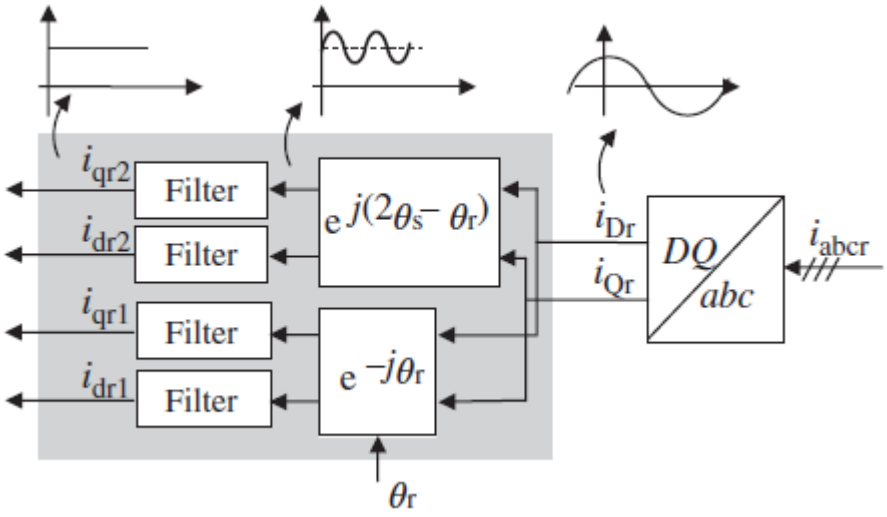

Figure 5.4. Sequence decomposition for the current loops [55].

PART 6

SIMULATION RESULTS

In this section, a detailed simulation result of a DFIG based wind turbine system is presented. The overall system has been carried out in MATLAB/Simulink software. This system consists of different models and sub-models, this includes the DFIG, wind speed, wind turbine model, RSC control, universal bridges (converters), PWM, GSC control, PI controller, and MPPT by indirect speed control strategy.

6.1. SIMULATION OF THE WIND TURBINE MODEL

As previously discussed in section 2, a practical wind turbine has a rated power of between 1.5 and 3 MW. Thus, this thesis chooses a 2.4 MW three-blade wind turbine for system simulations. Here, we assume that the wind turbine model is made up of several parts: a wind speed, an aerodynamic model, a drive train model, and an electrical generator.

6.1.1. Simulation of the Wind Speed Model

In this work, the wind speed model is designed by adding four constituents such as constant, turbulence, ramp, and gust constituents. The gust constituents can be used to describe unusual sudden changes in wind speed.

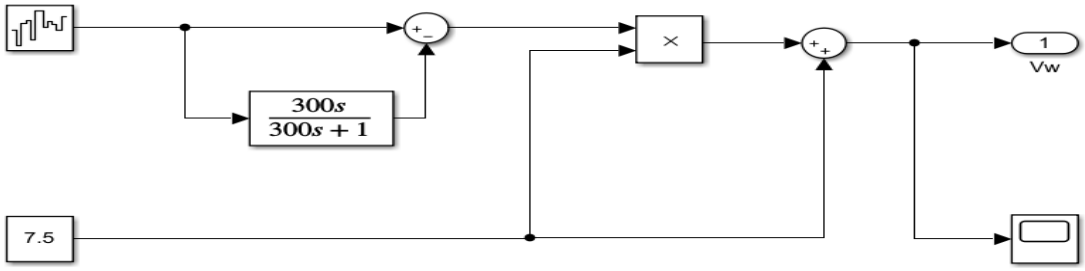

Figure 6.1. Wind speed model at 7.5 m/s.

Equation (2.4), explained in chapter 2, leads to the wind speed model represented in Figure 6.1. Thus, the simulation result of this model at 7.5 m/s of wind speed is shown in Figure 6.2.

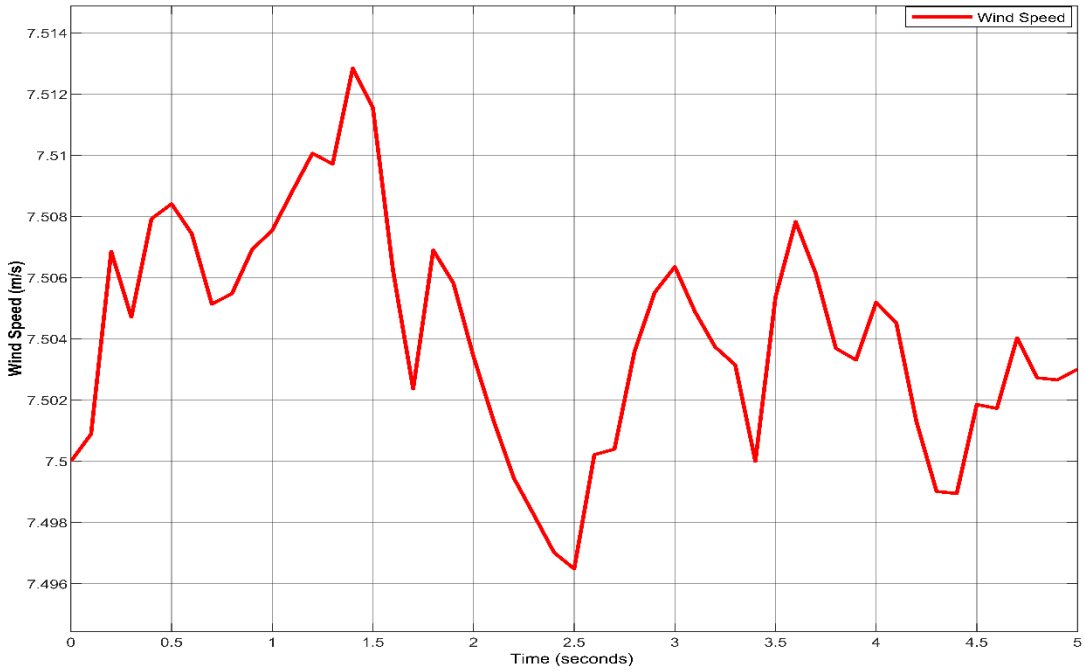

Figure 6.2. Wind speed profile.

6.1.2. Simulation of the Aerodynamic Model

It is possible to design the aerodynamic model by determining the turbine torque generated by the three-blade wind turbine. To do that, some parameters should be considered, such as the radius of the blade, turbine angular speed, wind speed, and turbine coefficient. Moreover, the gearbox ratio should also be considered in both the low-speed shaft and high-speed shaft.

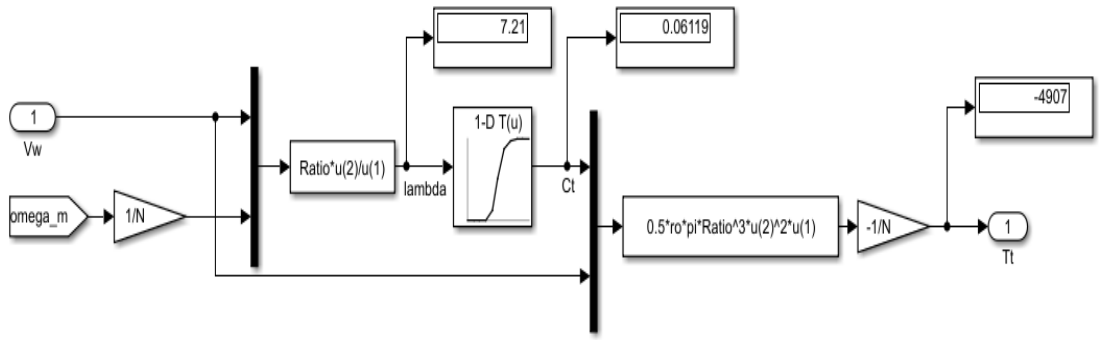

Figure 6.3. Simulink design of the aerodynamic model.

Equation (2.10) discussed in chapter 2 leads to the Simulink design of the aerodynamic model shown in Figure 6.3. The speed of the wind is set to 7.5 m/s and the value of the tip step ratio (lambda) which is 7.21 is maintaining the specified requirement where the optimum lambda has been considered to be 7.2 and the value of turbine coefficient (C_t) is 0.06. Thus, the torque generated by the three-blade wind turbine is -4907 N.m. The negative shows that the machine is operating as a generator convention.

6.2. SIMULATION OF THE DFIG SYSTEM

Figure 6.4 represents the Simulink design of the DFIG system. The system consists of a wound asynchronous induction machine (as a DFIG), two back-to-back converters, and RSC control.

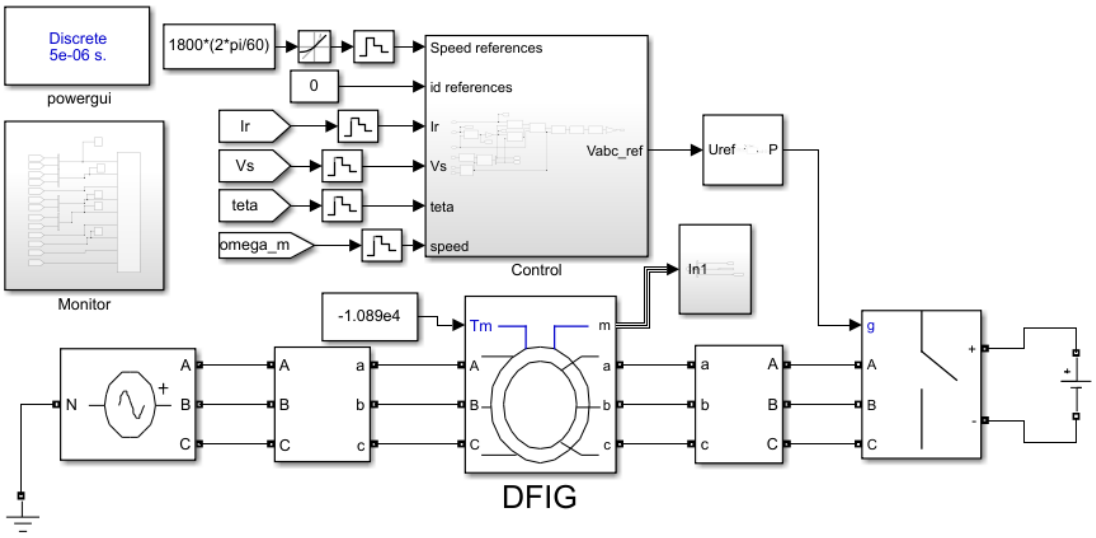

Figure 6.4. DFIG Simulink design.

The simulation result for the above model is presented in Figure 6.5. The speed reference is set at 1500 and 1800 rev/min. The electromagnetic torque is modified as the rotor speed changes. Accordingly, the electromagnetic torque depends on the rotor current. Thus, electromagnetic torque is regulated by the quadrature rotor current. Furthermore, the direct rotor current is always set to zero because the machine is magnetizing from the stator. Moreover, the stator voltage is constant and operates properly. Similarly, the rotor voltage references and stator and rotor currents are also working properly.

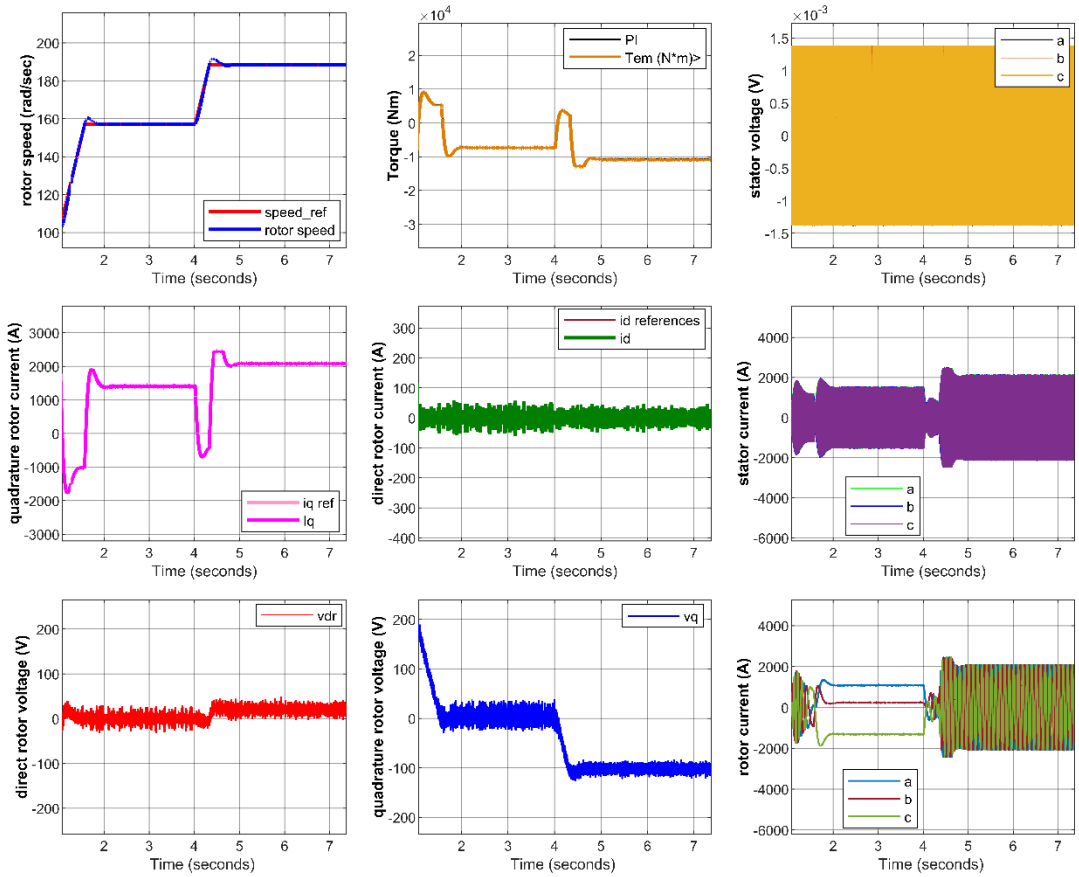

Figure 6.5. Magnitudes of the DFIG with the rotor speed and electromagnetic torque.

6.3. STEADY-STATE ANALYSIS OF DFIG

The MATLAB plot shown in Figure 6.6 is the most representative magnitudes of the model equations discussed in chapter 4 (see Table 4.2 and 4.3). In this case, as input is, a torque as a function of the rotational speed (rev/min). It can be realized that the torques are negative; therefore, the machine (DFIG) is operating as a generator. The machine represents something similar to the operation at the steady-state of a wind turbine based DFIG system.

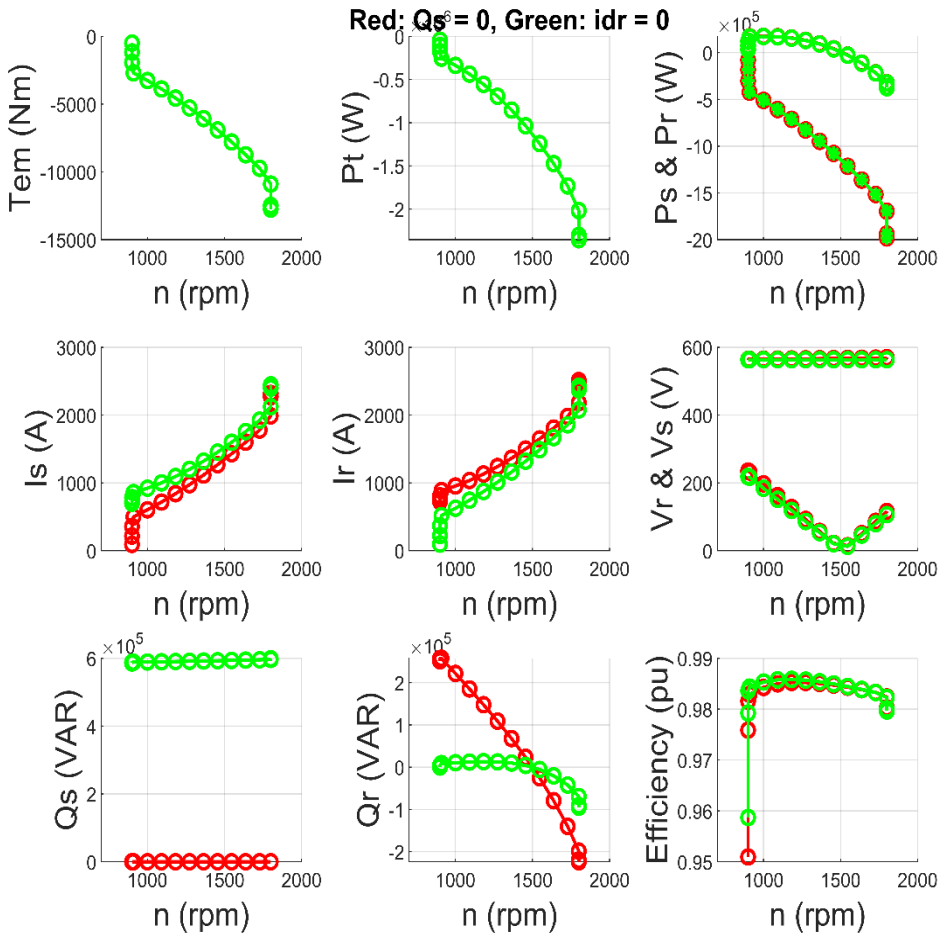

Figure 6.6. Steady-state analysis of DFIG.

The rotational speed is set between 900 and 1800 rpm and the value of the total mechanical power is almost the same as the product of torque and rotational speed. Furthermore, it has been calculated and realized that the stator active power (2 MW) is much greater than the rotor active power (400 kV). The rotor active power can be negative or positive depending on the rotational speed. Obviously, in case 1, when the stator reactive power (Q_s) is set at zero, the value of the maximum stator current will be lower. On the other hand, when direct rotor current (i_{dr}) is set to zero, it provides a lower stator current, but the reactive power will be high. Moreover, the stator voltage amplitude is always constant (690 V), while the rotor voltage depends on the rotor speed. For instance, the designed system (Figure 6.6) is tested for different rotational speeds. For example, at 1500 rpm the torque is -7341 Nm and at 1800 rpm the torque is -10890 Nm. Similarly, the results of the DFIG system (in Figure 6.5) exactly show

the same result. This clearly shows that the DFIG system is operating according to the Mitsubishi design. The objective of this steady-state analysis is to know the stable operating point of the system. Finally, it can be realized that the efficiency of the DFIG is good, reliable, sufficient, and constant between 900 and 1800 rpm.

6.4. SIMULATION OF DFIG BASED WIND TURBINE SYSTEM

In this section, detailed results and comparisons of a DFIG based wind turbine using MPPT by indirect speed control with typical PI and proposed controller is presented.

6.4.1. Simulation Results using PI Controller

Figure 6.7 shown below represents the simulated result of the system using PI control for different wind speed values (7.5 and 9.5 m/s). The rotational speed is set at 1800 rpm (188.5 rad/sec) through the operation.

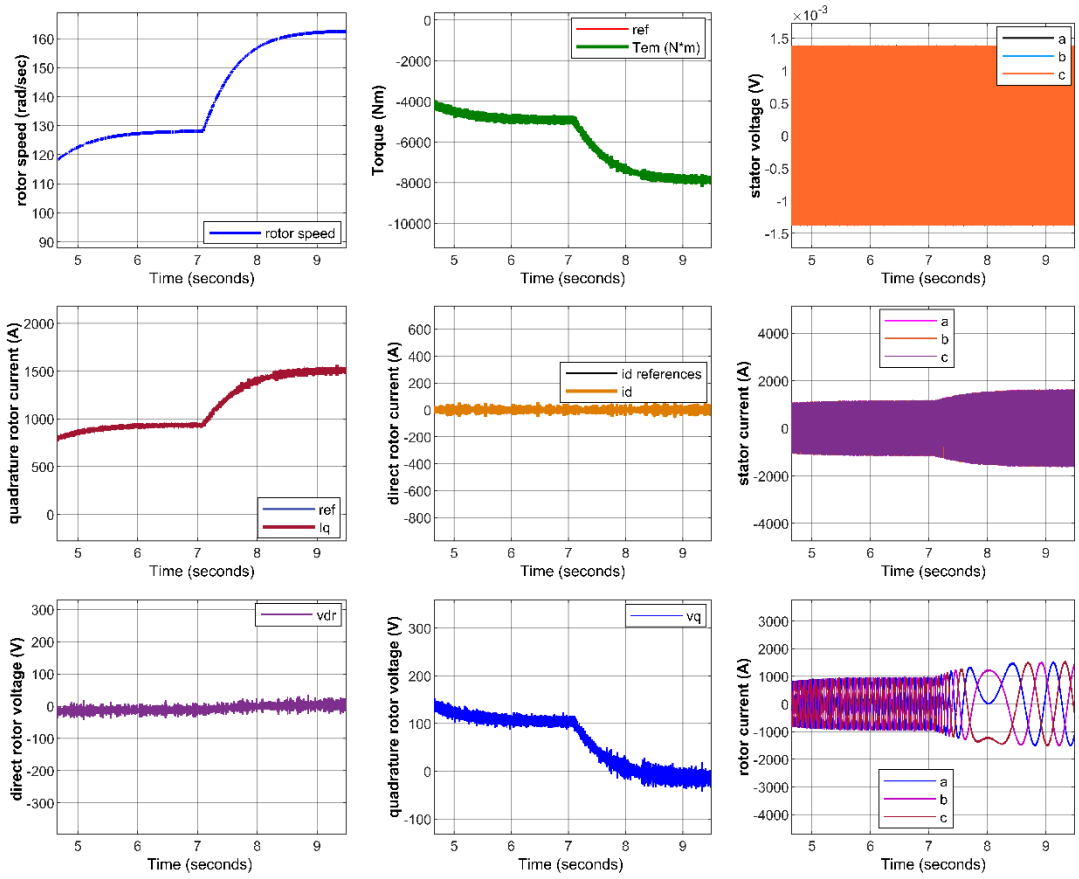

Figure 6.7. Performance of DFIG with PI control at different wind speed.

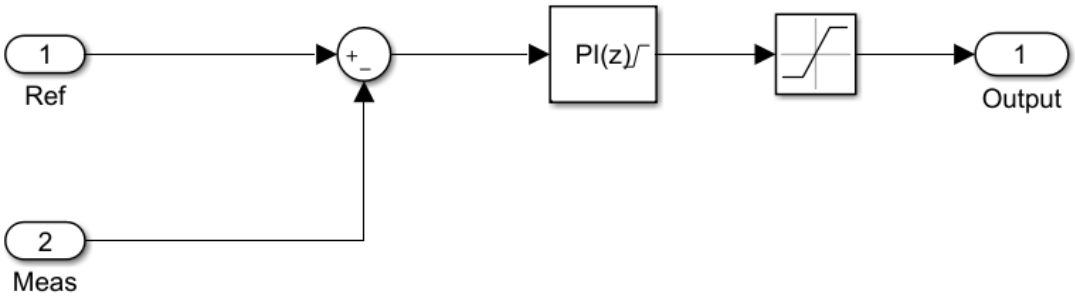

Figure 6.8. Typical PI controller design of the DFIG system.

Table 6. represents the value of the DFIG components at steady state-response with PI control at different wind speeds.

Table 6.1. Simulated results of the DFIG with PI controller at different wind speeds.

Wind speed	**Rotor speed**	**Torque**	**Power (generated)**
7.5 m/s	128.1 rad/sec	-4860 Nm	-0.622 MW
9.5 m/s	162.5 rad/sec	-7825 Nm	-1.271 MW
11.8 m/s	201.8 rad/sec	-12100 Nm	-2.44 MW

From Table 6.1 it can be realized that, as the wind speed increases, the rotor speed, torque, and generated power also increases. However, in this work, the wind speed doesn't go beyond 11.8 m/s. For instance, in case it exceeds that value, the pitch control will take place to limit the maximum extracted power. Even though, pitch controller is not implemented, instead a 2.4 MW three blade wind turbine has been carried out in MATLAB. Thus, the simulation result shown in Figure 6.7 has been verified with the proposed system (see Figure 4.15). Figure 6.9 represents steady-state response of the system with typical PI controller.

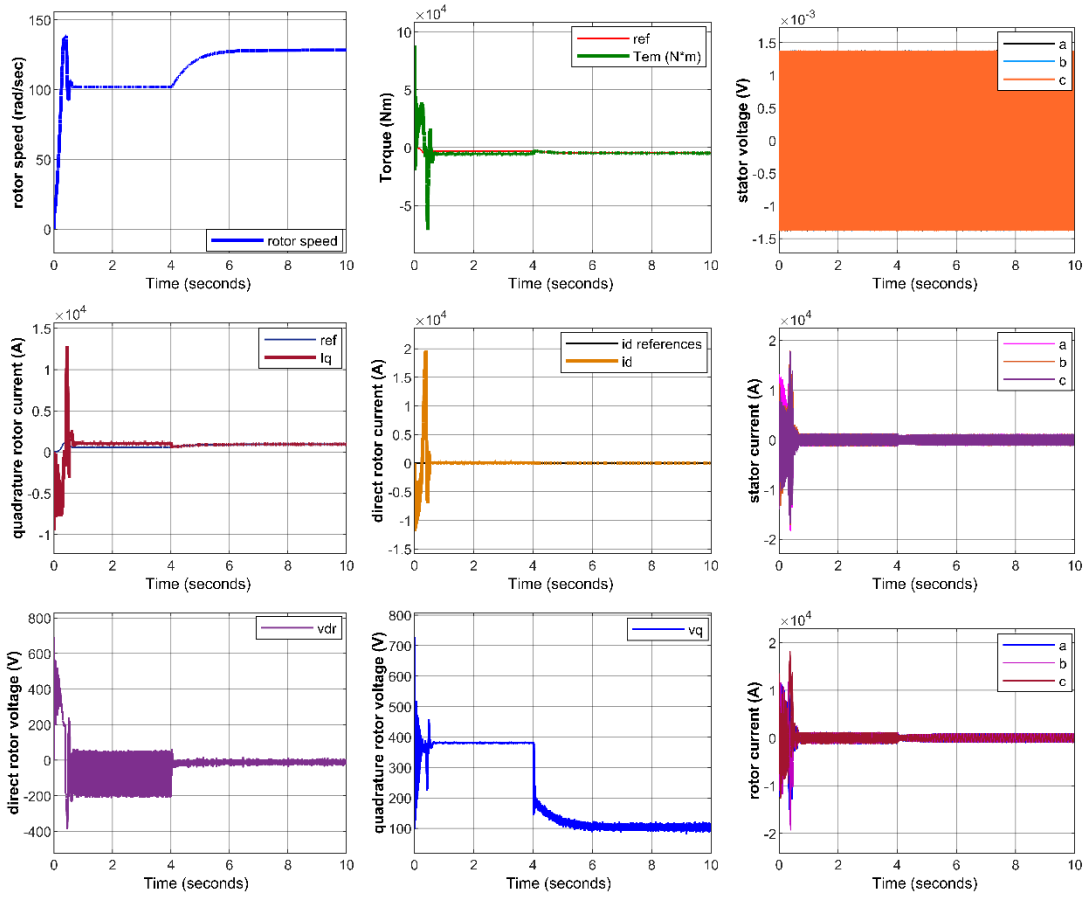

Figure 6.9. Steady-state response of DFIG with typical PI controller at 7.5 m/s.

Table 6.2 analyses the settling time of the DFIG components at different wind speed value for typical PI control.

Table 6.2. Settling time of DFIG components with typical PI at different wind speed.

	Settling Time (5%) (seconds)			
Wind speed (m/s)	**Rotor speed**	**Torque**	***iqr***	***idr***
7.5	4.665	4.896	5.168	1.117
9.5	3.71	3.914	4.476	1.03
11.8	3.218	3.64	4.1	0.91

6.4.2. Simulation Results of the Proposed Method

As shown in Figure 6.9 the performance of the system when PI controller is applied, it could not satisfy the specification of the DFIG, as there is higher settling time of the parameters and high overshoot/undershoot for all parameters. Therefore, an efficient controller is proposed by tunning the gains of i_d and i_q until the desired value is obtained. Figure 6.10 illustrates the proposed Simulink design.

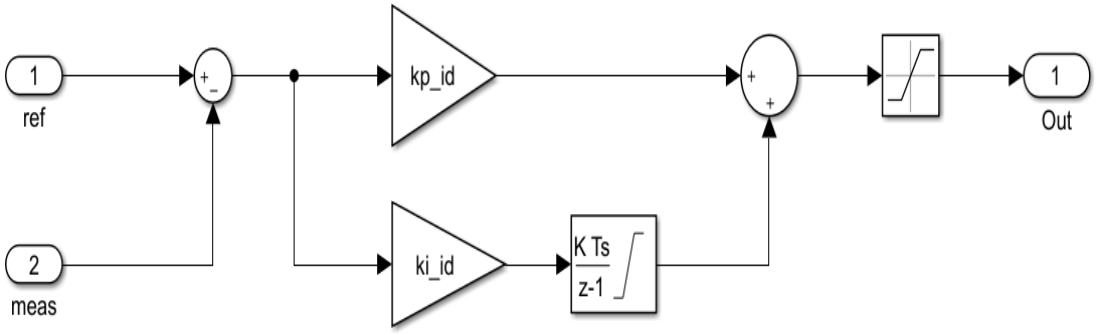

Figure 6.10. Proposed Simulink design of DFIG system.

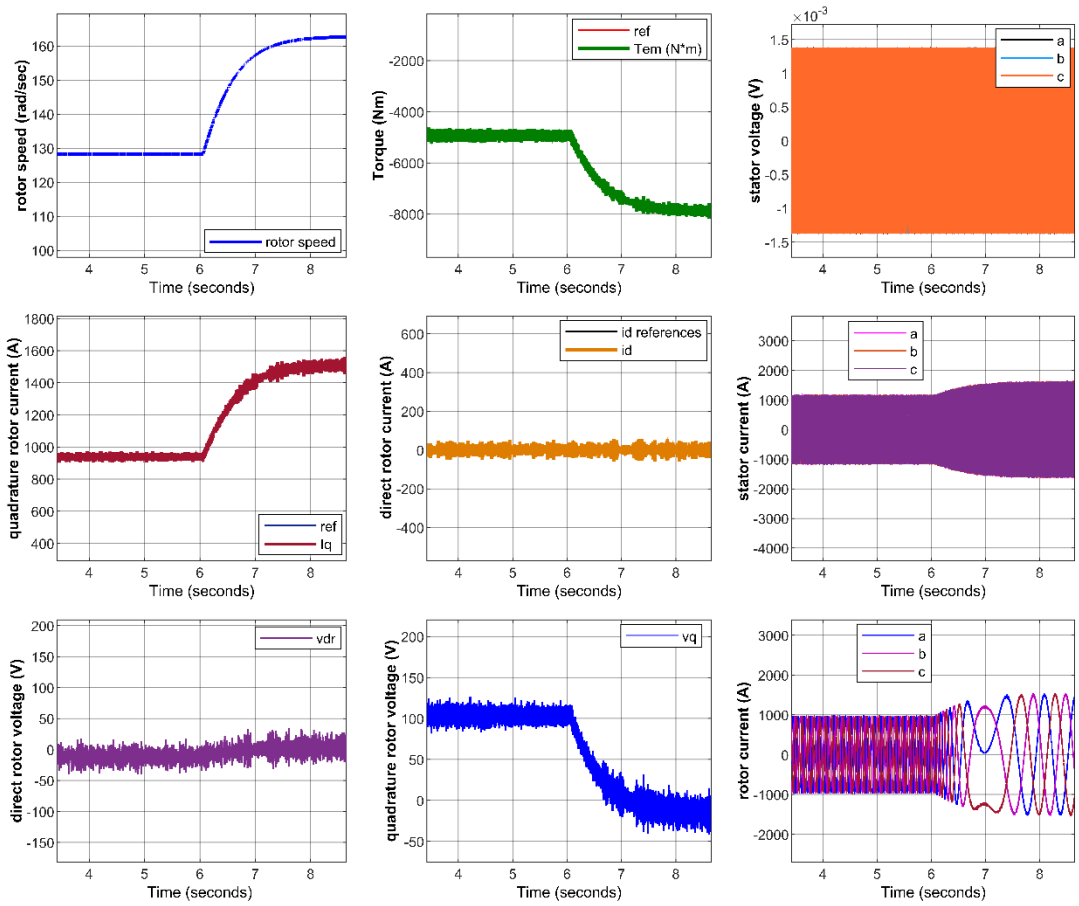

Figure 6.11. Performance of the proposed controller at different wind speed.

Table 6.3. represents the value of the DFIG components at steady state-response with the proposed method. It further shows that the generated powers at different wind speeds corresponds to Table 6.1. Therefore, at speed less than 11.8 m/s, the proposed system performs as desired. Figure 6.12 illustrates the steady-state performance of the proposed controller at 7.5 m/s.

Table 6.3. Results of the DFIG with the proposed method at different wind speeds.

Wind speed	**Rotor speed**	**Torque**	**Power (generated)**
7.5 m/s	128.24 rad/sec	-4900 Nm	-0.63 MW
9.5 m/s	162.79 rad/sec	-7850 Nm	-1.28 MW
11.8 m/s	201.86 rad/sec	-12200 Nm	-2.46 MW

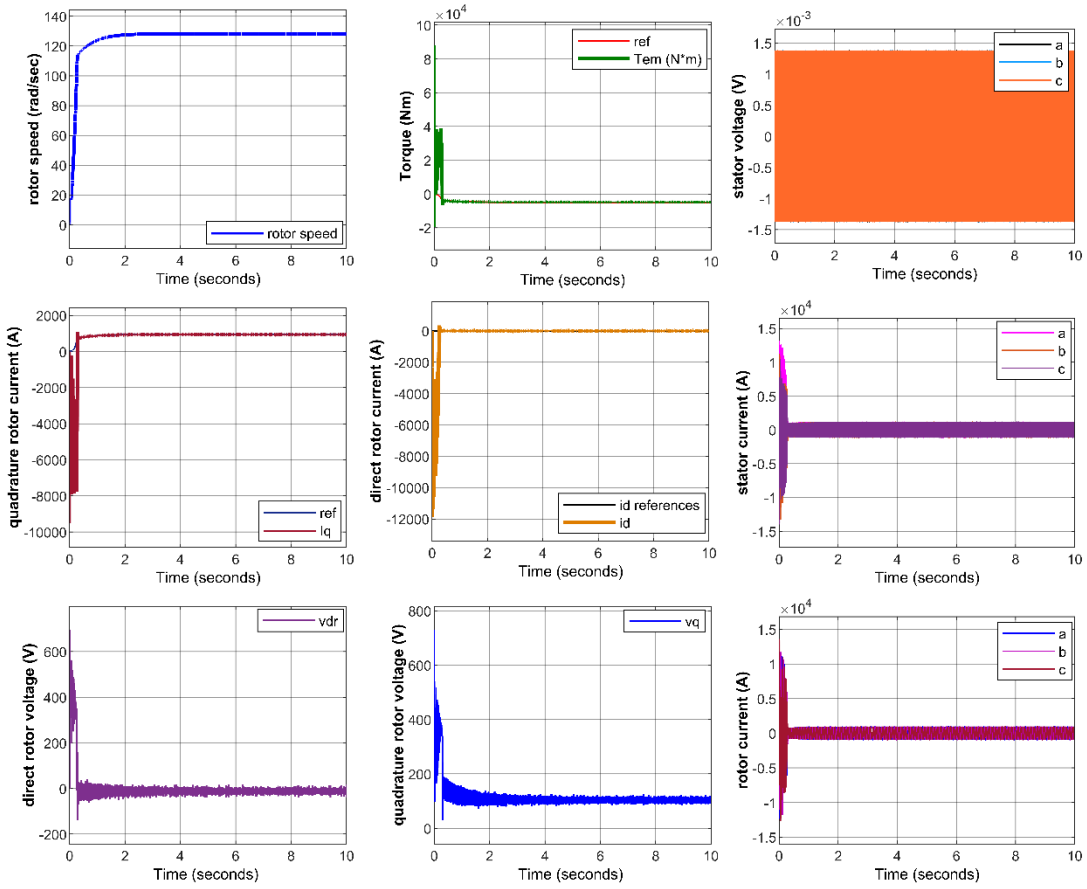

Figure 6.12. Steady-state performance of the proposed controller at 7.5 m/s.

Table 6.4. Settling time of the proposed method at different wind speed.

	Settling Time (5%) (seconds)			
Wind speed (m/s)	**Rotor speed**	**Torque**	***iqr***	***idr***
7.5	1.483	2.115	1.894	0.922
9.5	1.35	1.94	1.76	0.81
11.8	1.33	1.7	1.613	0.705

6.4.3. Comparison between Typical PI Controller and Proposed Method

When compared the relevant values in Table 6.2 and Table 6.4, it can be seen that the performance of DFIG based wind turbine with the proposed method improves in terms of settling time.

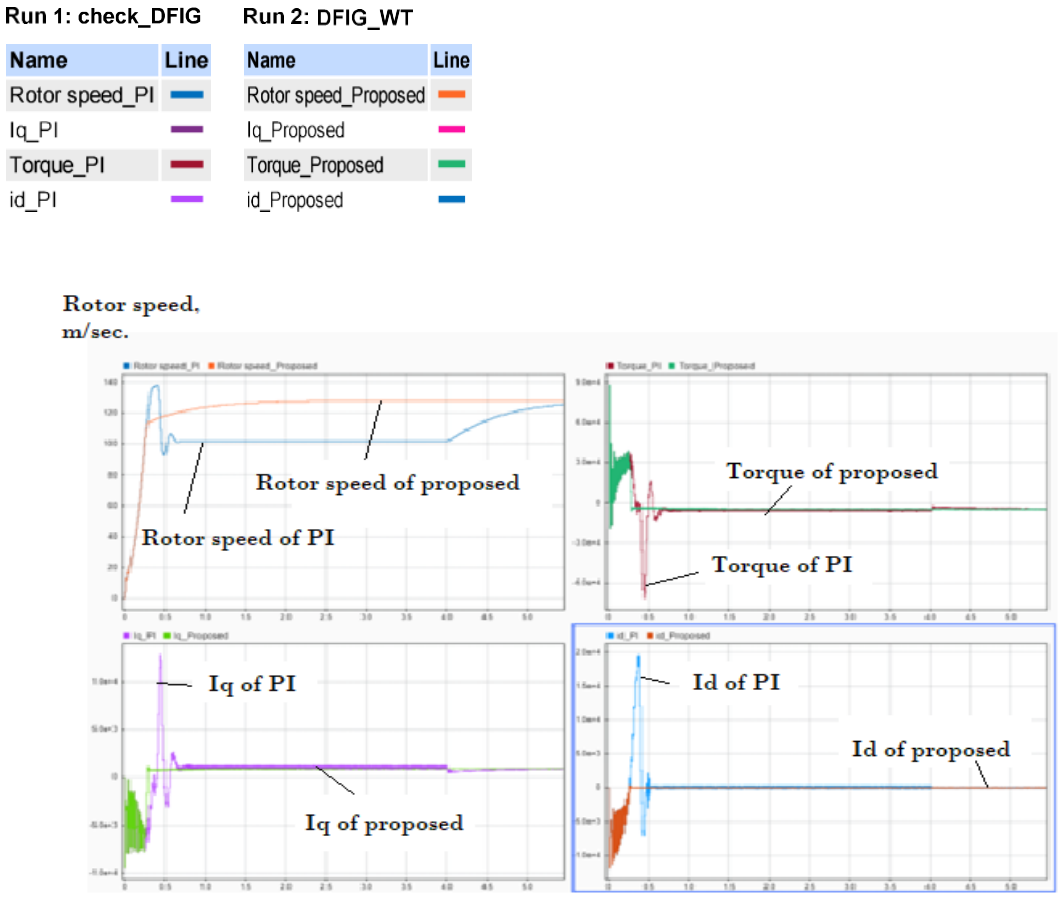

Figure 6.13. Steady-state performance with PI and proposed method at 7.5 m/s.

Figure 6.13. shows the steady-state performance for the PI controller and proposed method at 7.5 m/s. Moreover, it can be observed that the proposed method has less perturbations compared to the PI controller. Besides, the proposed method provides strong robustness for controlling the system with variable parameters. From the results, it is clearly obvious that the proposed method has better performance than the PI.

6.5. IMPLEMENTATION OF DFIG BASED WIND TURBINE SYSTEM

In this section, the implementation and control of a wind turbine based DFIG in RSC and GSC control is presented. Figure 6.14 represents the overall implementation of a wind turbine based DFIG.

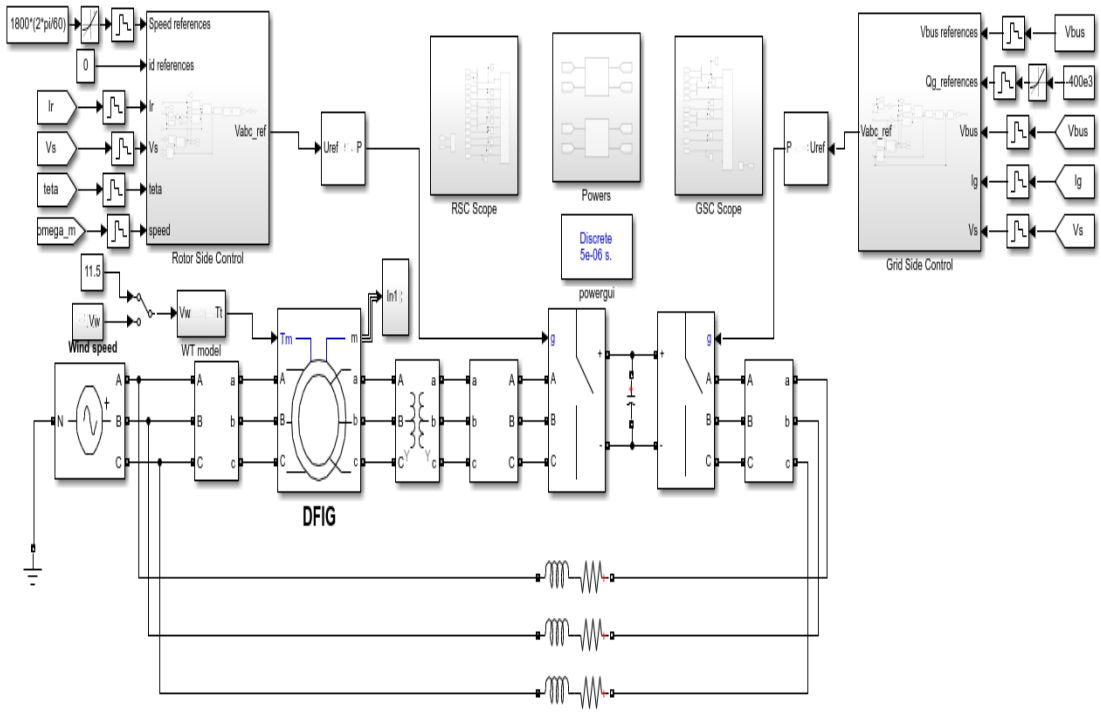

Figure 6.14. Overall implementation of DFIG based wind turbine.

6.5.1. Implementation of the RSC Control

The main purpose of RSC is to control the stator active power that enables the turbine to capture the maximum power, while also providing reactive power support to the grid. The RSC control is also responsible for the MPPT, Figure 6.15 shows indirect speed control Simulink design.

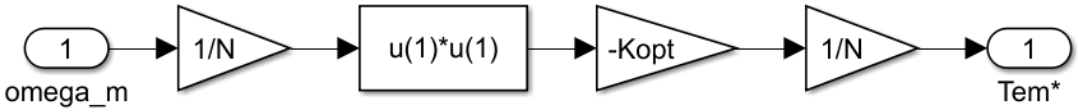

Figure 6.15. Indirect speed control.

In the RSC, we have rotor currents and rotor speed references which is used to generate the rotor voltage references.

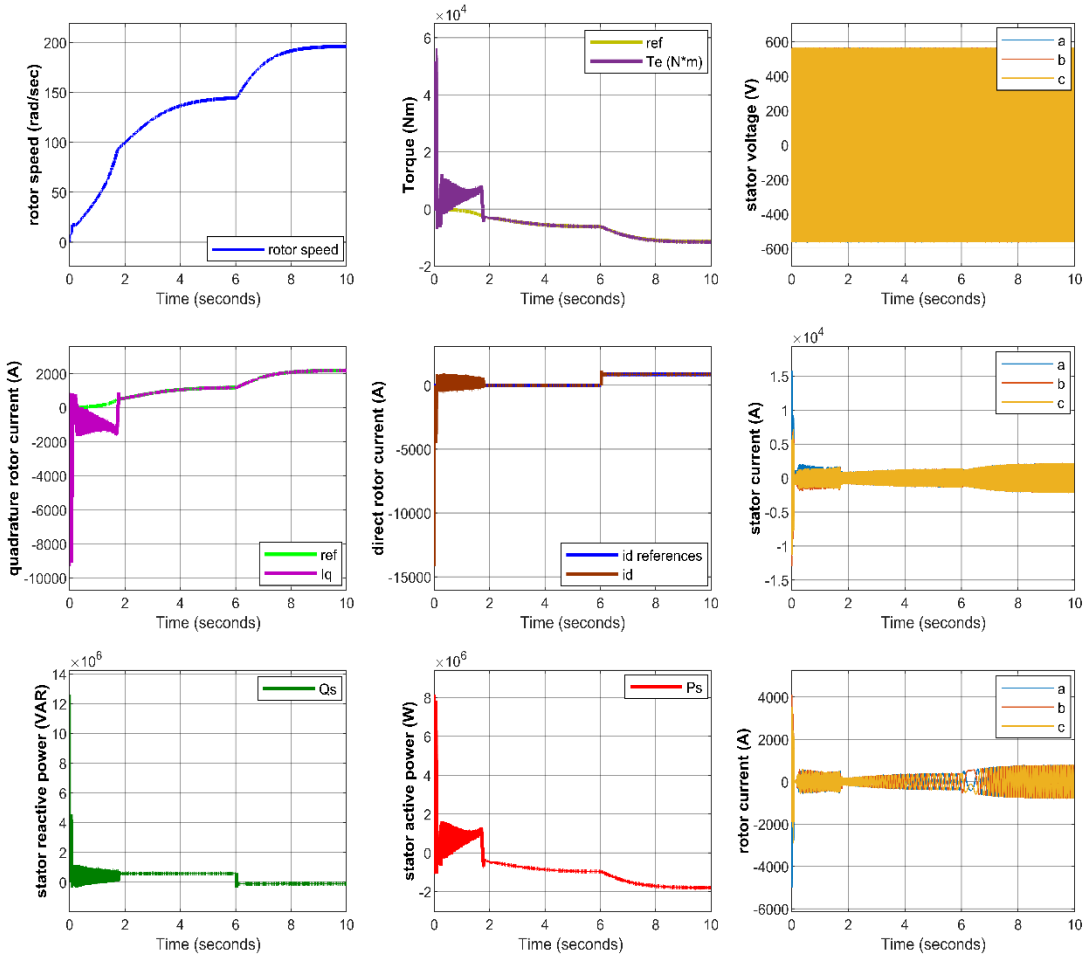

Figure 6.16. Steady-state response for the magnitudes of RSC at different wind speeds.

Figure 6.16 illustrates the most representative magnitudes of DFIG in the RSC control at different wind speed. From the result, it can be observed that the performance of the stator active power (Ps) is almost proportional to the torque. Furthermore, MPPT by indirect speed control can be realized. When the wind speed changes (8.5 to 11.5 m/s),

in this way, MPPT control algorithm operates. Accordingly, the rotor speed changes to a new (higher) operating point and the quadrature rotor current component (I_q) becomes higher, which maximizes the stator active power (Ps). For instance, as the direct rotor current (i_{dr}) component changes from 0 to 850 ampere, corresponding stator reactive power (Qs) also modifies. Thus, this provides decouple control of active and reactive power.

6.5.2. Implementation of the GSC Control

The main objectives of GSC are to maintain the DC bus voltage constant irrespective of the operating zone and to control grid reactive power reference. It operates at a unit power factor. Moreover, the power generated by wind turbine is partly delivered through the rotor of the DFIG. For example, the power flow that pass via the rotor also flows through the DC-link and then sent to the grid by the GSC.

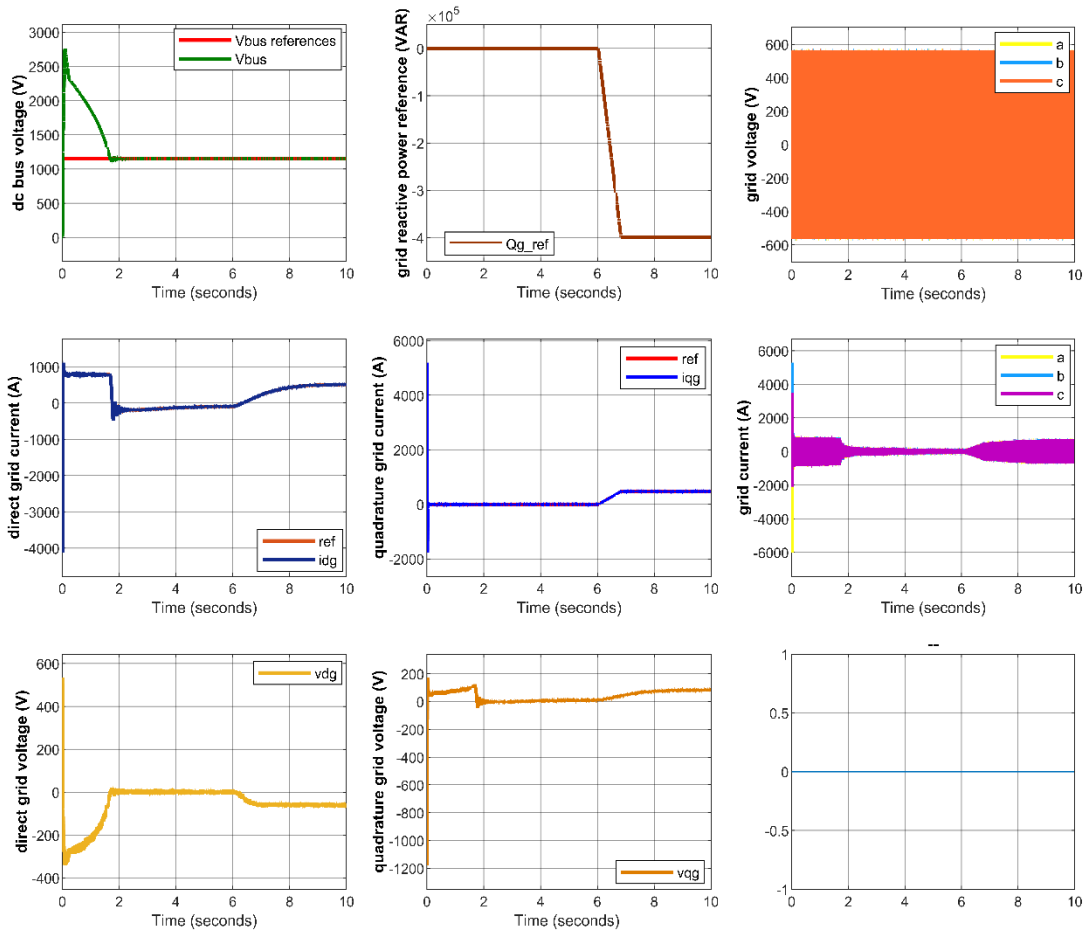

Figure 6.17. Steady-state response for the magnitudes of GSC at different wind speed.

Figure 6.17 indicates the most representative magnitudes of a vector controlled DFIG for the GSC at various wind speed. It can be realized that at the steady-state the DC bus voltage is kept constant. Moreover, the grid voltage references (vdg and vqg) are very small voltages because, we are using a feedback voltage of the grid. At 6 seconds, it has been performed a variation from 0 to -400 kVAR reactive power at the GSC and therefore, the quadrature grid current (iqg) is also being modified.

6.6. DYNAMIC ANALYSIS OF CURRENT LOOPS BEHAVIOR

This section investigates the dynamic analysis of current loops behavior in a wind turbine based DFIG. Figure 6.18 demonstrates the most representative magnitudes in the RSC.

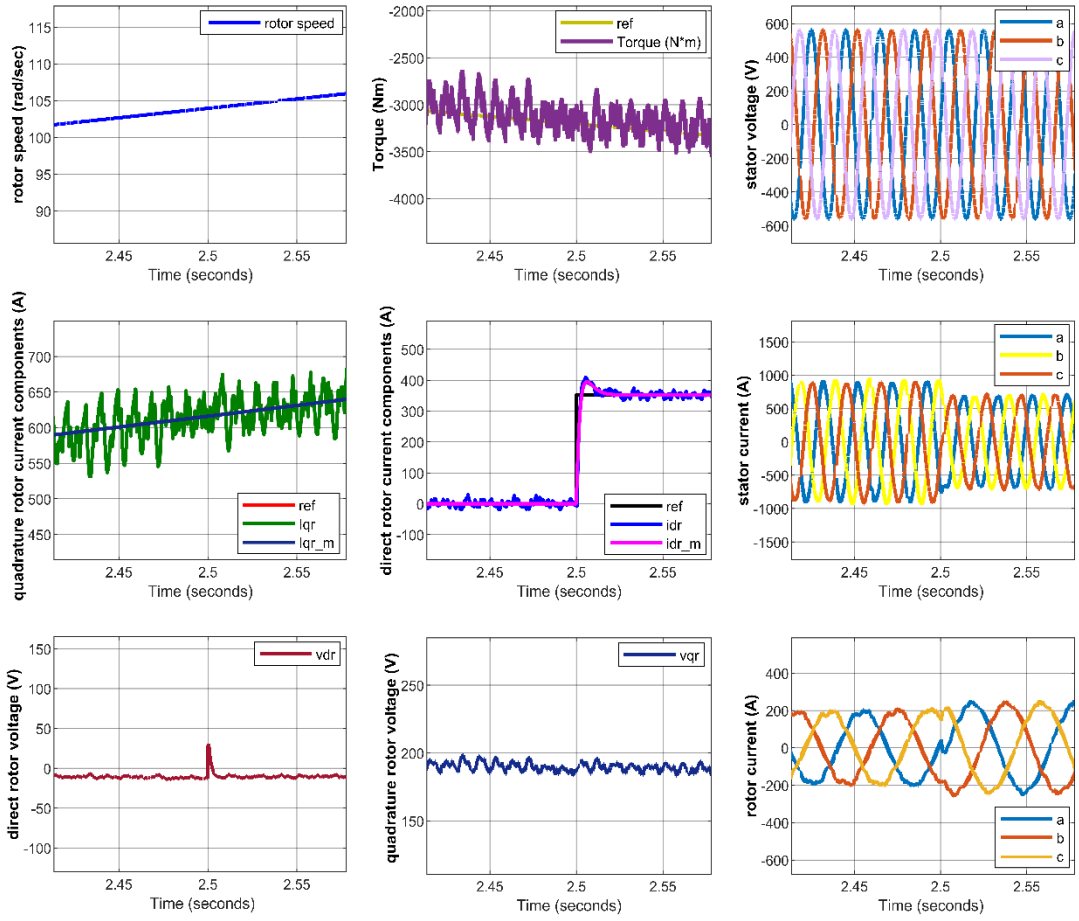

Figure 6.18. Most representative magnitudes of a wind turbine based DFIG in the RSC.

The implementation of this thesis represents the most representative magnitudes of a 2 MW grid-connected two-level (2L) converter. Figure 6.19 represents the magnitudes of DFIG based wind turbine in the GSC. The abc grid voltage is connected to the converter and this converter also controls the DC bus voltage.

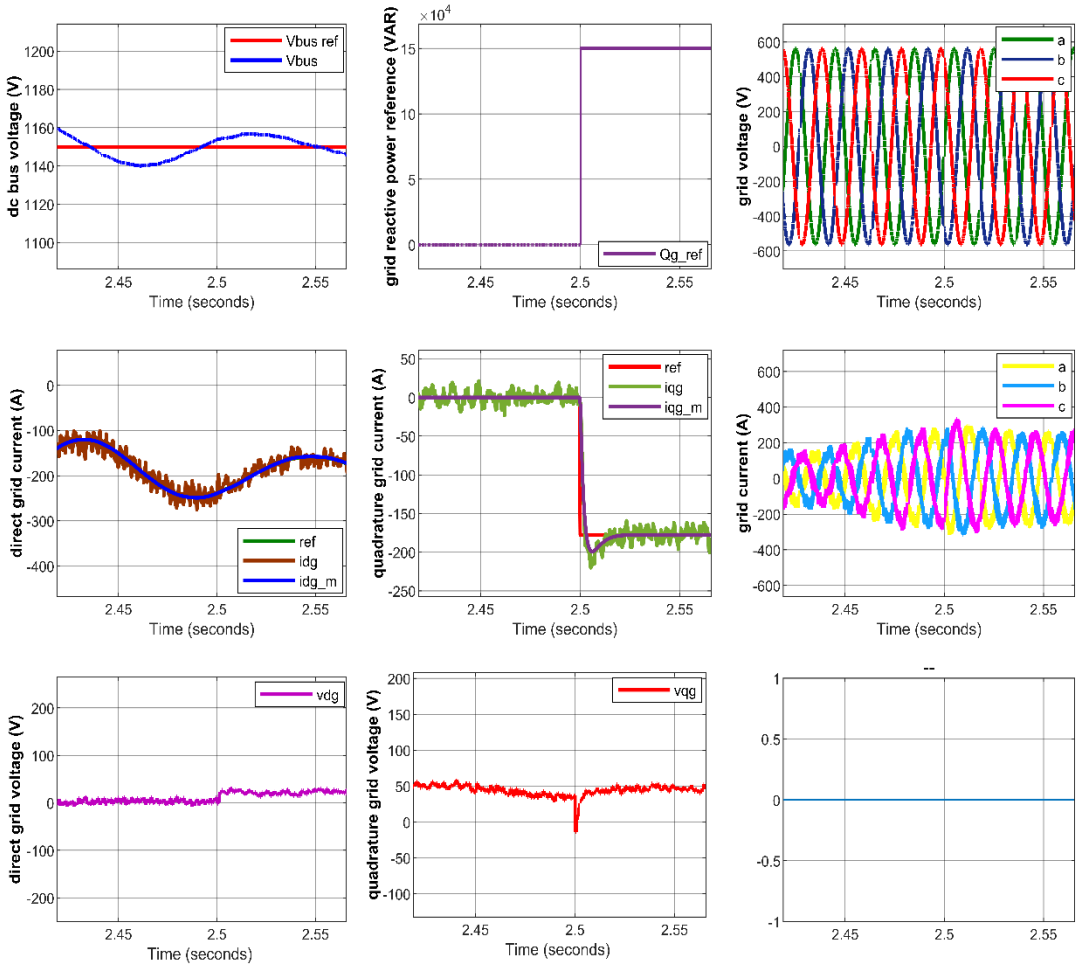

Figure 6.19. Most representative magnitudes of a wind turbine based DFIG in the GSC.

In Figure 6.18, it can be realized that the id component has been a little bit degraded but thanks to the compensation that the theoretical model (idr_m) fits quite well with the actual one (idr). Correspondingly, at the grid side (Figure 6.19) the theoretical model (iqg_m) is also similar to the actual model (iqg). Obviously, the actual one has a ripple due to the switching frequency that the simplified model (idr_m & iqr_m) doesn't take into account. In general hardware implementations, there is one delay between control and PWM or modulation implementations. In case the compensation of this delay is not used, the theoretical and actual model will be further way for both

RSC and GSC. Moreover, it can be observed how idg and iqg components are very accurate. It should be noted that to follow properly the dynamic performance of DFIG it is not required to reach the saturation of the voltage references. Finally, at the time instant 2.5 seconds, there is a reactive power variation from 0 to 150 kVAR and it can be observed, as the grid reactive power references (Q_ref) increases, the magnitudes of the grid current also increase.

6.7. PERFORMANCE ANALYSIS UNDER VOLTAGE DIPS

This section graphically presents the performance analysis of a grid-connected DFIG based wind turbine during symmetrical and asymmetrical voltage dips. The main findings are drawn from the parameters of a 2 MW, 690V DFIG based wind turbine.

6.7.1. Symmetrical Voltage Dips

This section demonstrates the simulation analysis of symmetrical voltage dips. When grid fault occurs, the converter is damaged. Hence, in order to overcome this kind of problematic issues, we have included a hardware element called crowbar protection. This protection is suddenly activated when the voltage dip occurs and return it under normal operation condition. Moreover, during the crowbar activation, the RSC should be disabled in order to protect the converter. Figure 6.20 shows the stator flux and the crowbar current fault analysis.

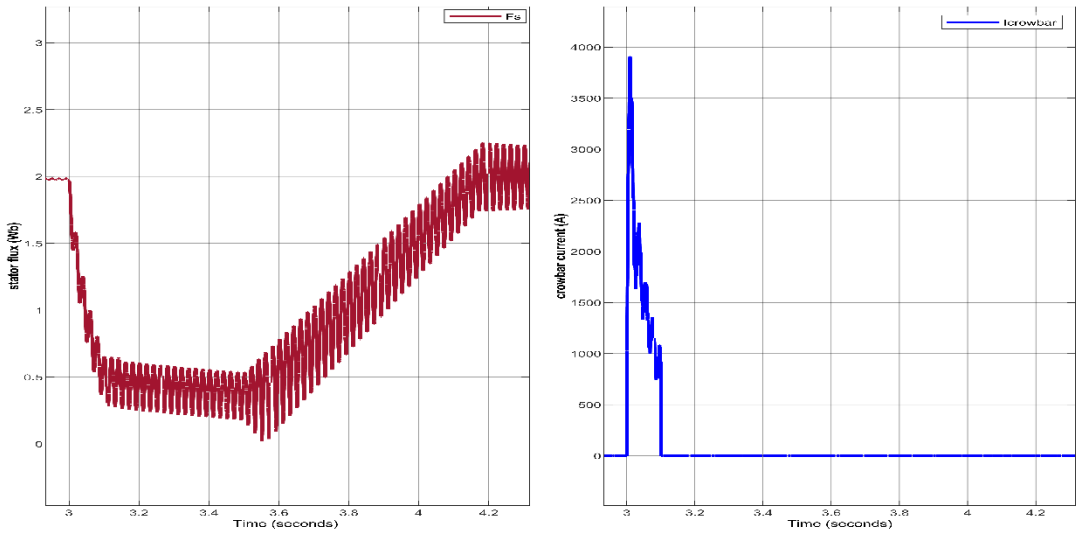

Figure 6.20. Stator flux and crowbar current under symmetrical voltage dip.

Figure 6.21 and 6.22 demonstrates the performances of the RSC and GSC during the dip.

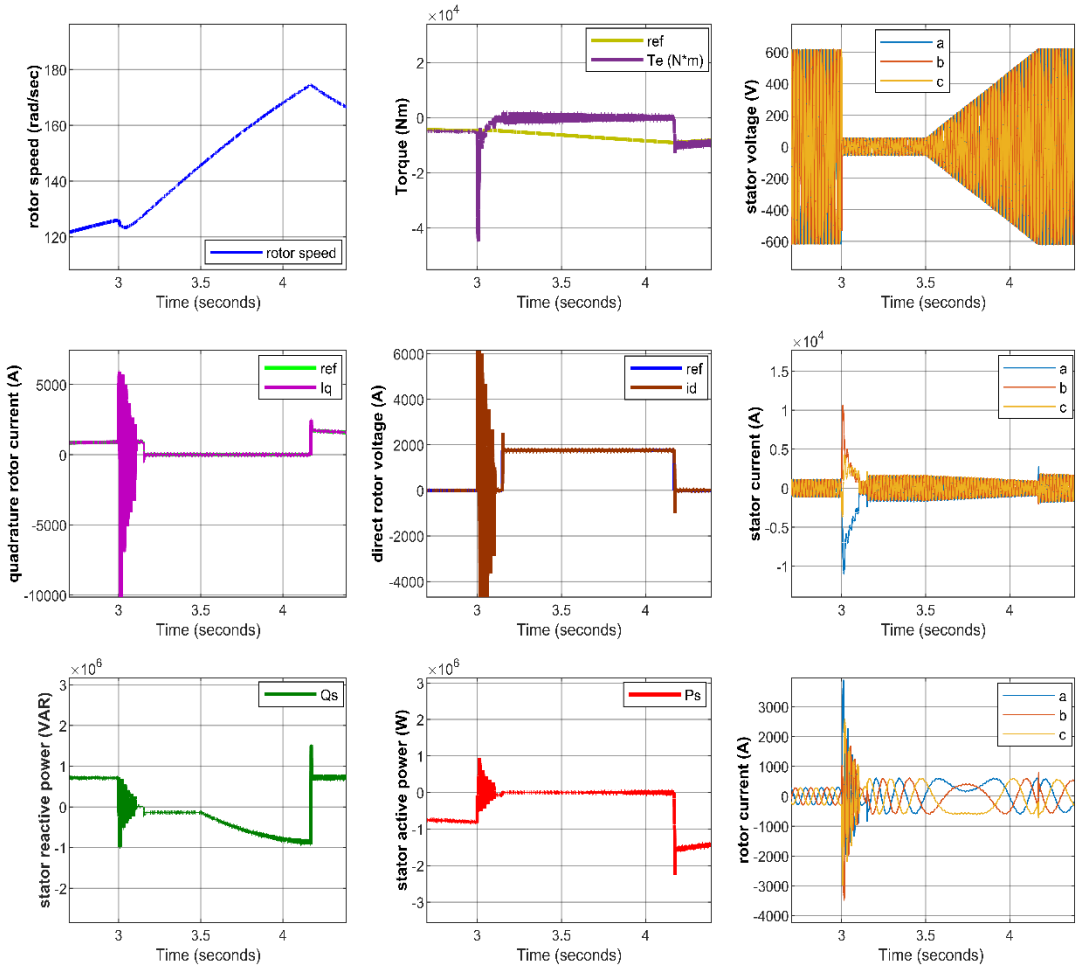

Figure 6.21. Performance of RSC magnitudes under symmetrical voltage dips.

From the above simulation, the voltage dip has been performed at 3 seconds and the remaining voltage at the grid is only 10 % of the normal voltage. Once the voltage dip occurs, the stator flux cannot progress to the steady-state as fast as the stator voltage. Then the crowbar protection is suddenly activated, this helps the stator flux to progress much faster and recover. Thus, during this time all the rotor currents goes through the crowbar protection, which results the RSC to be protected. Furthermore, during the voltage dip as demanded by the grid codes, it has been performed a high value of id rotor current, in order to provide reactive power through the stator.

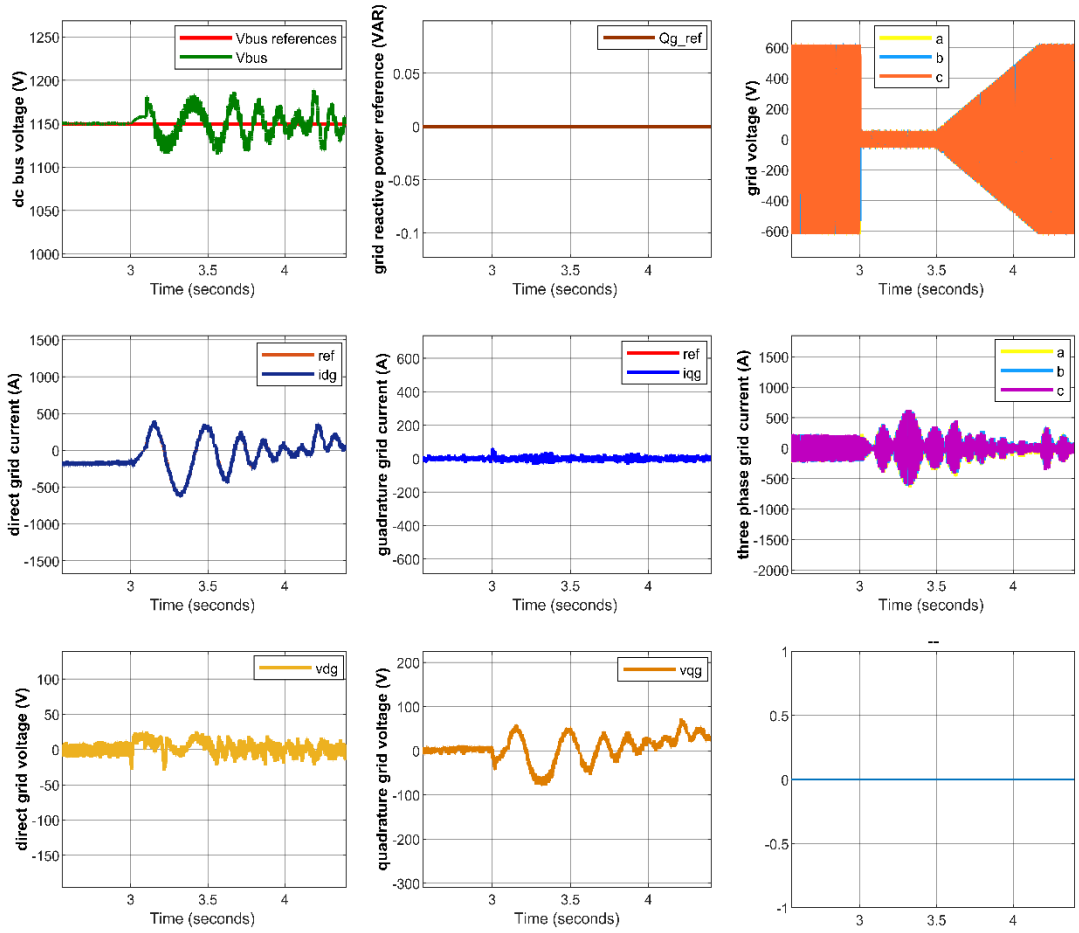

Figure 6.22. Performance of GSC magnitudes under symmetrical voltage dips.

Once the voltage at the grid is totally recovered, the control of the quadrature rotor current (iq) component is regained and this provides the torque and active power demanded by the MPPT algorithm. This means that the rotational speed is controlling properly. At the GSC, it can be realized that the voltage dip has provoked some variations in the DC bus voltage. However, this is not that much problematic because, the GSC is working properly during the dip. It has to be noted that, as demanded by the grid codes, a huge amount of reactive currents should be provided by a means of GSC and this can be done by providing grid reactive power reference (Q_g_ref) during the dip.

6.7.2. Asymmetrical Voltage Dips

This section exhibits the simulation analysis of asymmetrical voltage dips. Hence, the performance of the proposed control system is analyzed for 10 % asymmetrical voltage dip. Figure 6.23 represents the stator flux and the crowbar current performances.

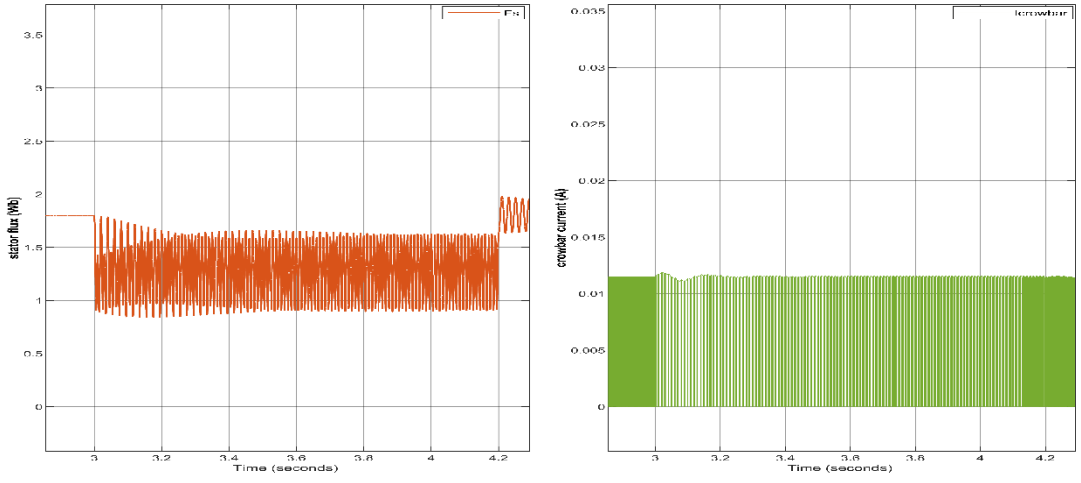

Figure 6.23. Stator flux and crowbar current under asymmetrical voltage dips.

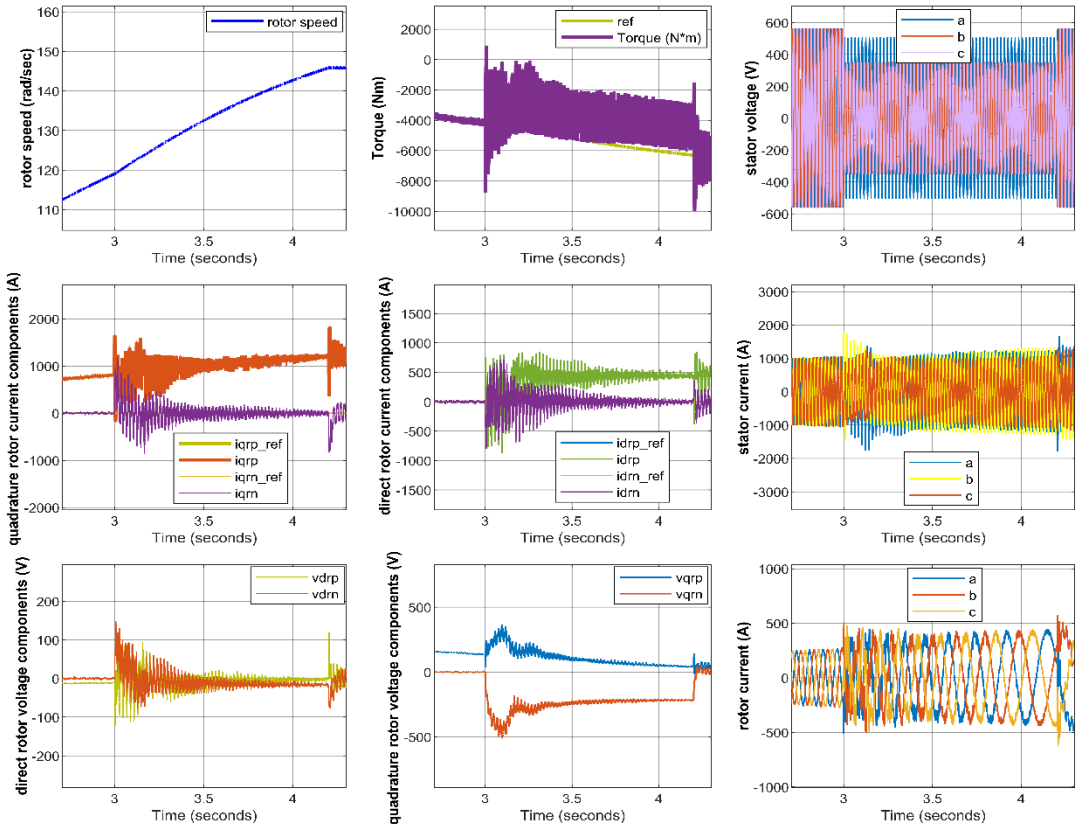

Figure 6.24. Performances of RSC magnitudes under asymmetrical voltage dips.

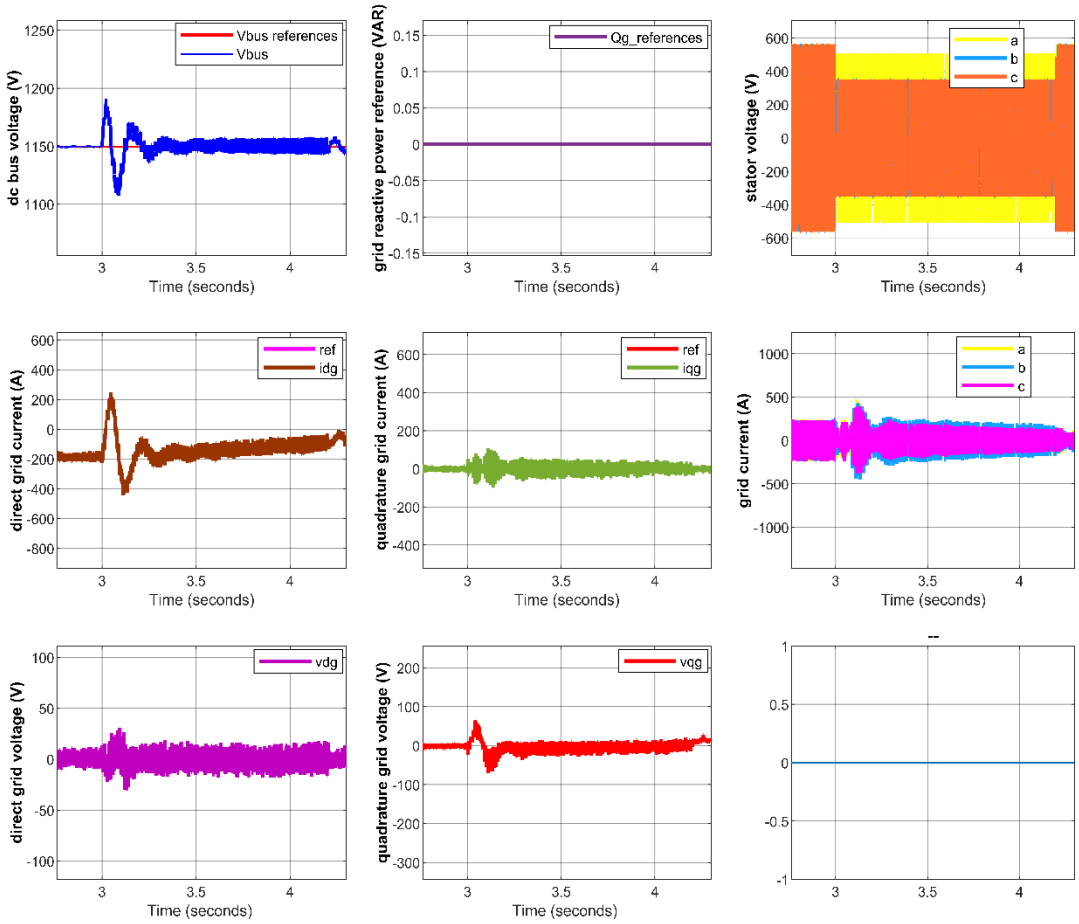

Figure 6.25. Performances of GSC magnitudes under asymmetrical voltage dips.

From the simulation above at the RSC, it can be observed that there is variation in the rotor speed and this is mainly because there is non-total control of voltage at the grid. Furthermore, the stator flux has moved down during the voltage dip and therefore there is no total control on the torque. Besides, there is oscillations at the torque and those oscillations are mainly because of the imbalance situation. Additionally, the zero sequence of the rotor currents that has been performed is maintaining (zero) properly. At the time instant 4.2 seconds, the grid voltage that recover again is a perturbation for the DFIG magnitudes but the system is still able to operate properly. However, the asymmetry has not been performed at the GSC for the sake of simplicity, but the GSC has been capable to cope with the DC bus voltage perturbation and the system is controlling the quadrature grid current (iqg) component to zero during the voltage dip.

PART 7

CONCLUSION

In this thesis, a detailed simulation result of DFIG based wind turbine connected to the power grid is extensively investigated. The main finding has been drawn from the specifications of a 2 MW, 690 V DFIG system. At first, all the key elements have been modeled including the wind turbine such as: wind speed model, aerodynamic model, drive train model, electrical model and DFIG. Furthermore, a comprehensive dynamic model of DFIG has been developed in a rotating dq reference frame by using Clarke and Park transformation technique, by first deriving and modeling the abc natural reference frame.

The most representative magnitudes, performance, and control of a wind turbine based DFIG has been illustrated. It further contains the findings of the steady-state analysis and simulation results that confirm the performance and control of the DFIG system. Different wind speed with the system has been evaluated and the finding shows that the system is capable of controlling the torque and power at variable speed. This means that the system is also capable of extracting the maximum power available by using MPPT. An indirect speed control strategy has been applied to drive the torque to track the maximum power curve.

Moreover, vector control approach of electrical machines has been implemented in the study. Vector control provides dynamic control of DFIG and it employs RSC and GSC. The objective of the RSC is to control the torque and flux of the machine and it's also responsible for the MPPT. Besides, the RSC assures decouple control of active and reactive stator power. The main purpose of GSC is to maintain the dc bus voltage constant irrespective of the region of operation and it also operates at a unit power factor. In addition, the comparisons of the performances of a wind turbine based DFIG with PI control and proposed method for different wind speed has been investigated.

Finally, the study provides extensive investigations of the transient behavior of DFIG based wind turbine under symmetrical and asymmetrical voltage dips. Furthermore, the asymmetrical voltage shows the existence of positive and negative sequence. Thus, dual vector control strategy has been implemented. It has been determined that this strategy is suitable for controlling the reactive power properly during the dip. Crowbar protection has been applied in order to protect the converter during the voltage dip and the simulation result of the most representative magnitudes of a wind turbine based DFIG has been analyzed.

7.1. CONTRIBUTIONS OF THESIS

The main contributions are presented as follows:

- Implementation and simulations of the DFIG system in the RSC using SFOVC.
- The study of steady-state analysis of the different magnitudes of DFIG system.
- Comparison between the typical PI controller and the proposed method in terms of settling time for different wind speeds.
- Implementation of grid-connected DFIG based wind turbine in the GSC using GVOVC.
- The study for dynamic analysis of current loops behavior in a wind turbine based DFIG.
- Investigation and performance analysis of DFIG based wind turbine connected to the grid under symmetrical and asymmetrical voltage dips.

7.2. FUTURE WORK

Even though various developments have been done in DFIG wind turbine, some future work that require to develop are listed below.

- Since vector control strategy which, for instance, require current control loops has been performed in this thesis. Thus, direct torque control and direct power control strategy should be examined because, these strategies do not require current control loops.

- Pitch controller should be designed in order to achieve good performances for much higher wind speed.
- Advanced control strategies of DFIG based wind turbine should be considered. Robust control strategy, hybrid control and optimal control strategies should be investigated for better transient and robustness.
- The DFIG system during asymmetrical voltage dips that has been developed in this thesis still need to improve by just integrating dc choppers instead of crowbar to further modify the oscillations in the dc bus voltage.

REFERENCES

1. Thakur, A., Panigrahi, S., and Behera, R. R., "A review on wind energy conversion system and enabling technology", ***IEEE International Conference on Electrical Power and Energy Systems***, 527-532 (2016).

2. Annoukoubi, M., Essadki, A., Laghridat, H., and Nasser, T., "Comparative study between the performances of a three-level and two-level converter for a Wind Energy Conversion System", ***IEEE International Conference on Wireless Technologies, Embedded and Intelligent Systems***, 1-6 (2019).

3. Morsi, A., Abbas, H. S., and Mohamed, A. M., "Wind turbine control based on a modified model predictive control scheme for linear parameter-varying systems", ***IET Control Theory and Applications***, 11(17): 3056-3068 (2017).

4. El-Sharkawi, M. A., "Wind energy: an introduction*"*, ***Taylor and Francis book on History of the Wind Energy Development***, 1-5 (2015).

5. Bianchi, F. D., De Battista, H., and Mantz, R. J., "Wind turbine control systems: principles, modelling and gain scheduling design*"*, ***Springer Book Advances in Industrial Control***, (19): (2007).

6. Ackermann, T., "Wind power in power systems*"* 200(5): (2005).

7. Sathyajith, M., and Philip, G. S. (Eds.)., "Advances in wind energy conversion technology", ***Springer Science and Business Media***, 3-8 (2011).

8. Pardalos, P. M., Rebennack, S., Pereira, M. V., Iliadis, N. A., and Pappu, V. (Eds.)., "Handbook of wind power systems", ***Springer Berlin Heidelberg***, 21-30 (2013).

9. IEA., "International Energy Agency Ministerial Meeting on Wind Power", **https://www.iea.org/reports/wind-power** (2022).

10. Tanvir, A. A., Merabat, A., and Beguenane, R., "Real-time control of active and reactive powerfor doubly fed induction generator (DFIG)-based wind energy convertion system", ***Energies***, 8(9): 10389-10408 (2015).

11. Jain, B., Jain, S., and Nema, R. K., "Control strategies of grid interfaced wind energy conversion system", ***An overview. Renewable and Sustainable Energy Reviews***, (47): 983-996 (2015).

12. Jena, D., and Rajendran, S., "A review of estimation of effective wind speed based control of wind turbines", ***Renewable and Sustainable Energy Reviews***, (43): 1046-1062 (2015).

13. Pati, S., and Samantray, S., "Decoupled control of active and reactive power in a DFIG based wind energy conversion system with conventional PI controllers", ***IEEE International Conference on Circuits, Power and Computing Technologies***, 898-903 (2014).

14. Ouyang, J., Tang, T., Yao, J., and Li, M., "Active voltage control for DFIG-based wind farm integrated power system by coordinating active and reactive powers under wind speed variations", ***IEEE Transactions on Energy Conversion***, 34(3): 1504-1511 (2019).

15. Kerrouche, K., Mezouar, A., and Belgacem, K., "Decoupled control of doubly fed induction generator by vector control for wind energy conversion system", ***Energy procedia***, (42): 239-248 (2013).

16. Ghoudelbourk, S., Dib, D., and Omeiri, A., "Decoupled control of active and reactive power of a wind turbine based on DFIG and matrix converter", ***Energy Systems***, 7(3): 483-497 (2016).

17. Aydin, E., Polat, A., and Ergene, L. T., "Vector control of DFIG in wind power applications", ***IEEE International Conference on Renewable Energy Research and Applications***, Birmingham, UK, 11, 20 (2016).

18. Jabr, H. M., Lu, D., and Kar, N. C., "Design and implementation of neuro-fuzzy vector control for wind-driven doubly-fed induction generator" ***IEEE Transactions on Sustainable Energy***, 2(4): 404-413 (2011).

19. Li, S., Haskew, T. A., Williams, K. A., and Swatloski, R. P, "Control of DFIG wind turbine with direct-current vector control configuration", ***IEEE transactions on Sustainable Energy***, 3(1): 1-11 (2011).

20. Wang, T., Ding, L., Yin, S., Jiang, J., Cheng, F., and Si, J., "A new control strategy of DFIG-based wind farms for power system frequency regulation", ***IEEE PES Asia-Pacific Power and Energy Engineering Conference***, 1-5 (2015).

21. Hughes, F. M., Anaya-Lara, O., Jenkins, N., and Strbac, G., "Control of DFIG-based wind generation for power network support", ***IEEE Transactions on Power Systems***, 20(4): 1958-1966 (2005).

22. Fdaili, M., Essadki, A., and Nasser, T., "Comparative analysis between robust SMC & conventional PI controllers used in WECS based on DFIG", ***International Journal of Renewable Energy Research***, 7(4): 2151-2161 (2017).

23. Azzaoui, M. E., and Mahmoudi, H., "Fuzzy-PI control of a doubly fed induction generator-based wind power system", ***International Journal of Automation and Control***, 11(1): 54-66 (2017).

24. Hamane, B., Benghanemm, M., Bouzid, A. M., Belabbes, A., Bouhamida, M., and Draou, A., "Control for variable speed wind turbine driving a doubly fed induction generator using Fuzzy-PI control", ***Energy Procedia***, (18): 476-485 (2012).

25. Zhu, R., Chen, Z., Tang, Y., Deng, F., and Wu, X., "Dual-loop control strategy for DFIG-based wind turbines under grid voltage disturbances", ***IEEE Transactions on Power Electronics***, 31(3): 2239-2253 (2015).

26. Tremblay, E., Atayde, S., and Chandra, A., "Comparative study of control strategies for the doubly fed induction generator in wind energy conversion systems: A DSP-based implementation approach", ***IEEE Transactions on sustainable energy***, 2(3): 288-299 (2011).

27. Nian, H., and Yi, X., "Coordinated control strategy for doubly-fed induction generator with DC connection topology", ***IET Renewable power generation***, 9(7): 747-756 (2015).

28. Wu, Y. K., and Yang, W. H., "Different control strategies on the rotor side converter in DFIG-based wind turbines", ***Energy Procedia***, (100): 551-555 (2016).

29. Tourou, P., and Sourkounis, C., "Review of control strategies for DFIG-based wind turbines under unsymmetrical grid faults", ***IEEE Ninth international conference on ecological vehicles and renewable energies***, 1-9 (2014).

30. Justo, J. J., Mwasilu, F., and Jung, J. W., "Enhanced crowbarless FRT strategy for DFIG based wind turbines under three-phase voltage dip", ***Electric Power Systems Research***, (142): 215-226 (2017).

31. Musarrat, M. N., Fekih, A., and Islam, M. R., "An Improved Fault Ride Through Scheme and Control Strategy for DFIG-Based Wind Energy Systems", ***IEEE Transactions on Applied Superconductivity***, 31(8): 1-6 (2021).

32. Wessels, C., Gebhardt, F., and Fuchs, F. W., "Fault ride-through of a DFIG wind turbine using a dynamic voltage restorer during symmetrical and asymmetrical grid faults", ***IEEE Transactions on Power Electronics***, 26(3): 807-815 (2010).

33. Das, T. K., and Zhang, J., "Counteracting the effects of symmetrical and asymmetrical voltage sags on DFIG-based wind power systems", ***IEEE International Conference on Advanced Mechatronic Systems***, Melbourne, Australia, 11, 30 (2016).

34. Döşoğlu, M. K., "Crowbar hardware design enhancement for fault ride through capability in doubly fed induction generator-based wind turbines", ***ISA transactions***, (104): 321-328 (2020).

35. Altimania, M. R., "Modeling of doubly-fed induction generators connected to distribution system based on eMEGASim® real-time digital simulator" (2014).

36. Gasch, R., and Twele, J. (Eds.)., "Wind power plants: fundamentals, design, construction and operation", ***Springer Science and Business Media***, 47-59 (2011).

37. Aissaoui, A. G., and Tahour, A. (Eds.)., "Wind turbines: design, control and applications", ***BoD–Books on Demand***. 83-92 (2016).

38. Hermann, J. W., and Mathur, J., "Introduction to wind energy systems: basics, technology and operation", ***Springer***, 50-51 (2009).

39. Bustos, G., Vargas, L. S., Milla, F., Sáez, D., Zareipour, H., and Nuñez, A., "Comparison of fixed speed wind turbines models: a case study", ***38th Annual Conference on IEEE Industrial Electronics Society***, 961-966 (2012).

40. Wu, B., Lang, Y., Zargari, N., and Kouro, S., "Power conversion and control of wind energy systems", ***John Wiley & Sons***, 12-19 (2011).

41. Noussi, K., Abouloifa, A., Katir, H., and Lachkar, I., "Modeling and control of a wind turbine based on a doubly fed induction generator", ***IEEE 4th World Conference on Complex Systems***, 1-5 (2019).

42. Abad, G., Lopez, J., Rodriguez, M., Marroyo, L., and Iwanski, G., "Doubly fed induction machine: modeling and control for wind energy generation", ***John Wiley & Sons***, (2011).

43. Junyent-Ferré, A., Gomis-Bellmunt, O., Sumper, A., Sala, M., and Mata, M., "Modeling and control of the doubly fed induction generator wind turbine", ***Simulation Modelling Practice and Theory***, 18(9): 1365-1381 (2010).

44. Jing, X., "Modeling and control of a doubly-fed induction generator for wind turbine-generator systems" (2012).

45. Michas, M., "*Control of turbine-based energy conversion systems*" (2018).

46. Yang, B., Jiang, L., Wang, L., Yao, W., and Wu, Q. H., "Nonlinear maximum power point tracking control and modal analysis of DFIG based wind turbine", ***International Journal of Electrical Power and Energy Systems***, (74): 429-436 (2016).

47. Instruments, T., "Clarke & park transforms on the tms320c2xx", ***Application Report BPRA***, (48): (1997).

48. Lamnadi, M., Trihi, M., Bossoufi, B., and Boulezhar, A., "Modeling and control of a doubly-fed induction generator for wind turbine-generator systems", ***International Journal of Power Electronivs and Drive System***, 7(3): 973-985 (2016).

49. Arifujjaman, M., Iqbal, M. T., & Quaicoe, J. E., "Vector control of a DFIG based wind turbine", ***IU-Journal of Electrical & Electronics Engineering***, 9(2): 1057-1066 (2009).

50. Meera, G. S., and Divya, N. A., "Rotor side converter control of DFIG based wind energy conversion system", ***International Journal of Engineering Research and Technology***, 4(8): 607-612 (2015).

51. Tuka, M. B., "DC Link Voltage and Power Flow Control of Doubly Fed Induction Generator in Wind Power System", ***IEEE PES/IAS PowerAfrica***, 1-5 (2020).

52. Hallak, M., Hasni, M., and Menaa, M., "Modeling and control of a doubly fed induction generator base wind turbine system", ***IEEE International Conference on Electrical Sciences and Technologies in Maghreb***, 1-5 (2018).

53. Bhushan, R., and Chatterjee, K., "Mathematical modeling and control of DFIG-based wind energy system by using optimized linear quadratic regulator weight matrices", ***International Transactions on Electrical Energy Systems***, 27(11): 1-23 (2017).

54. Puchalapalli, S., and Singh, B., "A novel control scheme for wind turbine driven DFIG interfaced to utility grid", ***IEEE Transactions on Industry Applications***, 56(3): 2925-2937 (2020).

55. Abu-Rub, H., Malinowski, M., and Al-Haddad, K., "Power electronics for renewable energy systems, transportation and industrial applications", ***John Wiley & Sons***, 270-317 (2014).

56. Elbashir, O. E., Zezhong, W., and Qihui, L., "Modeling and analysis of DFIG in wind energy conversion system", ***International journal of Energy and environment***, (5): 239-250 (2014).

57. Nadour, M., Essadki, A., and Nasser, T., "Comparative analysis between PI & backstepping control strategies of DFIG driven by wind turbine", ***International Journal of Renewable Energy Research***, 7(3): 1307-1316 (2017).

58. Al Zabin, O., & Ismael, A., "Rotor current control design for DFIG-based wind turbine using PI, FLC and fuzzy PI controllers", ***IEEE International Conference on Electrical and Computing Technologies and Applications***, UAE, 9 (2019).

59. Yonis, S. A., and Yusupov, Z., "Dynamic Analysis of Current Loops Behavior in a Wind Turbine Based Doubly-fed Induction Generator", ***Avrupa Bilim ve Teknoloji Dergisi***, Konya, Turkey, 3, 11 (2022).

60. Kumhar, A. R., "Vector Control Strategy to Control Active and Reactive Power of Doubly Fed Induction Generator Based Wind Energy Conversion System", ***IEEE 2nd International Conference on Trends in Electronics and Informatics***, 1-9 (2018).

61. Haseeb, I., Basit, A., Khan, R., and Asif, M., "Designing variable speed small hydro turbine with doubly fed induction generator (DFIG)", ***International Journal of Renewable Energy Sources***, (4): 1-10 (2019).

APPENDIX A

DFIG AND WIND TURBINE PARAMETERS

Table Appendix A.1. Initial parameters of DFIG and wind turbine.

PARAMETERS	VALUES (UNITS)
STATOR POWER	2 MW
ROTOR SPEED	1800 rev/min
NOMINAL VOLTAGE	690 V
NOMINAL CURRENT	1.76 kA
ELECTROMAGNETIC TORQUE	12.7 kN.m
STATOR FREQUENCY	50 HZ
ROTOR VOLTAGE	2.07 kV
ROTOR RESISTANCE	0.0029 Ω
ROTOR INDUCTANCE	0.0026 H
STATOR RESISTANCE	0.0026 Ω
STATOR INDUCTANCE	0.0026 H
STATOR/ROTOR TURNS RATIO	0.34
RATED WIND SPEED	11.8 m/s
GEARBOX RATIO	100
RADIUS OF THE BLADE	42 m
AIR DENSITY	1.225 kg/m^2
POLE PAIR	2

APPENDIX B

MATLAB/SIMULINK MODELS AND SUB-MODELS

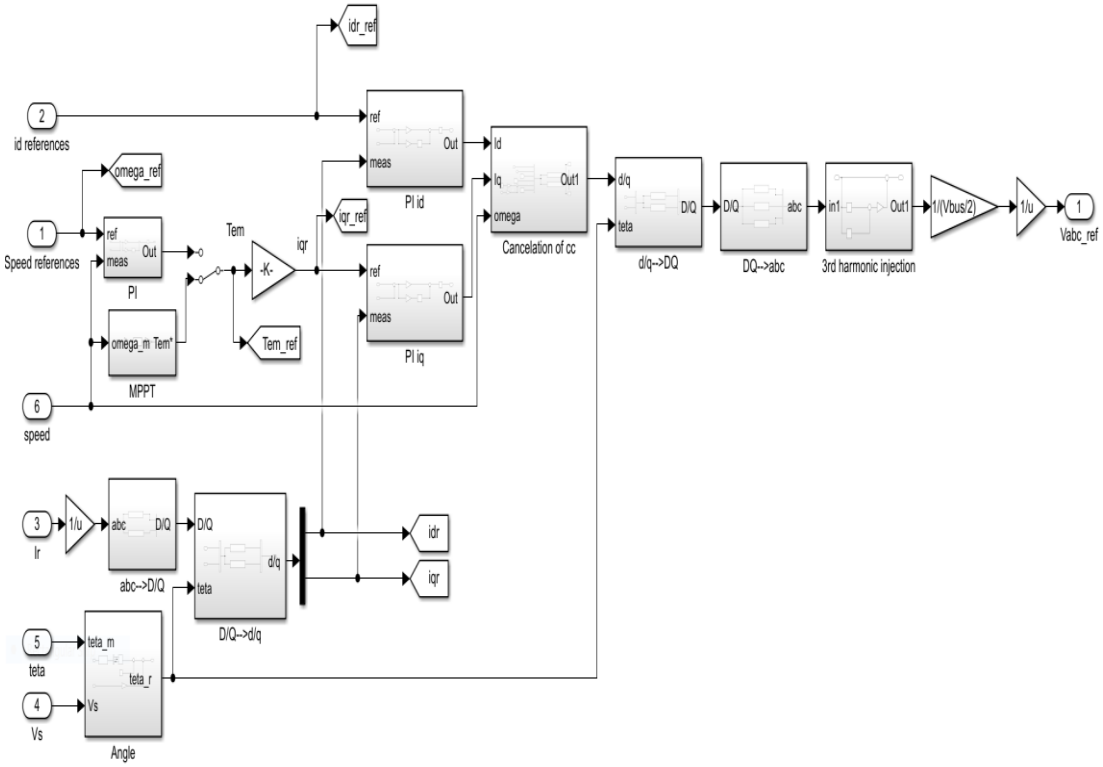

Figure Appendix B.1. RSC control block.

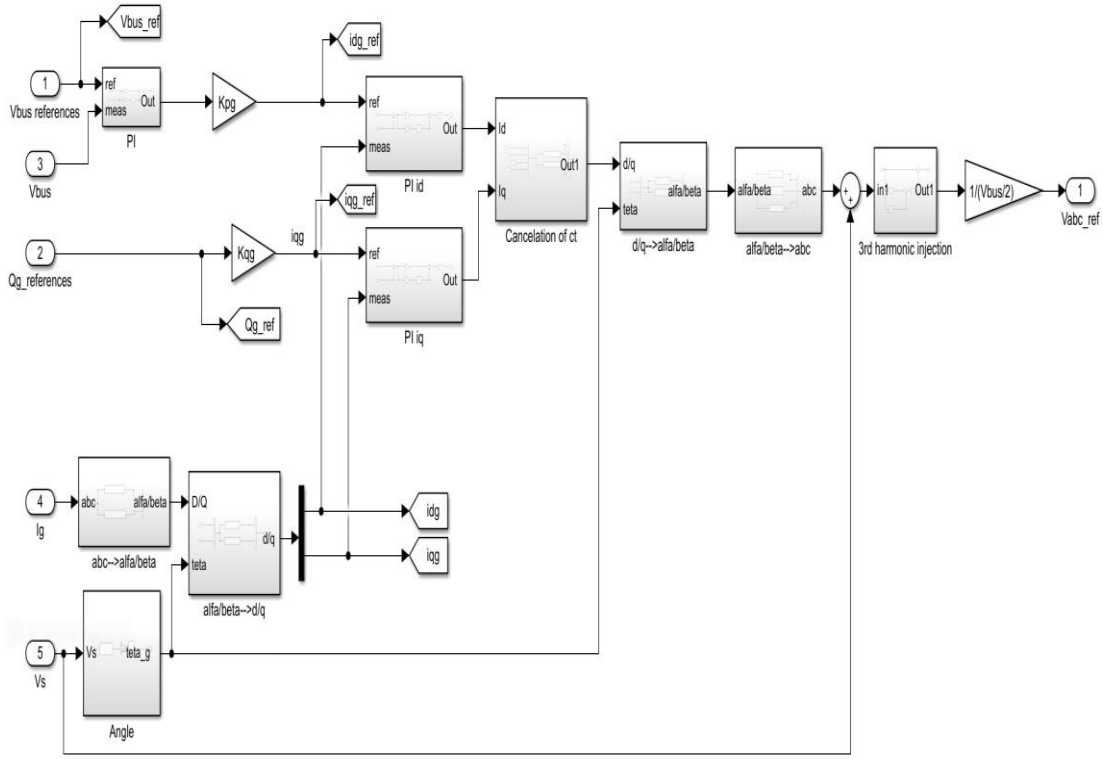

Figure Appendix B.2. GSC control block.

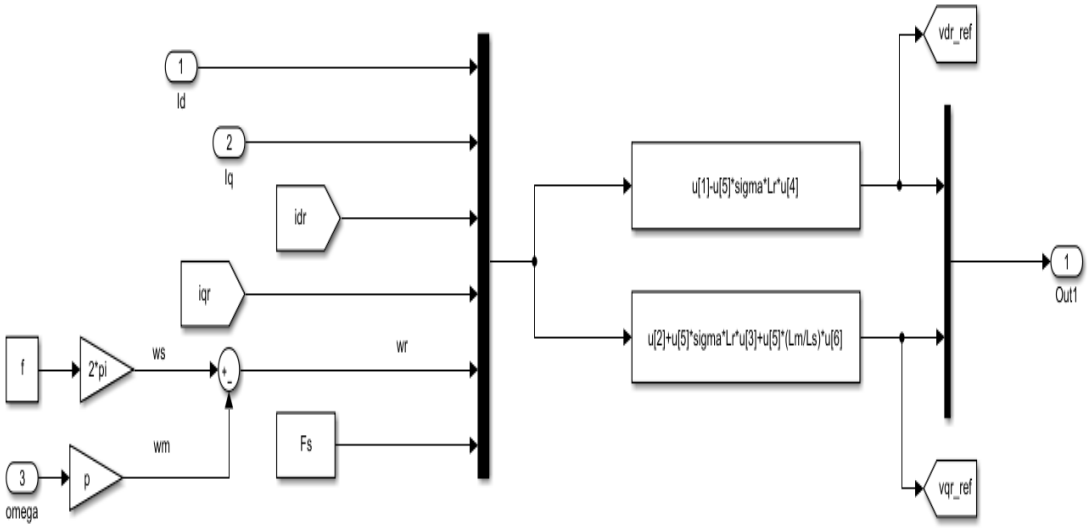

Figure Appendix B.3. Cancellations of coupling terms.

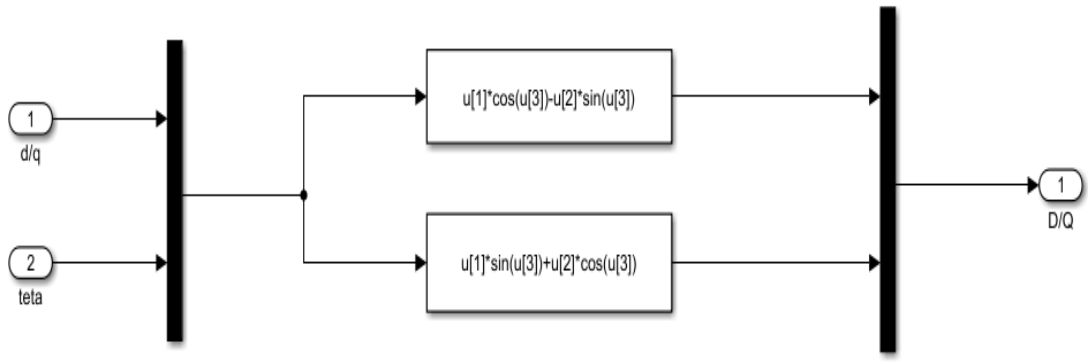

Figure Appendix B.4. d/q to D/Q transformation.

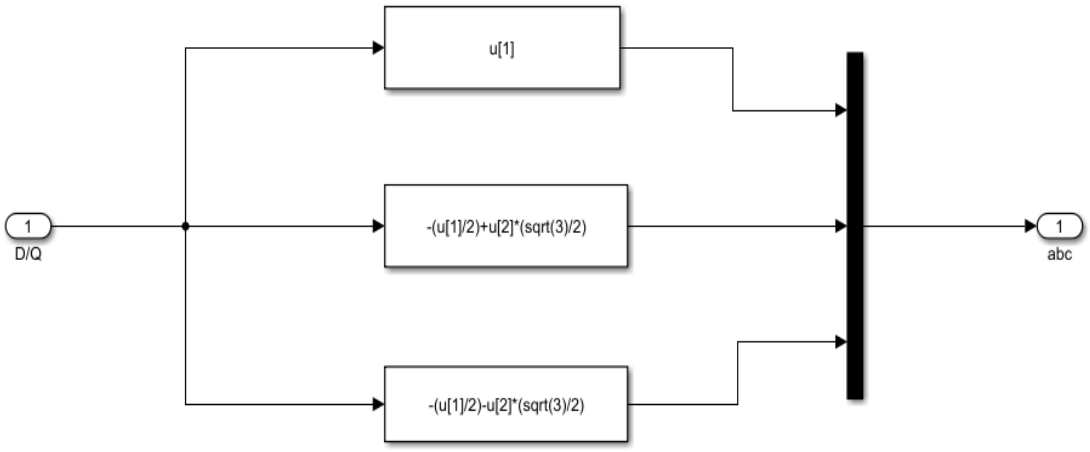

Figure Appendix B.5. D/Q to abc transformation.

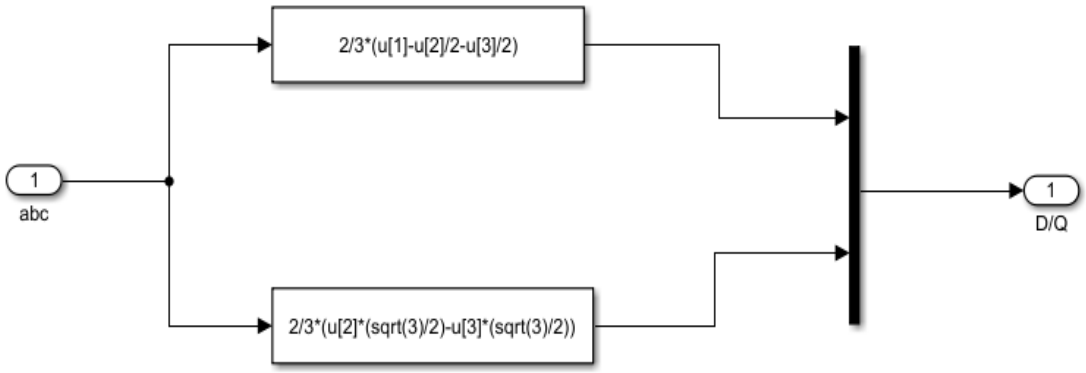

Figure Appendix B.6. abc to D/Q transformation.

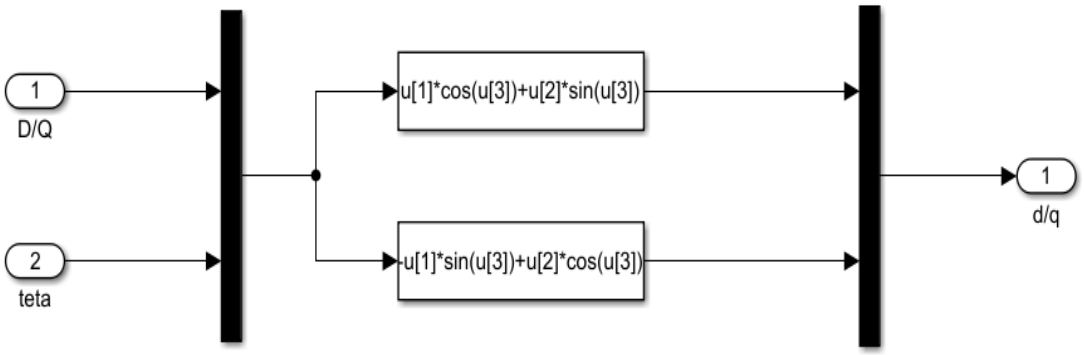

Figure Appendix B.7. D/Q to d/q transformation.

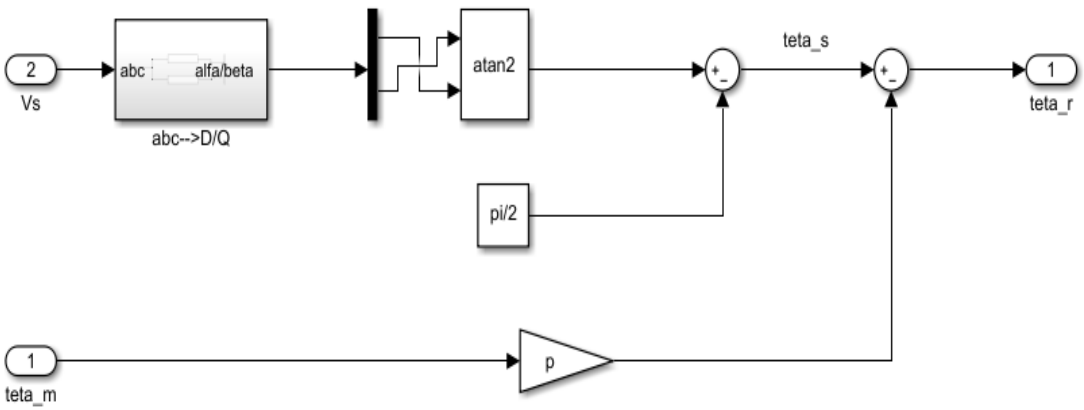

Figure Appendix B.8. PLL angle calculator.

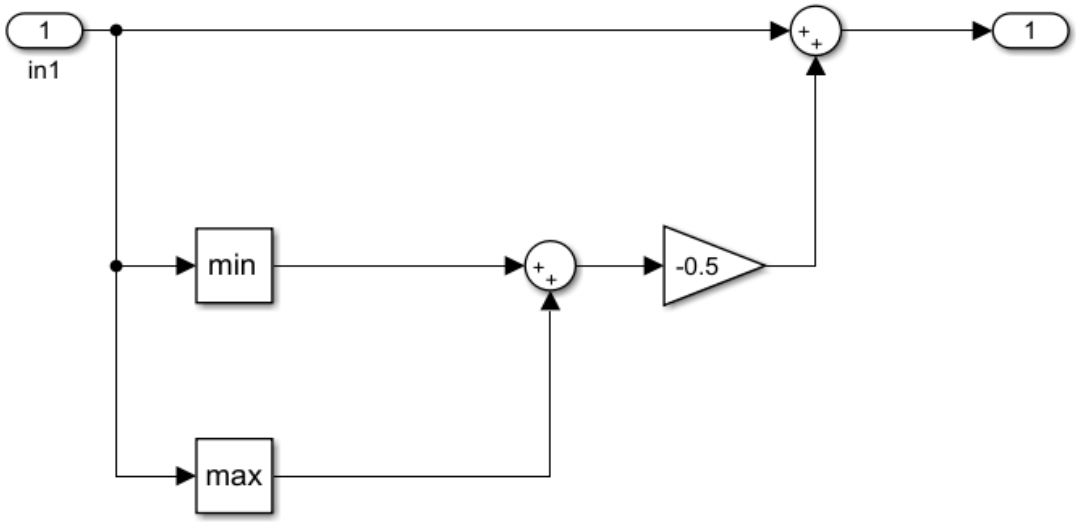

Figure Appendix B.9. Third harmonic injection.

APPENDIX C

INITIALIZATION PROGRAM

```
% Parameters of the DFIG

P= 2e6;
V= 0.69e2;
I = 1.76e3;
T = 12.7e3;
F= 50;
P= 2;                          % number of poles
vr = 2.07e3;
smax = 0.34;
n= 1.5e3;
vr_stator = (Vr*Smax) *u;
U= 0.34;
Rr = 2.9e-3;
Ls =0.087e-3;
Rs = 2.6e-3;
Lm = 2.5e-3;
Vbus = 1150;
σ = 1- Lm^2/(Ls*Lr);        % sigma
Ls = Lm + Ls;                % stator inductance
Lr = Lm + Ls;                % rotor inductance
Fs = V*Sqrt(2/3)/(2*pi*F);%Stator flux (approx.)

Ts = 1/fsw/50;               % sample time
J = 63.5;                    % inertia
fsw = 4000;                  % switching frequency
D = 0.001;                   % damping ratio

% The PI regulator

Tau_i = (σ *Lr)/Rr;
Tau_n = 0.05;
Wni = 100*(1/tau_i);
Wnn = 1/tau_n;


% The dq current regulators

Kp_id = (2*Wni* σ *Lr)-Rr;
Kp_iq = Kp_id;
Ki_id = (Wni^2)*Lr* σ;
Ki_iq = Ki_id;
```

```
% The regulators tuned as controller

Kp_n = (2*Wnn *J)/P;
ki_n = ((wnn^2) *J)/p;

% Parameter of wind turbines

Vw=11.8;                    %Wind speed
N = 100;
Ratio = 42;
ro = 1.225;                 %Air density
```

APPENDIX D

PUBLISHED PAPERS

TR Dizin-indexed Journal

1. Yonis, S. A., and Yusupov, Z., “Dynamic Analysis of Current Loops Behavior in a Wind Turbine Based Doubly-fed Induction Generator”, ***Avrupa Bilim ve Teknoloji Dergisi***, (34): 415-420 (2022).

CONFERENCES

1. Yonis. S. A., and Yusupov, Z., “Voltage Dips Analysis in a Doubly-fed Induction Generator Based Wind Turbine Using Active Crowbar Protection”, ***International Graduate Research Symposium***, Istanbul, Turkey, 3, 6 (2022).

RESUME

Samatar ABDI YONIS was born in Djibouti city in 1994 and he graduated first and elementry education in Dire-dawa, Ethiopia. He completed high school education in Al-falah secondary and preparatory islamic school, after that, he started undergraduate program in Haramaya University Department of Electrical and Computer Engineering in 2013. Then in 2020, he started a master degree in Karabuk University.